Project no. 505428 (GOCE)

AquaTerra

Integrated Modelling of the river-sediment-soil-groundwater system; advanced tools for the management of catchment areas and river basins in the context of global change

Integrated Project

Thematic Priority: Sustainable development, global change and ecosystems

Deliverable No.: TREND2.4
Title: Report on extrapolated time trends at test sites

Due date of deliverable: November 2005
Actual submission date: November 2005

Start date of project: 01 June 2004 **Duration: 60 months**

Organisation name *and contact* of lead contractor *and other contributing partners* for this deliverable:
Broers H.P[1], Visser A.[2],(eds.)
Pinault J.-L.[3], Guyonnet D.[3], Dubus I.G.[3], Baran N.[3], Gutierrez A.[3] & Mouvet C[3]
Batlle Aguilar J.[4], Ph. Orban4, Brouyere S.[4]

1 Netherlands Organisation for Applied Scientific Research TNO, Division Groundwater and Soil, Princetonlaan 6, P.O. Box 80015, 3508 TA Utrecht, The Netherlands. E-mail: h.broers@tno.nl (lead partner)
2 Universiteit Utrecht, Faculty of Geographical Sciences, Budapestlaan 4, 3584 CD Utrecht, The Netherlands.
3 BRGM, Water Division, BP 6009, 45060 Orléans Cedex 2, France.
4 GEOMAC, University of Liege, Building B52/3, 4000 Sart Tilman, Belgium.

Revision: M.H. Gerzabek / J.Barth

Project co-funded by the European Commission within the Sixth Framework Programme (2002-2006)		
Dissemination Level		
PU	Public	X
PP	Restricted to other programme participants (including the Commission Services)	
RE	Restricted to a group specified by the consortium (including the Commission Services)	
CO	Confidential, only for members of the consortium (including the Commission Services)	

SUMMARY

The establishment of tools for trends analysis in groundwater is essential for the prediction and evaluation of measures taken within context of the Water Framework Directive and the draft Groundwater Directive. This report describes the development of trend detection and extrapolation methods. A novel approach for demonstrating trends is presented for the Dutch Meuse case, based on back-scaling of time series using $^{3}H/^{3}He$ ages. The method yields convincing results, because it effectively reduces uncertainty in trend analysis, which is caused by groundwater age variations. Trend reversal was demonstrated for several chemical indicators and trend extrapolation was feasible using additional simple regression. The Wallonian Meuse case focuses on the complications caused by more-yearly fluctuations of nitrate in areas with thick unsaturated zones. A comparison was made between parametrical and non-parametrical methods to overcome these inherent sources of variability. Several innovative approaches are presented for the Brévilles catchment in France. Especially the impulse-response approach and the possibilistic regression approach helped to understand the functioning of the groundwater system with respect to pesticide transport. Advantages of these approaches are that the require only information on high temporal resolution monitoring data and rainfall inputs.

MILESTONES REACHED

T2.4: Statistical time trend estimation and extrapolation at test locations

The extrapolated trends in groundwater seems to be interesting for surface water – groundwater interaction studies in work packages FLUX and BASIN. The effective demonstration of trend reversal in groundwater due to effective Manure regulations in the lower Meuse basin is interesting within the work of EUPOL.

Table of Contents

1. Introduction to TREND 2 (TNO)

1.1 Background and objectives

The implementation of the EU Water Framework Directive (2000/60/EU) and the draft Groundwater Directive asks for specific methods to detect the presence of long-term anthropogenically induced upward trends in the concentration of pollutants in groundwater. Specific goals for trend detection have been under discussion during the preparation of the recent draft of the Groundwater Directive. The draft Directive defines criteria for the identification and reversal of significant and sustained upward trends and for the definition of starting points for trend reversal. Figure 3.1.1 illustrates the trend reversal concept, as communicated by EU Commission Officer Mr. Ph. Quevauviller. The figure 3.shows how the significance of trends is related to threshold concentrations which should be defined by the member states.

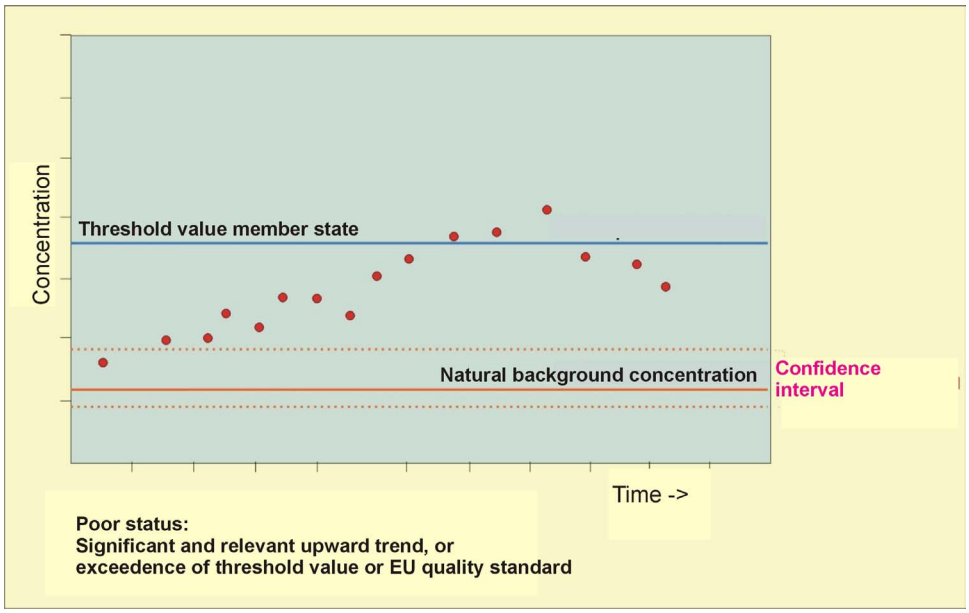

Figure 1.1 Trend reversal concept of the draft EU Groundwater Directive.

Trends should be reversed when concentrations increase up to 75% of the threshold concentration. Member states should reverse trends which present a significant risk of harm to associated aquatic ecosystems, directly dependent terrestrial ecosystems, human health, whether actual or poten
tial, of the water environment, through the program of measures referred to in Article 11 of the Water Framework Directive, in order to progressively reduce pollution of groundwater. Thus, there is a direct link between trends in groundwater and the status and trends in related surface waters. This notion is central to the overall objectives of the AQUATERRA research project.

> Working hypothesis 1:
> Groundwater quality is of utmost importance to the quality of surface waters. Establishment of trends in groundwater is essential for prediction and evaluation of measures taken within the Framework Directive and the draft Groundwater Directive.

Accordingly, the work package TREND-2 of Aquaterra is dedicated to the following overall objectives.

Development of operational methods to assess, quantify and extrapolate trends in groundwater systems. The methods will be applied and tested at various scales and in various hydrogeological situations. The methods applied should be related to the trend objectives of the Water Framework Directive and draft Groundwater Directive. In addition to the DOW, it is our ambition to link changes in groundwater quality to changes in surface water quality.
Linking changes in land use, climate and contamination history to changes in groundwater chemistry. We define a temporal trend as '*a change in groundwater quality over a specific period in time, over a given region, which is related to land use or water quality management',* according to Loftis 1991, 1996.

It should be noted that trends in groundwater quality time series are difficult to detect because of (1) the long travel times involved, (2) possible obscuring or attenuating effect of physical and chemical processes, (3) spatial variability of the subsurface, inputs and hydrological conditions and (4) short-term natural variability of groundwater quality time series. The TREND 2 package is dedicated to the development and validation of methods which overcome many of these problems.

Working hypothesis 2:
Detection of trends in groundwater is complicated by spatial variations in pressures, in flow paths and groundwater age, in chemical reactivity of groundwater bodies, and by temporal variations due to climatological factors. Methods for trend detection should be robust in dealing with this inherent variability.

Groundwater pollution is caused by both point and diffuse sources. Large scale groundwater quality, however, is mainly connected to diffuse sources, so that the TREND 2 project will concentrate on trends in groundwater quality connected to diffuse inputs, notably nutrients, metals and pesticides. We will consider a number of large basins in Europe and try to devise a trend monitoring method and network. Although trends in groundwater quality can occur at large scales, linking groundwater quality to land use and contamination history requires analysis at smaller scale, i.e. groundwater subsystems. Thus, the approach zooms in on groundwater system analysis around observation locations. Results will be extended to large scale monitoring.

1.2 General methods used in TREND 2

Research activities within TREND 2 focus on the following issues:
Inventory of monitoring data of different basins and sub-catchments. The inventory focuses on observation points with existing long time series. The wells should preferably be located in agricultural areas, because pesticides and nutrients are the main concern in trend detection for the Water Framework Directive. Additional information will be collected about historical land use changes and related changes in the input of solutes into the groundwater system.
Development of suitable trend detection concepts. Trend detection concepts include both statistical approaches (classical parametrical and non-parametrical methods, hybrid techniques) and conceptual approaches (time-depth transformation, age dating)
Methods for trend aggregation for groundwater bodies. The Water Framework Directive demands that trends for individual points are aggregated on the spatial scale of the groundwater bodies. The project will focus on robust methods for trend aggregation.
Trend extrapolation. Trend extrapolation will be based on statistical extrapolation methods and on deterministic modelling. Both 1D and 3D model may be applied to predict future changes and to compare these with measured data from time series.
Recommendations for monitoring. Results from the various case studies will be used to outline recommendations for optimizing monitoring networks for trend analysis

1.3 TREND 2 case studies

The following case studies have been selected for testing the methodologies:

Table 1.1: Case studies

Basin	Contaminants	Institutes
Meuse		
Dommel upper tributaries	Nitrate, sulfate, Ni, Cu, Zn, Cd	TNO/UU
Noord-Brabant region	Nitrate, sulfate, Ni, Cu, Zn, Cd	TNO/UU
Wallonian catchments:	Nitrate	Ulg
Néblon		
Pays Herve		
Hesbaye		
Floodplain Meuse		
Brévilles		
Brévilles catchment	Pesticides	BRGM
Elbe		IETU
Czech subbasins	Nitrate	
Schleswig-Holstein	Nitrate	

These cases have different spatial scales and different hydrogeological situations. Details on the various cases are provided in the subsequent chapters of this report.

1.4 Contents of the current report

This report describes the results of trend analysis, including both trend detection and trend extrapolation. A novel approach for demonstrating trends is presented for the Dutch case, based on back-scaling of time series using $^{3}H/^{3}He$ ages. The method yields convincing results, because it effectively reduces uncertainty in trend analysis which is caused by groundwater age variations. Trend reversal was demonstrated for several chemical indicators and trend extrapolation was feasible using additional simple regression. The Wallonian case focuses on the complications caused by more-yearly fluctuations of nitrate in areas with thick unsaturated zones. A comparison was made between parametrical and non-parametrical methods to overcome these inherent sources of variability. Several innovative approaches are presented for the Brévilles catchment in France. Especially the impulse-response approach and the possibilistic regression approach helped to understand the functioning of the groundwater system with respect to pesticide transport.

1.5 Structure of the report

This report describes statistical trend analysis results for the various cases of TREND 2. Chapters 2 to 4 describe the trend estimation and extrapolation for the the Dutch Meuse, the Wallonian Meuse and the Brévilles catchments, respectively. Chapter 5 gives a brief discussion on the results of the various cases, focusing on opportunities and limitations on the integration of methods for trend analysis.

1.6 Glossary

Parametrical methods	Methods of trend analysis based on an assumption of a specific frequency distribution (for instance normal distribution)
Non-parametrical methods	Methods of trend analysis which do not make assumptions on.
Impulse-response approach	Black box model to describe the response of hydraulic head to precipitation
Possibilistic regression approach	Regression methods that use mathematical tools that describe information that is incomplete or imprecise
OXC	oxidation capacity
SUMCAT	sum of cations
LOWESS smooth	LOcally WEighted Scatter-plot Smoothing
VMW	Vlaamse Maatschappij voor Watervoorziening), the Flemish water supply company
Mann Kendall test	Non-parametric trend test, recommended for use in large data sets where the normality assumption cannot be checked for all individual time series
Shapiro-Wilks test	Test for normality of data for small dataset: n<50
Shapiro- Francia test	Test for normality of data for large dataset: n>50
D'Agostino's test	Test for normality of data for large dataset
Normality	Gaussian distributed data
Kendall´s slope	Non-parametrically determined trend slope
Sen's slope	Non-parametrically determined trend slope
TEMPO computer tool	Windows-based tool which facilitates groundwater data analysis and enables the modelling of time series through iterative calibrations of combinations of transfer functions
Holt's two parameter method	method for exponential smoothing of a time series
SVM	support vector machine

2. Demonstrating trend reversal using tritium-helium age scaling: results for the Dutch Meuse subcatchment (TNO/UU)

A. Visser[1], H.P. Broers[2] & B. van der Grift[2]
[1]Department of Physical Geography, Utrecht University
[2]TNO-NITG - Division of Soil and Groundwater

TNO-NITG
Princetonlaan 6 / P.O. Box 80015
3508 TA Utrecht, The Netherlands
Tel: +31 30 2564750
Fax: +31 30 2564755
h.broers@nitg.tno.nl

2.1 Introduction

In this section we present a new method for the interpretation of groundwater quality time series using modern groundwater travel time determination. This method involves the back-scaling of the individual time series by the $^3H/^3He$ groundwater age, resulting in figures that show the measured concentrations plotted against the estimated time of recharge. These figures can directly be compared to the input functions of the targeted chemicals. We will show that the results of trends in historical inputs can easily be observed and detected from these concentration - recharge date plots.

Using simple regression statistics between the aggregated back-scaled time series and the estimated input function gives us a tool to extrapolate future time trends, based on presumed land use- input scenarios.

2.1.1 Theoretical groundwater age - depth relationship

For groundwater flow to a fully penetrating drain or watercourse, the following travel time distribution can be used (Raats, 1978, 1981):

$$t_z = \frac{\varepsilon D}{N} \ln\left(\frac{D}{D-z}\right) \qquad (2.1)$$

where t_z; age at depth z [years]; D: aquifer thickness [m]; ε: porosity; N: groundwater recharge [m/year] and z: depth below land surface [m]. Equation (2.1) yields a horizontal pattern of isochrones (lines of equal groundwater travel time) which is shown in Figure 2.1. The equation has proved useful for a range of Dutch conditions, because the Netherlands has a flat topography and thick, permeable aquifers.

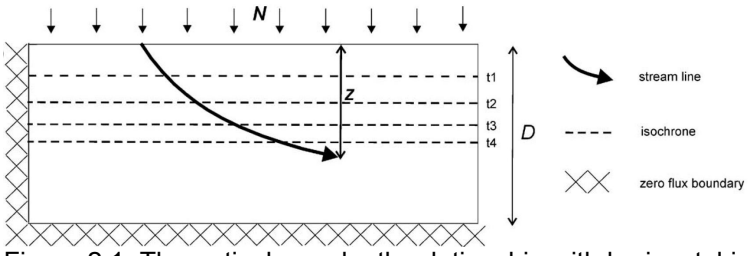

Figure 2.1: Theoretical age-depth relationship with horizontal isochrones, applicable to recharge areas in the Dutch Meuse basin (After Broers and Van der Grift, 2004)

2.1.2 Variation in groundwater ages

On a regional scale, the parameters that control this relationship may vary. For instance, the aquifer thickness is known to be less in the western part of the Dutch Meuse basin (Meinardi, 1994). Heterogeneity in the subsurface will also cause deviations from the ideal theoretical case, as can be seen in Figure 2.2. In this theoretical example, a discontinuous layer with low permeability affects the flow-field such that younger water is able to infiltrate locally to greater depths, replacing older water.

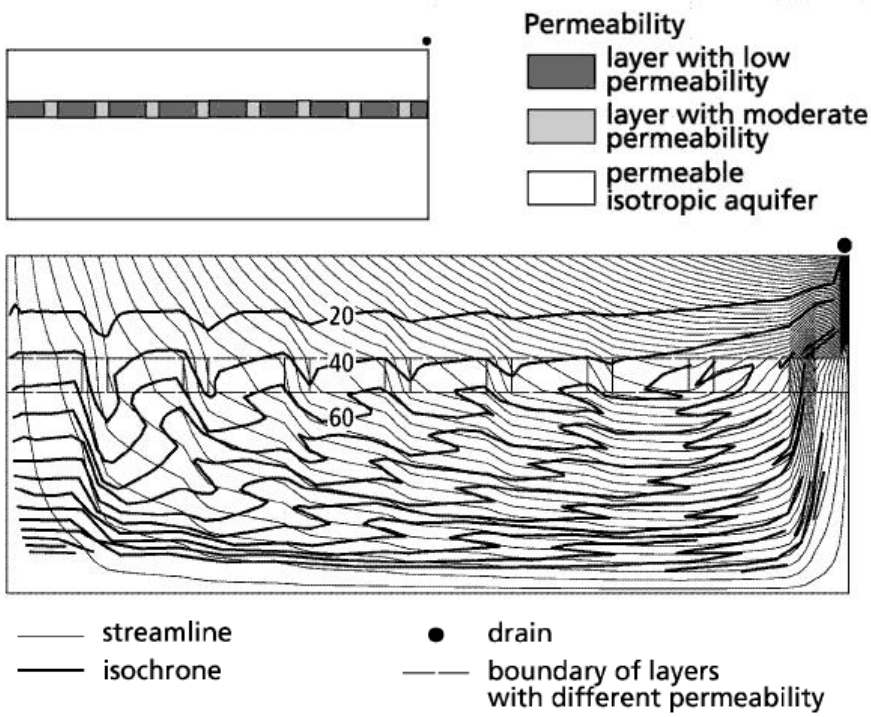

Figure 2.2: Effect of a discontinuous layer with low permeability on the flow field and age distribution. (After Broers and Van der Grift, 2004)

These variations in groundwater age distribution will cause erroneous interpretation of the groundwater quality time series if the ideal theoretical relationship is assumed. Figure 2.3 shows the groundwater ages, as determined by $^{3}H/^{3}He$ groundwater dating (as presented in Deliverable T2.3) plotted against the groundwater ages predicted by equation 2.1, to show the variation in groundwater ages.

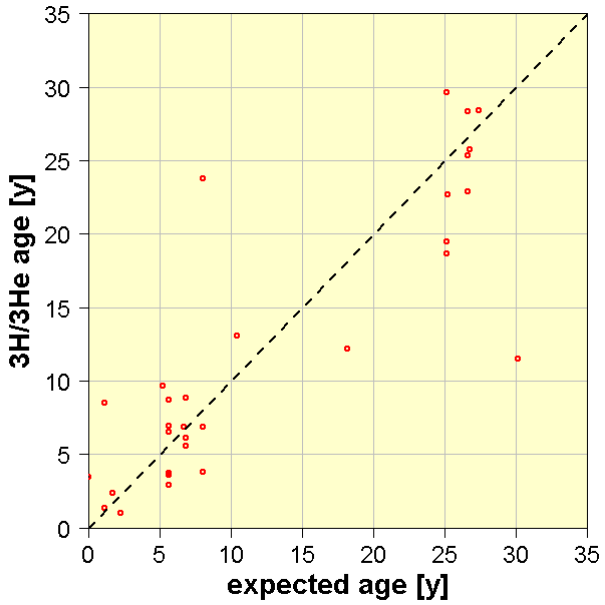

Figure 2.3: $^{3}H/^{3}He$ ages plotted against the expected theoretical ages.

2.2 Data

The data used for the profiles mentioned in the title were described Table 2.2 of Deliverable T2.1. Summarizing, the data include time series since 1980 or 1991 of the chemical composition of the groundwater sampled at 14 locations in agricultural recharge areas in the lower Meuse basin (shown on Figure 2.4). Measurements include field parameters (pH, EC and dissolved oxygen) concentrations of major cations (Na, K, Ca, Mg, Fe, Al and NH_4) and anions (Cl, NO_3, SO_4, HCO_3 and PO_4) and trace metals (i.e. Cd, Cu, Ni, Zn). These data were readily avaiblable from the provincial monitoring network.

For the present study, thirty-one screens between 4 and 26 m below surface level were sampled for tritium-helium. Samples were analyzed by the Institut für Umweltphysik of the Bremen University (Sültenfuß et al., 2004). The measurements were interpreted with an estimated recharge temperature of 10°C, an elevation of 0 m above sea level and a salinity of zero. See for further details deliverable T2.3. Tritium-helium ages were preferred over CFC and SF6 ages, because they were considered more reliable. This relates to the associated dissolved noble gas measurements which gave indications of age uncertainties.

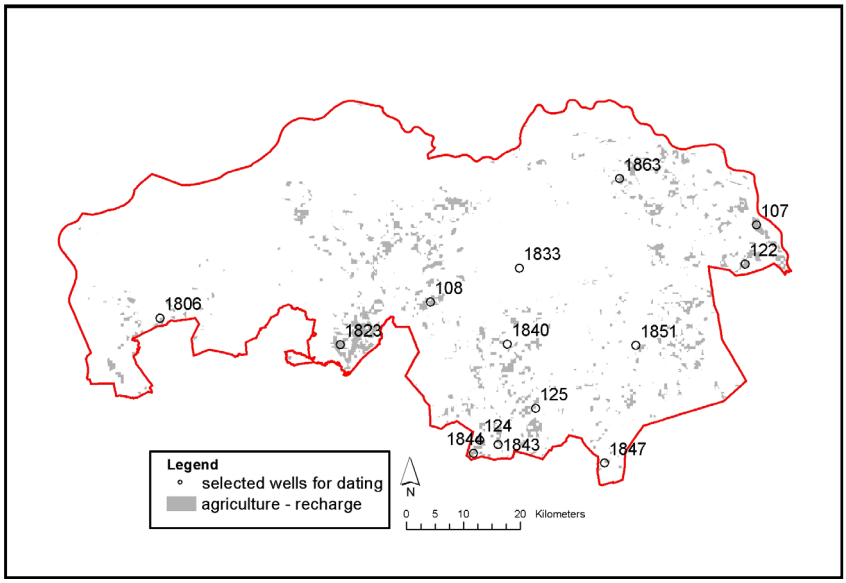

Figure 2.4: Well locations in the agricultural recharge areas in the lower Meuse basin, listed in Table 2.2 of Deliverable T2.1

Chemical indicators

The results of this procedure will be presented for six chemical indicators: three reactive targeted contaminants (*nitrate, aluminum and potassium*), and three conditionally conservative indicators (*oxidation capacity* (OXC), the *chloride concentration* and the *sum of cations* (SUMCAT)). These three chemical indicators are used because they are insensitive to specific subsurface reactions.

The *oxidation capacity* was defined as the weighted sum of molar concentrations of NO3 and SO4 after Postma et al. (1991): $\mathrm{OXC} = 5 * [\mathrm{NO_3^-}] + 7 * [\mathrm{SO_4^{2-}}]$

OXC behaves conservatively during the process of nitrate reduction by pyrite oxidation under the condition that no other reactions occur, i.e. no subsurface denitrification by organic matter.

Chloride is a conservatively transported ion under normal pH conditions.

The *sum of cations* (in fact, major cations: Na, K, Mg, Ca, Fe, Al, NH_4) is useful as a conditionally conservative indicator when cation-exchange processes dominate the transport of the cations and mineral dissolution does not occur. Moreover, the sum of cations is an indicator of the total load of solutes in the groundwater.

2.3 Back-scaling of time series

2.3.1 Method

Better knowledge of the age distribution among the wells enables the use of an alternative trend approach, which is based on “back-scaling” the time series with the known groundwater age. The main assumption is that groundwater age at a certain monitoring screen is constant in time (for example Goode, 1996) This assumption seems reasonable given the long time scales of transport compared with the time scales of seasonal transient effects. The individual time series which cover the monitoring period 1992–2004 were scaled back in time using the tritium-helium age. For example, the time series of a monitoring screen with an age of 9 years is scaled back to the period 1983–1995.

2.3.2 Example: Oxidation capacity

Figure 2.5 shows the back-scaled time series of the oxidation capacity are presented. Each individual time series is assigned a unique color to distinguish between the time series. The time series now reflect the approximate recharge period. The advantages

of the method are 2-fold: (a) every time series provides information over a range of recharge years, and (b) data of multiple time series is available for each recharge year. A LOWESS smooth (LOcally WEighted Scatter-plot Smoothing, Cleveland & Devlin, 1988) was used to generate a trend line through all the time series data in the graph. This trend line reflects the local median of all measurements, which in fact reflects the area aggregated median trend. This enables the direct comparison of the measured concentrations with the regional historical inputs, which were described in deliverable T2.2.

A LOWESS smooth through all the time series is plotted in black. This curve indicates the local median of all the time series. The LOWESS smooth is interpreted as the aggregated median trend for the agricultural recharge areas of Figure 2.4. The dashed black lines are the LOWESS smooths through the residuals between the back-scaled time series and the original LOWESS smooth. These indicate the local 25 and 75 percentile trend of all the time series. This indicates a confidence interval around the LOWESS smooth. We are confident that a certain trend is well described by the LOWESS smooth, if the confidence shows the same trend.

Since each data point of the time series is plotted at the year of recharge, the median curve or LOWESS smooth should resemble the curve of the historical surplus input of the agricultural recharge areas which was derived in deliverable T2.2 (red line).

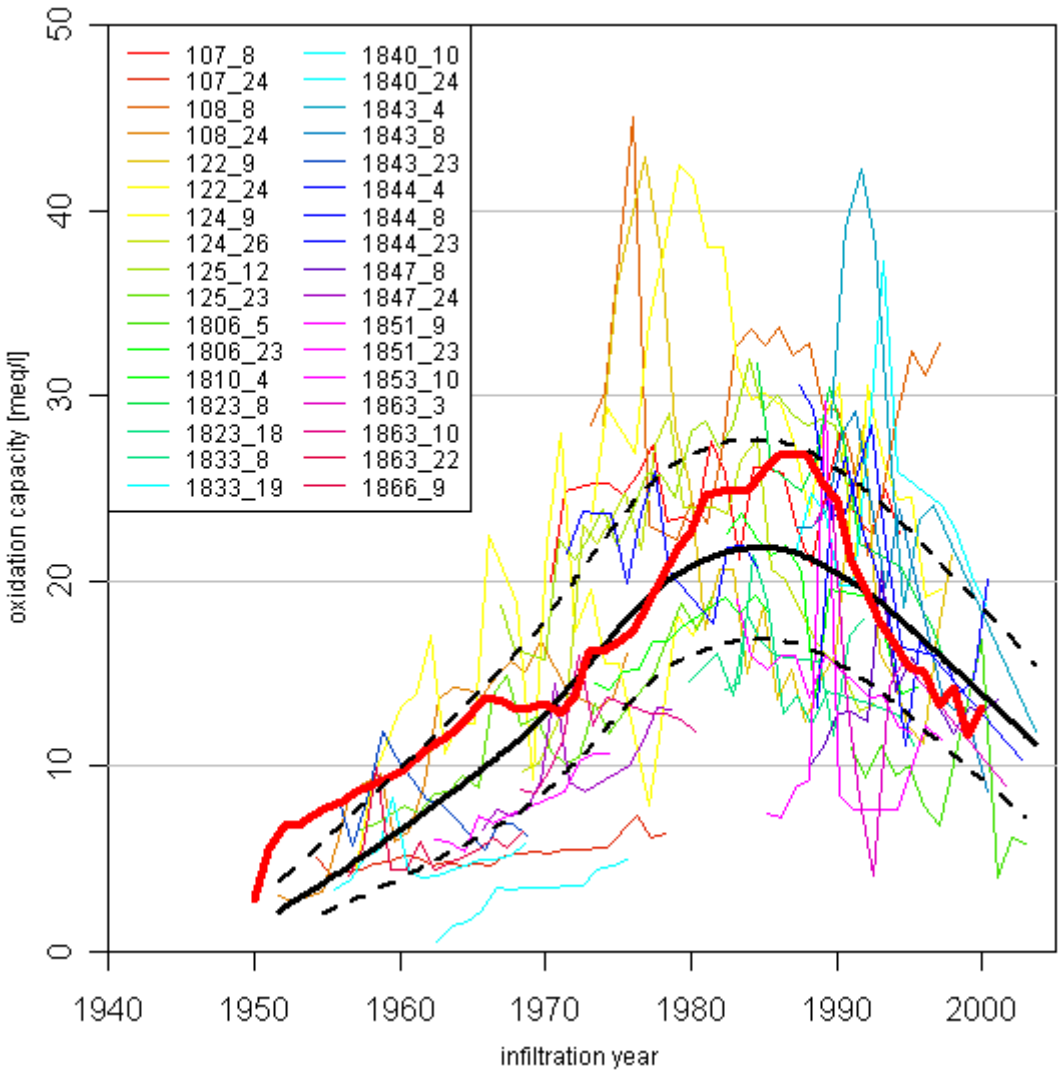

Figure 2.5: Time series of oxidation capacity back-scaled to the year of recharge of the samples. A LOWESS smooth (black line) is used to show the overall trend in these data. Dashed black lines indicate the 50% confidence interval around the LOWESS smooth. Red line indicates expected values based on historical inputs. Individual time series from selected piezometers have unique colors.

A few remarks can be made about this plot. First of all, there is a large noise in the individual time series. From individual time series it is hard to distinguish a trend in oxidation capacity. However, combining all the measured data into an aggregated trend using the LOWESS smooth, a clear trend reversal is demonstrated for OXC with a peak concentration around the year 1985. Both the LOWESS smooth itself, as the 25 and 75 percentile smooths increase towards a maximum observed oxidation capacity in groundwater that has recharged in 1985. Younger water shows a downward trend, resulting from the establishment of the Manure Law in 1985 and reduction of manure inputs from that time onward.

2.3.3 Results

From the study of the historical inputs, as described in Deliverable T2.2, we expect an upward trend in the concentrations in water recharging before 1985, and a downward trend in groundwater recharging after 1985 for solutes that travel with the same velocity as the groundwater itself. The following figures of back-scaled time series of conservative chemical indicators (OXC, Cl^- and SUMCAT) confirm these expectations. The reactive indicators (NO_3^-, Al and K^+) show a somewhat different behaviour, as a result of subsurface reaction and consequently non-conservative transport.

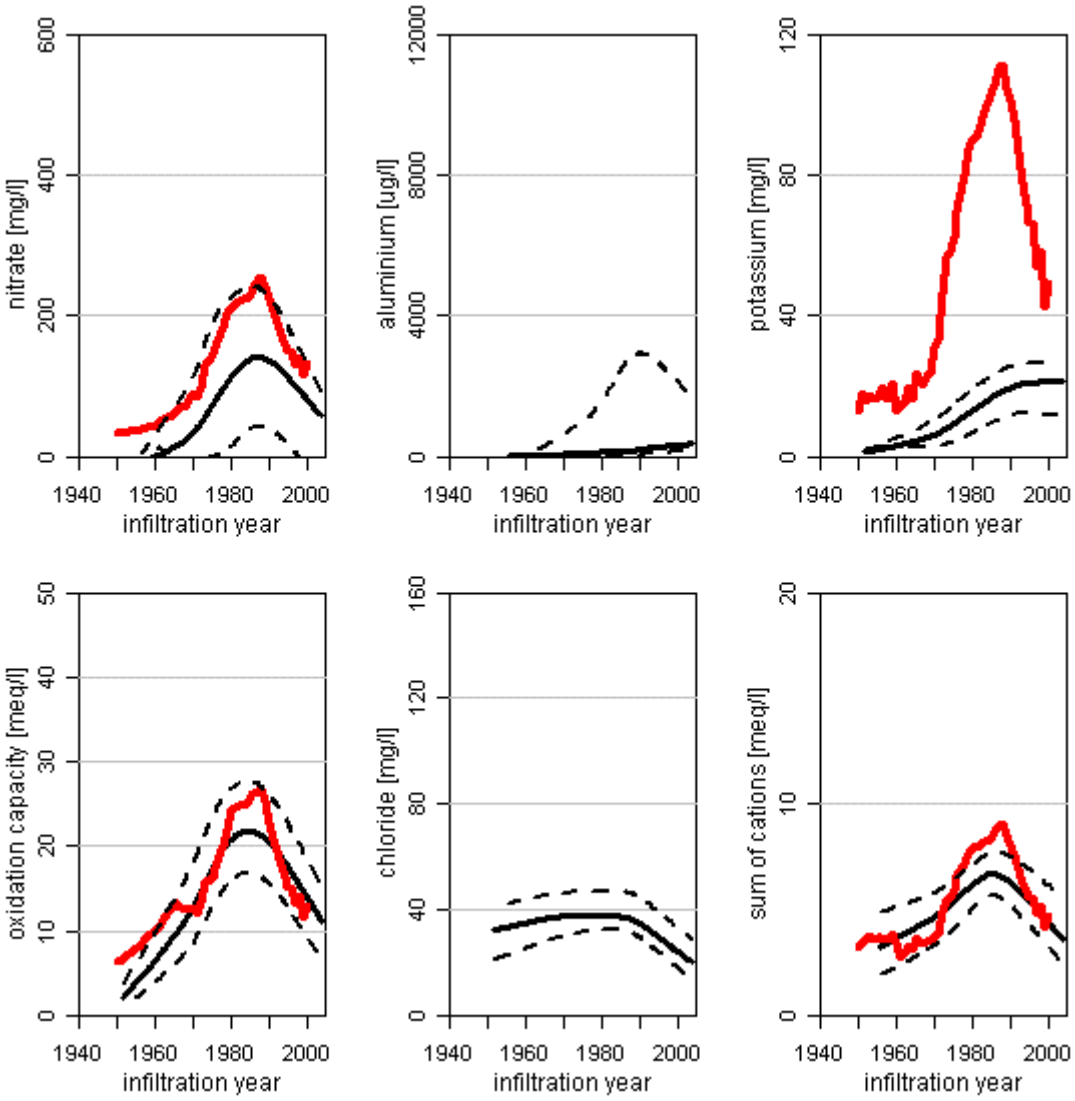

Figure 2.6: Comparison of measured trends (LOWESS smooths through back-scaled time series of six chemical indicators, in black) with historical inputs (red). Reactive indicators (top) show large discrepancies with historical inputs. Conservative indicators (bottom) are consistent with the expected trends.

2.3.4 Conservative indicators

The LOWESS smooth in Figure 2.6 indicates an increasing trend over the period 1950–1985 for all conservative indicators (bottom), a trend reversal and decreasing trends after 1985. There is a striking similarity between the estimated historical inputs and the trend derived from the monitoring data, even though the individual time series showed large fluctuations and probable measurement errors. This confirms the expectation that *OXC* and the *sum of cations* behave conservatively in the subsurface and confirms the increase of concentrations until the introduction of the Netherlands Manure Law in 1985 and the decrease afterwards.

2.3.4 Reactive chemical constituents

The discrepancy between the expected and actual concentrations of *nitrate (t*op left) are probably caused by denitrification by pyrite oxidation or organic matter in the saturated zone. Nitrate concentrations are lower than expected when nitrate would have been transported conservatively. The 25 percentile trend even indicates that 25% of the agricultural areas have concentrations below 50 mg/l for all infiltration years. However, the median aggregated nitrate trend clearly shows trend reversal with a peak

around 1985. Given the close resemblance between the OXC measured and expected trends, we propose that the main mechanism of nitrate removal is the oxidation of pyrite. Earlier studies indeed show the presence of abundant pyrite in the Noord-Brabant subsoil (for example Broers 2004).

Aluminum shows strong adsorption and retardation. The upper confidence limit of the LOWESS smooth does indicate the expected trends, but the median aggregated LOWESS smooth is still increasing in the low concentration range. This is attributed to the slow vertical movement of the acidification front.

Similarly, the *potassium* concentrations are increasing slowly in younger groundwater, unlike the input curve. Although the input curve is sharply decreasing since 1985, the aggregated median trend mooth is increasing slowly into the 1990s. The concentrations remains constant in younger waters, but no trend reversal can be observed. This is attributed to the retarding effect of cation exchange between potassium and calcium and magnesium; the ratio between the slopes of the input curve and the actual measured trend slope give some indication on the effective retardation factor, which is about three. This would mean that the maximum concentrations might only be reached after the year 2020.

2.3.5 Conclusions

A groundwater dating method such as $^{3}H/^{3}He$ provides a novel tool to detect trend reversal, aggregating monitoring data for larger areas. This removes the uncertainty in trend analysis that is caused by groundwater age variations. Large year to year variation in concentrations remain, but the back-scaling of time series yields a large number of data points for each year of infiltration. Trends are readily observed in back-scaled time series. The observed trend reversal in the aggregated monitoring data could well be related to the pattern of historical inputs. The upward trend in concentrations up to 1985 is clear in all conservative indicators. Even better visible is the trend reversal and subsequent downward trend since 1985, caused by the establishment of the Manure Law and the subsequent reduction of manure inputs.

Overall, the described novel approach for detection of trend reversal is well suited to meet the objectives of the draft Groundwater Directive, as illustrated in Figure 1.1.

The observed trend can well be related to the reconstructed historical inputs. This allows the trend propagation and extrapolation based on estimates of future land use, which will be presented in the following sections.

2.4 Trend extrapolation

2.4.1 Correlation of back-scaled time series with historical inputs

To propagate the trends observed in the time series into the future, we rely on the extrapolation of the input curves and expected future land use. To do so, we need to know whether these input curves are reliable in hindsight. Correlating the historical inputs to the observed trends will yield such information. So before extrapolating the observed trends using land use scenarios, a simple linear regression between the input curves and the LOWESS smooths was applied. This was performed for oxidation capacity and sum of cations (being conservative indicators) and nitrate. Because of the non-conservative transport of the reactive indicators, this simple trend propagation is not valid for other indicators and would require modelling of the transport of these chemicals incorporating the subsurface reactions, which is beyond the scope of this document. Examples of such an approach were given in Broers & van der Grift (2004).

The linear regression plots of the oxidation capacity and sum of cations are presented below. In each plot, the predicted concentrations are on the horizontal axis. On the vertical axis are the data points of the observed LOWESS smooth and data points of the LOWESS smooth indicating the 25 and 75 percentile.

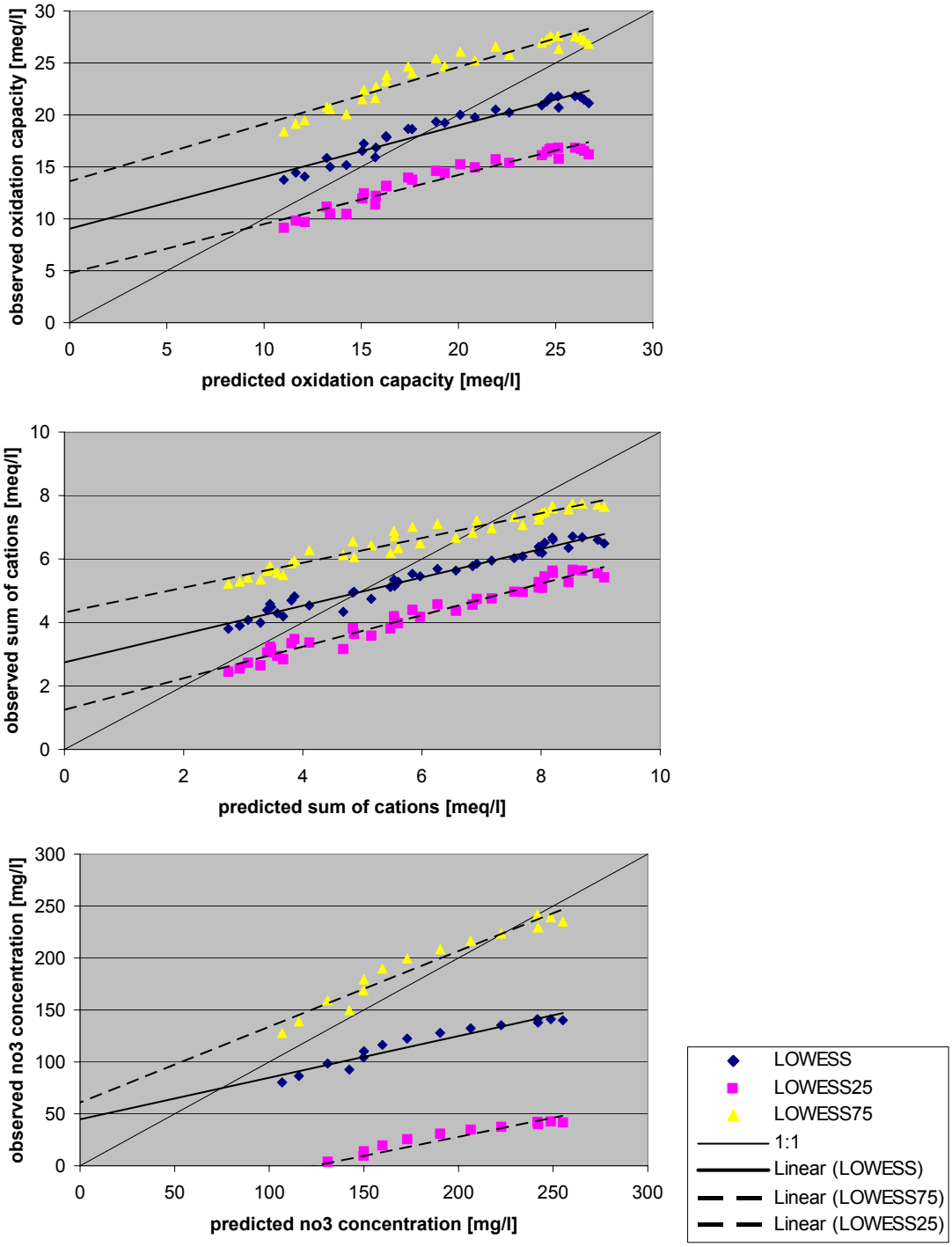

Figure 2.7: Linear regression between the predicted oxidation capacity (a), sum of cations (b) and nitrate concentration (c) from historical inputs and the LOWESS smooth through the observed data.

There is an excellent correlation between the historical inputs and the observed concentrations. The correlation coefficients for the LOWESS smooth are as high as 0.96, 0.98 and 0.94 for oxidation capacity, sum of cations and nitrate respectively. However, this relationship is not proportional. The prognosis seems to overestimate

high concentrations and underestimate lower concentrations. The result is a set of regression lines with a considerable intercept and a slope angle of less than 1. All parameters of the regression lines are presented in Table 2.1.

Table 2.1: Regression statistics of predicted and observed oxidation capacity, sum of cations and nitrate.

	oxidation capacity			sum of cations			nitrate		
	P25	LOWESS	P75	P25	LOWESS	P75	P25	LOWESS	P75
correlation coefficient	0.96	**0.96**	0.95	0.98	**0.98**	0.97	0.94	**0.94**	0.95
intercept	4.62	**8.88**	13.4	1.25	**2.75**	4.32	-47.9	**42.1**	55.9
Slope	0.48	**0.50**	0.56	0.50	**0.45**	0.39	0.23	**0.25**	0.45
R-squared	0.92	**0.92**	0.90	0.97	**0.96**	0.94	0.89	**0.89**	0.91
standard deviation of residuals	0.72	**0.75**	0.94	0.19	**0.18**	0.20	6.81	**7.35**	11.89

Although there does not seem to be a 1:1 relationship between input and observed concentrations, we will use these regression lines to circumvene this. The residual error of the regression line has a standard deviation of 0.75 and 0.18 for oxidation capacity and sum of cations respectively. Under the assumption that the underlying processes do not change, we would be able to predict the LOWESS smooth of the oxidation capacity with a confidence interval of 1.5 meq/l on either side.

Back-scaled time series give the opportunity to 'validate' the estimates of the historical inputs. Here we used a simple linear regression to relate the historical inputs to the actually observed values of oxidation capacity and sum of cations. This linear regression showed that there is a good correlation between the predictions based on historical input and the observed series. The relationship is not proportional, and large values are over predicted by the input function.

The historical curve for oxidation capacity seems not to fit the observed curve well before 1970. The estimates for the atmospheric deposition of this period are quite uncertain. To obtain a better correlation, we have used only data on groundwater that has recharged after 1970. Especially since this regression line will be used to predict ahead future concentrations, the error introduced by the uncertainty in atmospheric deposition is unwanted.

The historical curve for the sum of cations structurally overestimates the observed curve before 1960. This error seems to have propagated from the (over) estimated use of (calcium) fertilizer in this period. Again, to improve the regression line, we have only used data of the period 1960-present.

The upward part of the trend of nitrate is affected by pyrite oxidation and denitrification in deeper and older water. This does not affect the downward part of the trend as much and therefore only recent (post 1985) groundwater data was used in the regression.

2.4.2 Future inputs of agricultural pollution

A new system of regulating manure and fertilizer use will be in place in the Netherlands as of January 1st 2006. This scheme reduces the maximum allowable amount of nitrogen and phosphor that may be applied to agricultural land, with respect to the current legislation. The aim of the new system is to furhter comply with EU Nitrates Directive and specifically to reduce the concentration of nitrate in the upper five meter of groundwater to the required level of 50 mg/l.

In the period 2006 to 2008, maximum allowed manure use is reduced gradually towards levels which are to comply with the 50 mg/l standard. Failure to reach this limit will result in further reduction of the inputs.

Using the same accounting system of manure and fertilizer distribution as described in Deliverable T2.2, the effects of the measures on the deposition of other chemicals has been calculated. The following assumptions have been made to perform these calculations:

- land use ratios remain constant
- concentrations of chemicals in manure, fertilizer and crops remain constant
- crop yield remains constant
- atmospheric deposition remains constant

Furthermore, we assume that the Netherlands will comply to the EU threshold in 2010, and that the 2010 regulations remain in effect in the following years.

2.4.3 Trend extrapolation

Under these assumptions, the following input curves for nitrate, oxidation capacity and sum of cations are obtained. These were used to extrapolate the LOWESS smooth through the back-scaled time series graphs, as in Figure 2.8 .

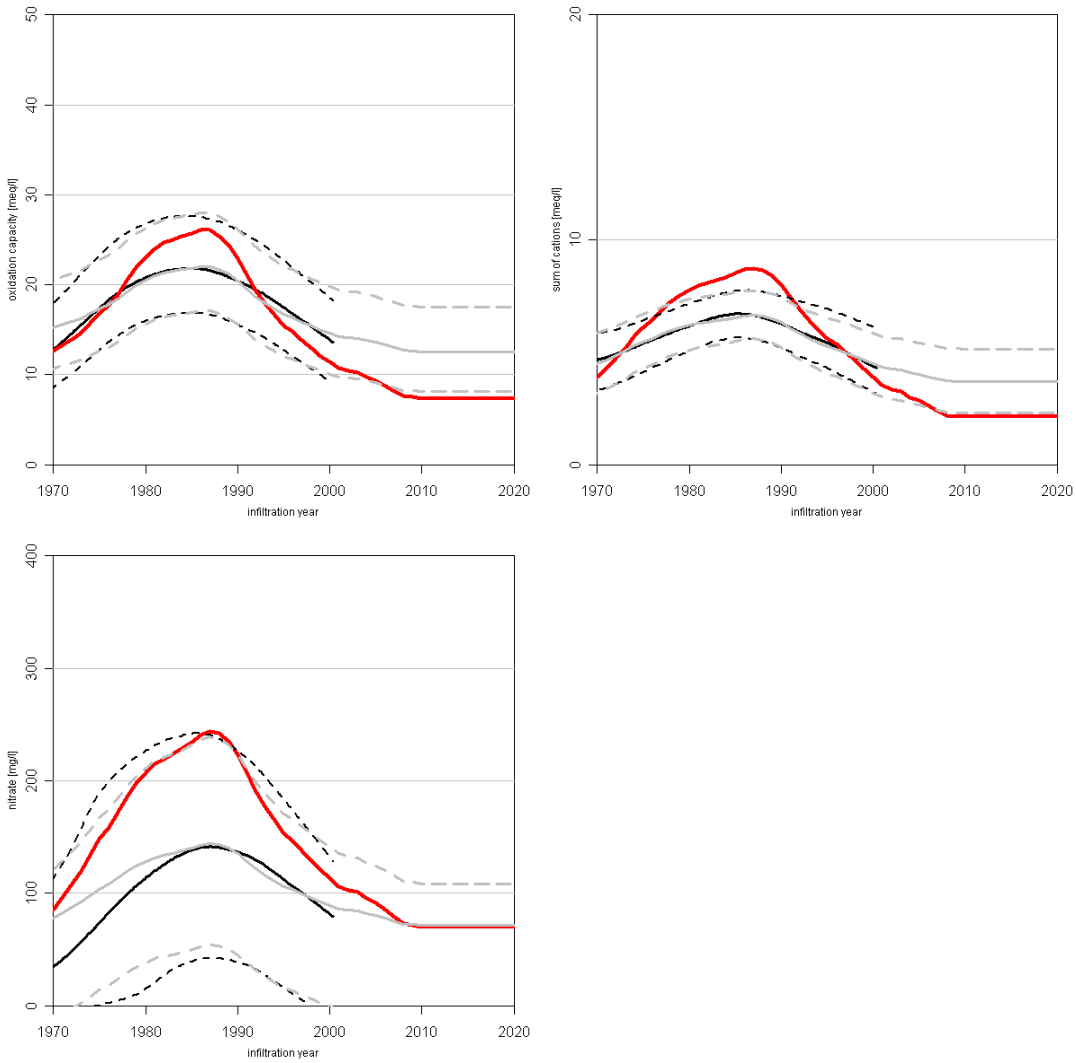

Figure 2.8: Extrapolated time trends of oxidation capacity, sum of cations and nitrate concentration. Extrapolation (gray) uses linear regression between observed LOWESS smooth curves (black) and predicted concentrations (red).

The extrapolated time trend of oxidation capacity shows only a gradual decrease over the period 2000-2020. This extrapolated trend seems to be weaker than the one observed in the LOWESS smooth, but keep in mind that the most recent years of the LOWESS smooth are based on very few measurements.
The extrapolated time trend of sum of cations seems more consistent with the observed trend of the LOWESS smooth. It shows a gradual decrease towards about 5.5 meq/l.

The extrapolated median time trend of nitrate very slowly decreases towards about 80 mg/l in 2020. As with oxidation capacity, the predicted decrease seems to be weaker than the trend in the LOWESS smooth. Note that the concentrations still seems to stay above 100 mg/l in 25% the cases, based on the extrapolated P75 trend). These results derived from measured data indicate that the proposed manure reduction might not be enough to actually reach the standard of 50 mg/l in groundwater.

Using the groundwater ages in the sampled wells, it is possible to predict the median concentrations of chemical indicators in groundwater that will be sampled during the next 10 or 20 years. So for each well, a median (and P25 and P75) prediction can be made for some time in the future. The median of these individual predictions will serve as the predicted concentration for the agriculture-recharge area. Individual time series may vary strongly from this median. This procedure has been applied to the shallow and deep screens separately, to gain insight in the changes in concentrations at different depth intervals.

Table 2.2: Predicted median and maximum of regional averaged OXC, SUMCAT and NO_3 concentrations at the shallow and deep screen level.

		OXC		SUMCAT		NO_3	
	year	Median (LOWESS)	Max (P75)	Median (LOWESS)	Max (P75)	Median (LOWESS)	Max (P75)
shallow	2005	**15.0**	27.2	**4.7**	7.5	**91.7**	220.5
	2010	**13.8**	28.0	**4.1**	7.7	**81.3**	239.0
	2015	**12.7**	24.2	**3.7**	7.0	**71.6**	198.6
	2030	**12.6**	18.0	**3.7**	5.3	**70.8**	115.1
	year						
deep	2005	**18.4**	28.0	**5.8**	7.7	**113.6**	239.0
	2010	**20.3**	27.8	**6.2**	7.7	**128.9**	237.3
	2015	**20.4**	28.0	**6.2**	7.7	**127.3**	239.0
	2030	**13.6**	22.0	**4.0**	6.5	**79.8**	170.4

It shows that improvements in groundwater quality at a certain depth will be very slow, largely because of the variation in groundwater ages. Median groundwater quality in shallow screens will slowly improve. Improvement of the maximum of the P75 prognosis will only occur in 25 years, because groundwater in all screens has than been recharged with low inputs groundwater. Before that time, some screens will still sample groundwater from around the nitrate peak. Groundwater quality in deep screens is expected to deteriorate in the near future – until the arrival of the 1985 manure peak – before improving.

2.4.4 Discussion

Groundwater age dating has proven to be very helpful when researching trends in groundwater quality. Part of the variation in measured concentrations can be explained by variation in groundwater ages, and when this part is reduced, the trends resulting from changes in land use become more apparent. The trend reversal and subsequent downward trend have been observed in conservative chemical indicators (oxidation

capacity and sum of cations) and the downward trend can now also be observed in the concentrations of nitrate in young groundwater.
With this concentration-recharge year relationship, the concentration time series can be extrapolated using a prediction of future land use. The correlation between the predicted concentrations and the measured concentrations was such that a reliable prediction for the future can be made. The largest source of uncertainty is in the estimates of manure and fertilizer use. These were based on the policy measures laid out for the period until 2010. Policy changes after evaluation of these measures may yield a stronger or a weaker downward trend in shallow groundwater quality.

Using the groundwater ages and the extrapolated time trends to predict future groundwater quality shows that regional improvements of groundwater quality will be very slow because of the variation in groundwater ages. Monitoring screens from which relatively old water is sampled will produce polluted water for a longer period of time than screens with young water. These “older screens” cause the long waiting time before groundwater quality has improved over the whole region at a certain depth level.

3. Point by Point Statistical Trend Analysis and Extrapoled Time Trends at Test Sites in the Meuse BE (ULg)

J. Batlle Aguilar[1], Ph. Orban[1], S. Brouyère[1,2]
[1]Group of Hydrogeology and Environmental Geology, HGULg
[2]Aquapôle Ulg

University of Liège, Building B52/3,
4000 Sart Tilman, Belgium
Tel: +32.43.662377
Fax: +32.43.669520,
Serge.Brouyere@ulg.ac.be

3.1 Introduction

The Hydrogeology Group of University of Liège (HGULg) has selected 4 main groundwater bodies in the Walloon Meuse basin to study groundwater nitrate concentration trends: The Hesbaye groundwater body (Geer basin), the Pays of Herve groundwater body, the Néblon basin and the alluvial plain of the Meuse river (Figure 3.1).

The present deliverable describes in detail the dataset of nitrate measurements (number of points, main features…) collected in these basins and the statistical trend analysis that has been performed on these data.

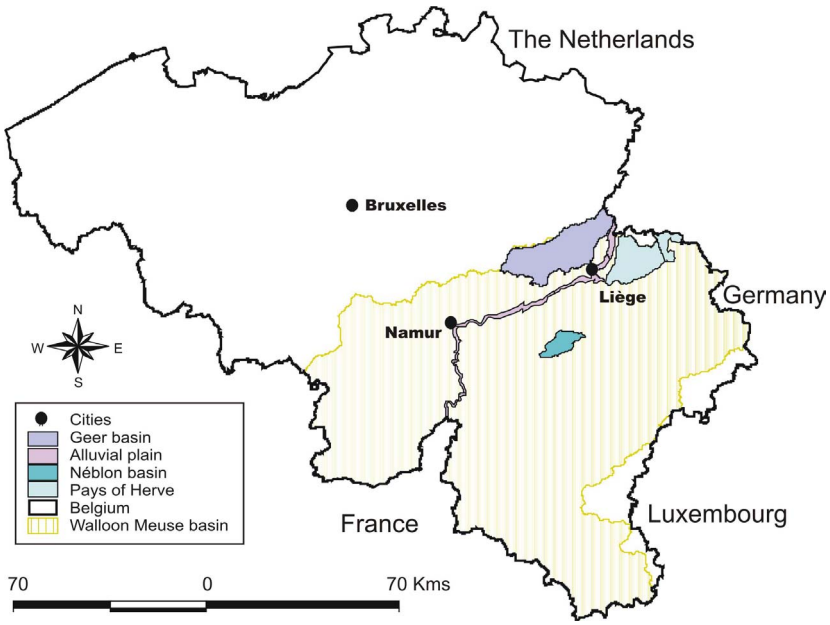

Figure 3.1. Location of groundwater bodies selected.

3.2 Description of the dataset of nitrate measurements

3.2.1 Update of the nitrate dataset

Nitrate concentrations used in this study are mainly from the Nitrate Survey Network established by the Walloon Region Government. In this network, boreholes, springs, galleries and traditional wells, where sampling and water analyses are carried out regularly are considered as monitoring points. This network provides a spatial and

temporary representation of nitrate contents in the aquifers. Nevertheless, gaps exist in the datasets and in the spatial distribution of monitoring points.
Annual data obtained from these analyses are stored in a database owned by the Walloon Region authorities. Up to now, the latest data available comes from the end of 2003. The 2004 dataset is still under compilation in the Walloon Region and it was not yet available at the time of preparing this deliverable
During the last months, contacts have also been established with the VMW (Vlaamse Maatschappij voor Watervoorziening), the Flemish water supply company, in order to have access to data and to water supply wells in the North of the Hesbaye groundwater body (included in the Geer basin). In Flanders, the Hesbaye chalk aquifer is confined, in contrast to the unconfined part of the aquifer within Walloon Region territory.
Some points has been deleted from table presented in Deliverable T2.1, because the number of records were clearly not enough to carry out a trend analysis, and new points from the VMW has been added for the Geer basin (denoted with the HF code in Table 1).
Table 3.1, 3.2, 3.3 and 3.4 in Appendix 3.1 present an updated summary of data availability for nitrate trend analysis in groundwater bodies selected in the Walloon Meuse basin.

3.2.2 Dataset features

Time-series graphs are presented for some sampling points to have a first idea of the main features of the datasets (seasonality, outliers…) and the presence of trends. Some interesting general features are pointed out here after.

Spatial variations in nitrate contents in the Hesbaye aquifer

Because of the geological context of the Hesbaye plateau, hydrogeological conditions prevailing in the chalk aquifer change from unconfined in the Southern part of the basin to confined conditions in the Northern part. As a direct consequence, nitrates are almost absent in groundwater of the North of the basin, while concentrations are close to the drinking limit in the South. Figure 3.2 and 3.3 shows characteristic time-series from the South and North part respectively. The absence of nitrate in the North may have two explanations: the occurrence of denitrification processes in the confined part of the aquifer or the occurrence of very old, still uncontaminated groundwater. This will be discussed later on.

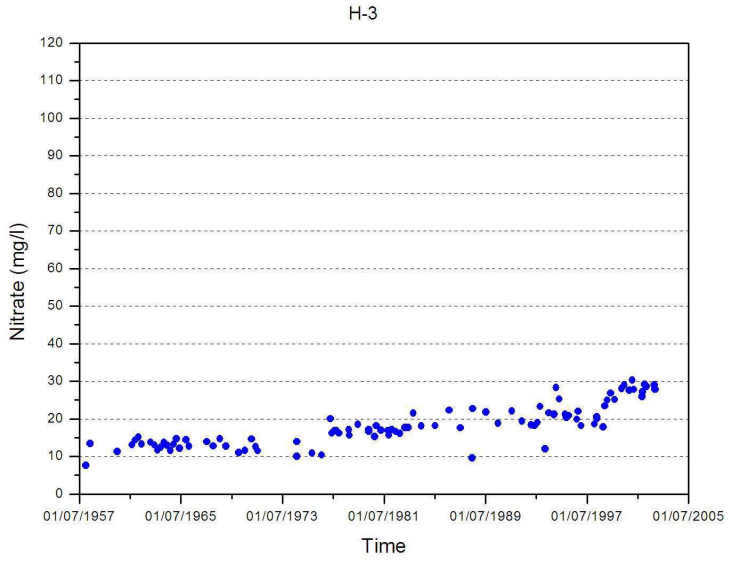

Figure 3.2. Characteristic time-series from a point located in the Southern part of the Hesbaye aquifer.

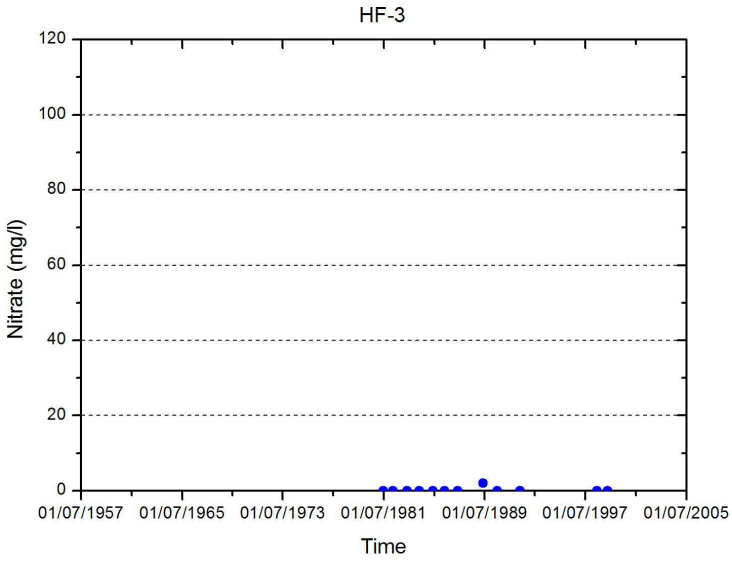

Figure 3.3. Characteristic time-series of a point located in the Northern part of the Hesbaye aquifer.

Periodic ("seasonal") variations in nitrate contents

Many datasets coming from the Hesbaye and the Pays de Herve groundwater bodies exhibit clear periodic variations in nitrate concentrations (Figure 3.4 and 3.5). As discussed by Brouyère *et al.,* (2004), such periodic variations are explained by groundwater table fluctuations in the variably saturated dual-porosity chalk. In principle, nitrate spread over the land surface progressively infiltrate across the unsaturated zone and migrate slowly downward through the unsaturated chalk matrix. Under low groundwater level conditions, the nitrate contamination front is disconnected from the aquifer and nitrate concentrations in the aquifer tend to diminish because of dispersion and mixing processes. When groundwater levels rise, the contamination front is quickly reached and leached: the contamination source is re-activated and nitrate concentrations are likely to increase rapidly in the saturated zone. This effect is observed in the Geer basin and in the Pays of Herve but not in the Néblon basin (mostly limestone aquifers) and in the alluvial plain aquifer (gravel aquifer).

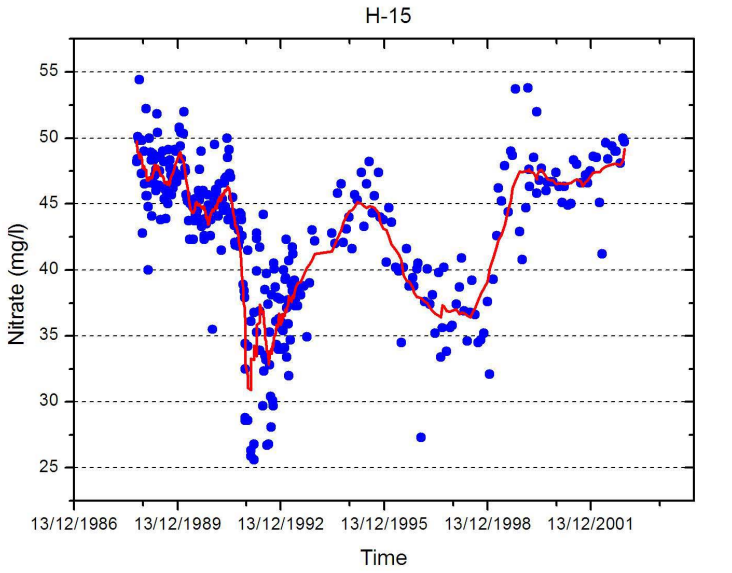

Figure 3.4. Multi-annual variations in nitrate concentration at sampling point H-15 in the Geer basin.

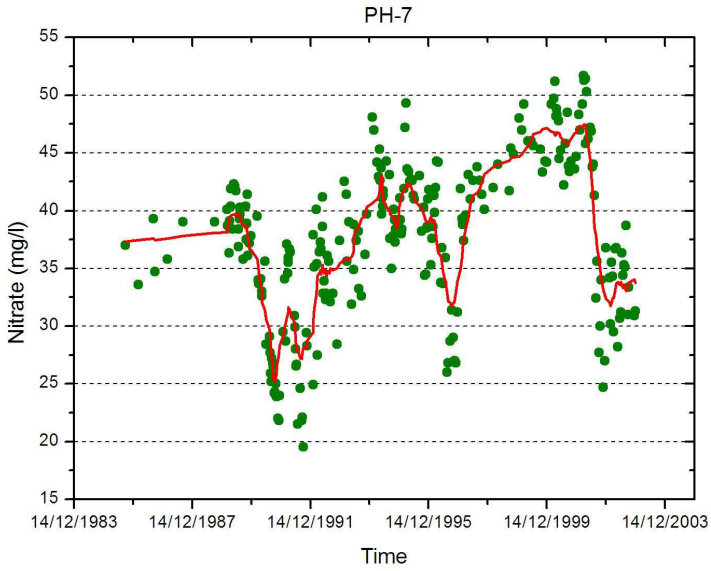

Figure 3.5. Multi-annual variations in nitrate concentration at sampling point PH-7 in the Pays of Herve groundwater body.

In the Geer basin, a very dense network is available for monitoring variations in groundwater levels. As an illustration, Figure 3.6 shows groundwater table variations for the longest datasets available in the basin (from 1951 to 2003). Unfortunately, this network does not necessarily correspond to nitrate sampling locations.

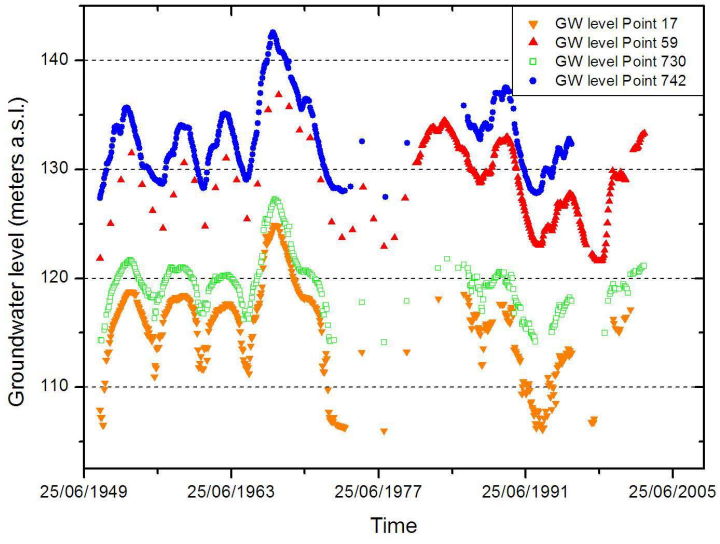

Figure 3.6. Groundwater level measurements from 1951 to 2003.

Figure 3.7 and 3.8 show groundwater level and nitrate concentration time plots at neighbouring observation points. These examples confirm the major impact of periodic variations in groundwater levels on the dynamics of nitrate in the chalk aquifer. In the subsequent statistical analysis, the seasonal effect of such periodic variations has not

been accounted for explicitly because of the difficulty in defining the periodicity of such effects that are related to pluri-annual variations in precipitations.
Neglecting the seasonality is not a problem in trend detection provided that the datasets integrate several periods so that the periodic variations compensate and the global trend emerges. Doing so on a reduced period of time could of course lead to wrong conclusions. In a shorter observation window, the general trend is less likely to be observed.
As an example, performing a trend calculation on a sub-dataset corresponding to decreasing groundwater levels could probably lead to the conclusion of a decrease of nitrate concentrations in the aquifer with time. Reliability of results depends on the length of the time series: longer series will yield more reliable results. This is the case for datasets H-9 and H-11 (see Annex). Dataset H-9 provide nitrate data on a long period of time, while dataset H-11 is relatively short. For H-9, the result is “evidence of an upward trend”, while for H-11, there is “no evidence of a trend”. Such a difference in the result can be explained by the length of H-11, which does not allow one detect anything in the trend analysis.
For the datasets in the Geer and Pays of Herve groundwater bodies, the analysis has been carried out having this potential problem in mind. However, most of the time, datasets that were too short were naturally “eliminated” at the trend detection level, the regression test or the Mann Kendall test, which is robust enough to conlude that no trend is present.

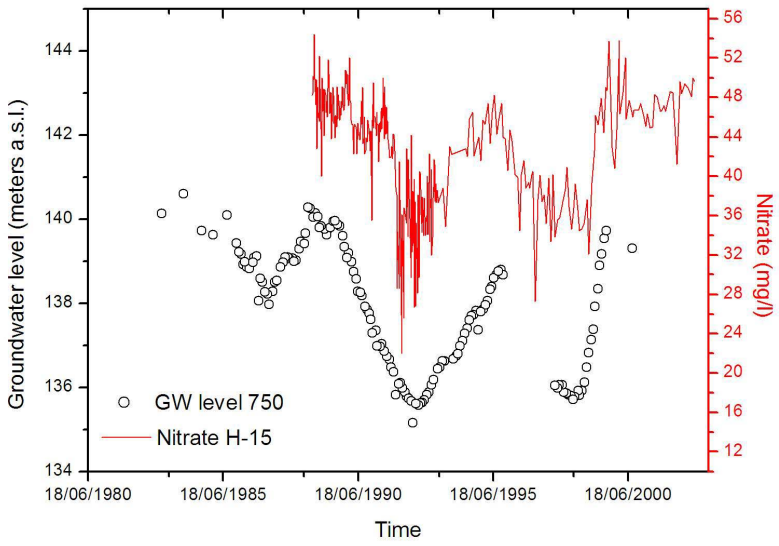

Figure 3.7. Time series of nitrate concentration (point H-15) and groundwater level measurements (point 750).

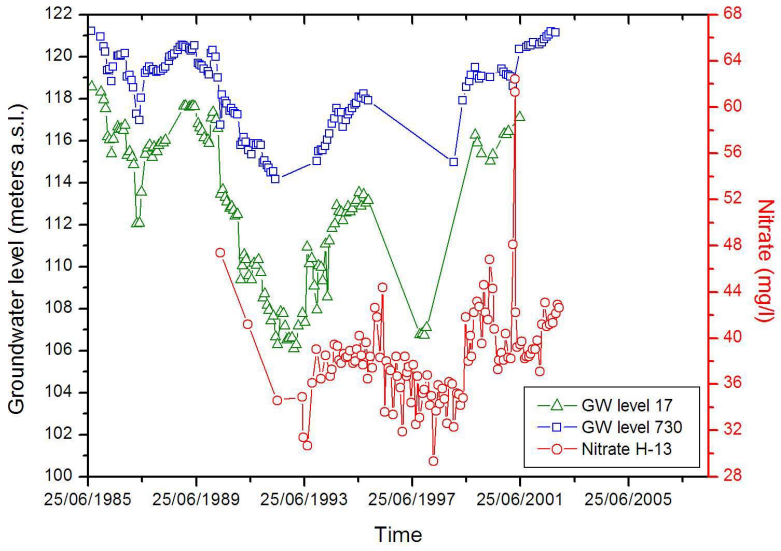

Figure 3.8. Time series of nitrate concentration (point H-13) and groundwater level measurements (points 17 and 730).

Presentation of the nitrate datasets

A total of 97 time-series is presented for the four selected groundwater bodies in Appendix 3. The same time and concentration scales are used for each dataset of a given groundwater body to allow visual comparison of data from one point to another. Figure 3.9 shows an example of a nitrate time plot for each of the four selected groundwater bodies considered in the Walloon part of the Meuse basin.

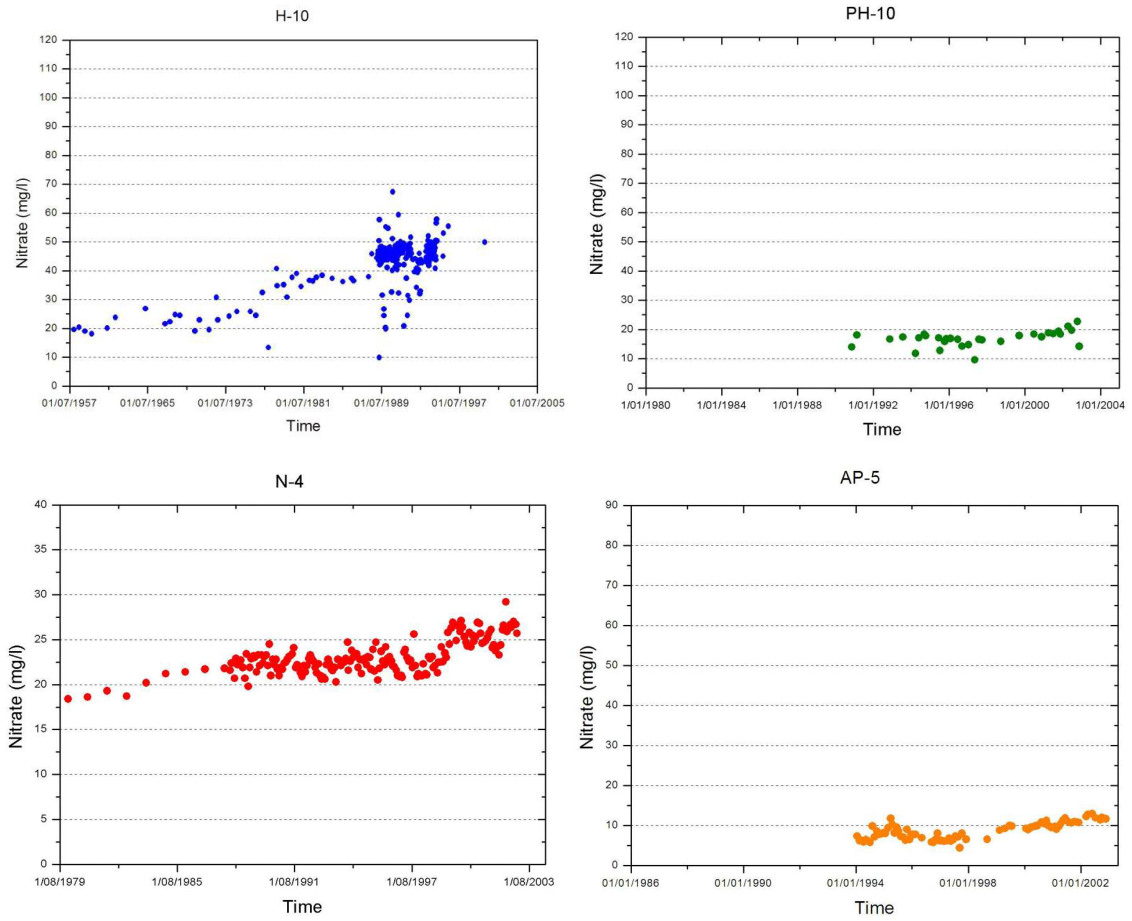

Figure 3.9. Nitrate concentration time-series for the Geer basin (top left), Pays of Herve (top right), Néblon basin (bottom left) and the alluvial plain aquifer (bottom right).

3.3 Statistical trend analysis

3.3.1 Methodology

For the trend analyses of groundwater quality data in the Walloon region, the following procedure has been used (Figure 3.10):

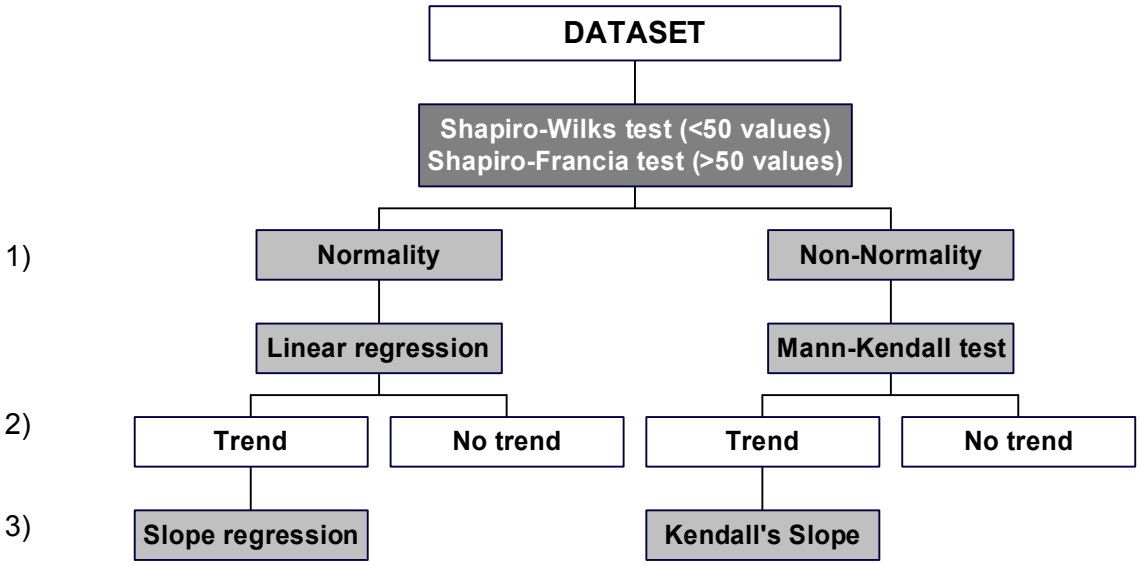

Figure 3.10. A three step procedure is adopted for trend analysis of nitrate concentrations in the selected groundwater bodies: 1) normality test; 2) trend detection; 3) trend estimation.

(1) Normality of the dataset

The first step is to evaluate whether the dataset is normally distributed or not. If the number of records is less than 50, the Shapiro-Wilks test is used. If the number of records is equal or larger than 50, the Shapiro-Francia test is used. D'Agostino's test has been also used to corroborate the results obtained using the two other techniques. For most datasets, the D'Agostino's test corroborates the result obtained with one of the two other tests. For the datasets for which the results of the normality test are contradictory, it has been decided to apply both trend detection techniques.

The choice of trend detection method is a function of the results obtained in this step: parametric tests are performed on normally distributed datasets and non-parametric tests are performed on non-normally distributed datasets.

(2) Trend detection

The second step consists in performing a test aiming at detecting whether a trend exists or not in the dataset. For normally distributed datasets, linear regression is applied. The correlation coefficient r is used as an indicator of the existence of the trend. In accordance with (Carr 1995), three ranges of correlation degree (trend robustness) have been considered for the correlation between time and nitrate concentrations:

- strong correlation for r values ranging between 0..8 and 1 (or -0.8 and -1);
- moderate correlation for r values ranging between 0..5 and 0..8 (or -0.5 and -0.8);
- weak correlation for r values ranging between 0.1 and 0.5 (or -0.1 and -0.5);
- no correlation for r values ranging between -0.1 and 0.1.

For trend detection on non-normally distributed datasets, the non-parametric Mann-Kendall test has been selected. It has to be mentioned that this test is very appropriate for groundwater quality data, when the amount of records is often limited and the data distribution usually not known. It has been applied previously with reliable results in numerous studies, including hydrological applications (Hirsch *et al.,* 1982; Lettenmaier *et al.,* 1991; Loftis *et al.,* 1991; Zetterqvist 1991; Smith and McCann 2000; Hanson 2002; Libiseller and Grimvall 2002; Schnabel 2002; Yue *et al.,* 2002; Robinson *et al.,* 2003; Zhang and Zwiers 2004). The Mann-Kendall test determines the existence of a trend by the calculation of an index reflecting the frequency with which concentrations observed in later samples are greater or less than those observed in earlier samples. It is based on the calculation of differences between pairs of successive data. For deciding if a trend exists in the Mann-Kendall test, a significance level of 99% has been considered, corresponding to a threshold value of 2.32634 for the Mann-Kendall index.

(3) Trend estimation

The third step in the trend analysis is the trend estimation or quantification. For normally distributed datasets, the trend magnitude is defined by the slope of the linear regression equation. For non-normally distributed datasets, the trend magnitude is based on the calculation of the Sen's slope, by calculating the median of all data pairs in dataset (Hirsch *et al.,* 1991). Is less affected by data errors, outliers or missing data than the linear regression (Hanson 2002).

3.3.2 Results from trend analysis on individual time series

Table 3.1 summarizes the results of trend analysis grouped by groundwater bodies. Estimations of slopes values are given in mg per year. Detailed results are presented in Tables 3.2 to 3.5.

Groundwater body	Number of nitrate points	Number of downward trends	Number of upward trends	Percent of significant trends
Geer basin	26	0	15	57.7%
Pays of Herve	12	2	6	66.6%
Néblon basin	6	1	4	83.3%
Alluvial plain	38	15	11	68.4%

Table 3.1. Summary of trend tests results for each groundwater body

Table 3.5 shows the number of significant trends (both upward and downward) at the nitrate points where statistical test was carried out. One can observe, except for the Néblon sub-basin, that in about 60% of the time series a significant trends is present. For the Néblon sub-basin just 6 points were taken into account, which could explain the high percentage of significant trends.

Code	Normality test			Trend detection				Trend estimation (mg/y)		Trend analyse result
	Sh.-Wilks test	Sh.-Francia test	D'Agostino's test	Linear Regression		Mann-Kendall		Linear Slope	Sen's slope	
				r	Correlation	Comparison level	Trend			
H-1		Non-norm.	Non-norm.	---		8.63554	Upward	---	0.4756	▲
H-2		Non-norm.	Normality	0.3791	Weak	3.92641	Upward	0.2555	0.2450	▲
H-3		Non-norm.	Normality	0.8405	Strong	9.94543	Upward	0.3285	0.3647	▲
H-4		Non-norm.	Non-norm.	---		0.43333	No trend	---	---	●
H-5		Non-norm.	Non-norm.	---		2.78247	No trend	---		●
H-6	Non-norm.		Non-norm.	---		1.31197	No trend	---	---	●
H-7		Normality	Normality	0.8881	Strong	8.93565	Upward	0.584	0.5883	▲
H-8		Non-norm.	Non-norm.	---		5.54954	Upward	---	0.5408	▲
H-9		Non-norm.	Non-norm.	---		4.96828	Upward	---	0.0928	▲
H-10		Non-norm.	Non-norm.	---		7.69519	Upward	---	0.3868	▲
H-11	Non-norm.		Non-norm.	---		-2.14892	No trend	---	---	●
H-12		Non-norm.	Non-norm.	---		5.50093	Upward	---	0.3249	▲
H-13		Non-norm.	Non-norm.	---		3.82585	Upward	---	0.3075	▲
H-14		Non-norm.	Normality	0.5292	Moderate	4.42336	Upward	0.4745	0.4525	▲
H-15		Non-norm.	Non-norm.	---		-0.49318	No trend	---	---	●
H-16	Normality		Normality	0	Null	0	No trend	0	---	●
H-17	Non-norm.		Non-norm.	---		2.22759	No trend	---	---	●
H-18		Non-norm.	Non-norm.	---		7.15834	Upward	---	0.4803	▲
H-19		Non-norm.	Normality	0.1442	Weak	2.07958	No trend	0.146	---	●

Code	Normality test			Trend detection				Trend estimation (mg/y)		Trend analyse result
	Sh.-Wilks test	Sh.-Francia test	D'Agostino's test	Linear Regression		Mann-Kendall		Linear Slope	Sen's slope	
				r	Correlation	Comparison level	Trend			
H-20		Normality	Normality	0.3632	Weak	3.68364	Upward	7.7745	1.6489	▲
HF-1	No nitrate									
HF-2	No nitrate									
HF-3	No nitrate									
HF-4	No nitrate									
HF-5	No nitrate									
HF-6	No nitrate									
HF-7	No nitrate									
HF-8	No nitrate									
HF-9	No nitrate									
HF-10	No nitrate									
HF-11	No nitrate									
HF-12	No nitrate									
HF-13	No nitrate									
HF-14	No nitrate									
HF-15	No nitrate									
HF-16	No nitrate									
HF-17		Non-norm.	Normality	0.6875	Moderate	11.436	Upward	0.7665	0.8058	▲
HF-18	Normality		Normality	0.0954	0	0	No trend	-0.073	---	●
HF-19	Normality		Non-norm.	0.4277	Weak	---		-0.9125		●
HF-20		Non-norm.	Normality	0.6905	Moderate	11.6486	Upward	0.803	0.8004	▲
HF-21		Non-norm.	Non-norm.	---		1.58516	No trend	---	---	●

Code	Normality test			Trend detection				Trend estimation (mg/y)		Trend analyse result
	Sh.-Wilks test	Sh.-Francia test	D'Agostino's test	Linear Regression		Mann-Kendall		Linear Slope	Sen's slope	
				r	Correlation	Comparison level	Trend			
HF-22		Non-norm.	Non-norm.	---		10.3717	Upward	---	0.3266	▲

Table 3.2. Point-by-point trend results for the Geer basin (▲ evidence of upward trend; ▼ evidence of downward trend; ● no evidence of trend).

Code	Normality test			Trend detection				Trend estimation (mg/y)		Trend analyse results
	Sh.-Wilks test	Sh.-Francia test	D'Agostino's test	Linear Regression		Mann-Kendall		Linear Slope	Sen's slope	
				r	Correlation	Comparison level	Trend			
PH-1	Normality		Normality	0.6022	Moderate	---	---	-4.3800	---	▼
PH-2	Non-norm.		Normality	0.7281	Moderate	3.1244	Upward	1.6060	1.7528	▲
PH-3	Normality		Normality	0.2629	Weak	-0.9826	No trend	-0.2555	---	●
PH-4	Normality		Normality	0.4243	Weak	2.6965	Upward	0.4380	0.5320	▲
PH-5	Normality		Non-norm.	0.8433	Strong	---	---	0.4745	---	▲
PH-6	Normality		Non-norm.	0.0721	0	---	---	0.0365	---	●
PH-7		Normality	Normality	0.3391	Weak	5.7037	Upward	0.5475	0.7335	▲
PH-8		Non-norm.	Non-norm.	---		0.0702	No trend	---	---	●
PH-9	Normality		Normality	0.8848	Strong	---	---	5.4750	---	▲
PH-10	Normality		Normality	0.4401	Weak	2.3416	Upward	0.3285	0.3166	▲
PH-11	Non-norm.		Non-norm.	---		-2.7072	Downward	---	-0.3760	▼

Table 3.3. Point-by-point trend results for the Pays of Herve groundwater body (▲ evidence of upward trend; ▼ evidence of downward trend; ● no evidence of trend).

Code	Normality test			Trend detection				Trend estimation (mg/y)		Trend analyse result
	Sh.-Wilks test	Sh.-Francia test	D'Agostino's test	Linear Regression		Mann-Kendall		Linear Slope	Sen's slope	
				r	Correlation	Comparison level	Trend			
N-1	Normality		Normality	0.6210	Moderate	-3.31628	Downward	-0.8395	-0.8773	▼
N-2		Normality	Normality	0.8281	Strong	11.2545	Upward	0.5840	0.6881	▲
N-3		Non-norm.	Non-norm.	---		10.7388	Upward	---	0.1929	▲
N-4		Non-norm.	Non-norm.	---		8.77369	Upward	---	0.1677	▲
N-5		Non-norm.	Non-norm.	---		11.1355	Upward	---	0.2536	▲
N-6	Normality		Normality	0.1153	Weak	-0.334242	No trend	0.0730	---	●

Table 3.4. Point-by-point trend results for the Néblon basin (▲ evidence of upward trend; ▼ evidence of downward trend; ● no evidence of trend).

Code	Normality test			Trend detection				Trend estimation (mg/y)		Trend analyse result
	Sh.-Wilks test	Sh.-Francia test	D'Agostino's test	Linear Regression		Mann-Kendall		Linear Slope	Sen's slope	
				r	Correlation	Comparison level	Trend			
AP-1		Non-norm.	Non-norm.	---		0.8895	No trend	---	---	●
AP-2		Normality	Normality	0.2569	Weak	-1.3817	No trend	-0.4380	---	▼
AP-3		Non-norm.	Non-norm.	---		0.1322	No trend	---	---	●
AP-4		Normality	Normality	0.3886	Weak	2.4662	Upward	0.1825	0.1497	▲
AP-5		Non-norm.	Normality	0.7408	Moderate	6.5608	Upward	0.5475	0.5714	▲
AP-6		Normality	Normality	0	0	-0.5452	No trend	0	--	●
AP-7		Normality	Normality	0.2383	Weak	-2.2253	No trend	-0.2555	---	▼
AP-8	Normality		Normality	0.6068	Moderate	-5.9796	Downward	-2.1170	-2.5489	▼
AP-9	Non-norm.		Non-norm.	---		-0.6719	No trend	---	---	●
AP-10	Normality		Normality	0.4695	Weak	2.7363	Upward	0.5840	0.6461	▲
AP-11	Normality		Normality	0.1217	Weak	1.0722	No trend	0.2920	---	●
AP-12	Normality		Normality	0.4518	Weak	-2.2111	No trend	-6.1320	---	▼
AP-13	Non-norm.		Non-norm.	---		1.5310	No trend	---	---	●
AP-14	Non-norm.		Non-norm.	---		-0.3409	No trend	---	---	●
AP-15	Normality		Normality	0.1407	Weak	---	---	0.2555	---	●
AP-16	Non-norm.		Normality	0.6127	Moderate	-4.6418	Downward	-2.2630	-5.2647	▼
AP-17	Normality		Normality	0.5128	Moderate	-1.7127	No trend	-2.2995	---	▼
AP-18	Normality		Normality	0.6709	Moderate	3.2337	Upward	0.8760	0.7964	▲

Code	Normality test			Trend detection				Trend estimation (mg/y)		Trend analyse result
	Sh.-Wilks test	Sh.-Francia test	D'Agostino's test	Linear Regression		Mann-Kendall		Linear Slope	Sen's slope	
				r	Correlation	Comparison level	Trend			
AP-19	Normality		Normality	0.4309	Weak	2.4539	Upward	0.5475	0.5548	▲
AP-20		Normality	Normality	0.2573	Weak	0.8073	No trend	0.5840	---	▼
AP-21	Non-norm.		Non-norm.	---		-2.8890	Downward	---	-0.2276	▼
AP-22	Normality		Normality	0.3297	Weak	1.6274	No trend	0.8395	---	▲
AP-23	Non-norm.		Normality	0	0	-1.0072	No trend	0	---	●
AP-24		Normality	Normality	0.2032	Weak	1.5057	No trend	0.4015	---	▲
AP-25		Normality	Normality	0.5545	Moderate	5.2465	Upward	1.0220	1.3371	▲
AP-26		Non-norm.	Non-norm	---		-0.1017	No trend	---	---	●
AP-27		Non-norm.	Non-norm.	---		4.8967	Upward	---	0.3896	▲
AP-28		Normality	Normality	0.4310	Weak	2.8865	Upward	0.6570	0.5713	▲
AP-29		Normality	Normality	0.2263	Weak	1.0288	No trend	0.4745	---	▲
AP-30		Normality	Normality	0.1497	Weak	-3.5609	Downward	-0.2555	-0.7343	▼
AP-31		Normality	Normality	0.1562	Weak	-3.3449	Downward	-0.2920	-0.5367	▼
AP-32	Non-norm.		Non-norm.	---		-4.4726	Downward	---	-6.2159	▼
AP-33	Normality		Normality	0.5867	Moderate	---	---	-2.0440	---	▼
AP-34	Normality		Normality	0.4939	Moderate	-1.2368	No trend	-1.7520	---	▼
AP-35	Non-norm.		Non-norm	---		0.4333	No trend	---	---	●

Code	Normality test			Trend detection				Trend estimation (mg/y)		Trend analyse result
	Sh.-Wilks test	Sh.-Francia test	D'Agostino's test	Linear Regression		Mann-Kendall		Linear Slope	Sen's slope	
				r	Correlation	Comparison level	Trend			
AP-36	Non-norm.		Non-norm.	---		-4,1748	Downward	---	-1,9967	▼
AP-37	Normality		Normality	0,8123	Strong	---	---	-7,5190	---	▼
AP-38		Non-norm.	Normality	0,3106	Weak	-3,4551	Downward	-0,4745	-0,6294	▼

Table 3.5. Point-by-point trend results for the alluvial plain groundwater body (▲ evidence of upward trend; ▼ evidence of downward trend; ● no evidence of trend).

3.3.3 Spatial trend distribution

In order to have an overview of the spatial trend distribution, trend analysis results are represented in Figure 3.11 to 3.14.

Figure 3.11 shows the distribution of nitrate trends in the Geer basin. As expected, a general upward trend is observed in the entire basin. However, as mentioned in point 2.2, two zones can be differentiated: the Southern part, corresponding to the unconfined part of the chalk aquifer, where high concentrations of nitrate are encountered, and the Northern part corresponding to the confined part of the chalk aquifer, where nitrate has not been detected (or at very low concentrations only).

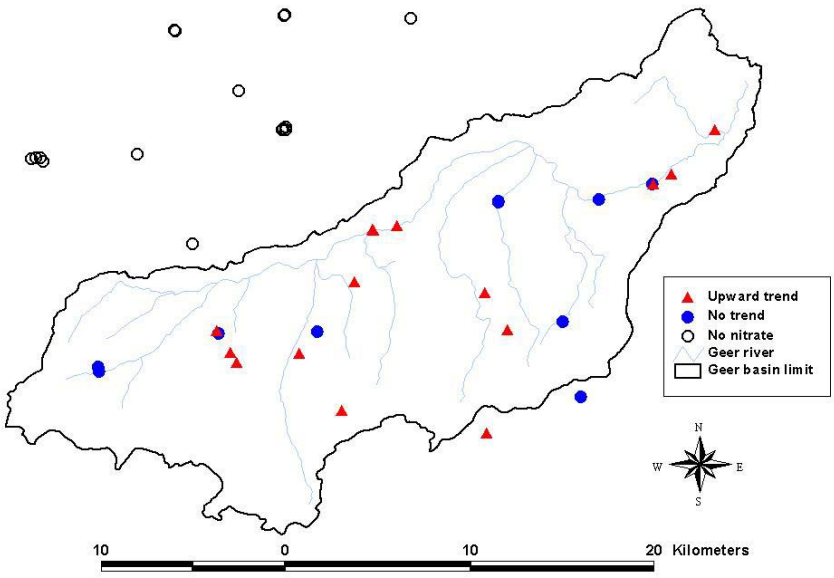

Figure 3.11. Spatial trend distribution in the Geer basin.

Figure 3.12 shows the distribution in nitrate trends in the Pays de Herve groundwater body. The monitoring network is not as developed as in the Geer basin, however, a upward trend is generally observed.

In these two groundwater bodies (Geer and Herve), it is logical to obtain similar results because of the same geology (fissured dual porosity chalk overlain by loess formations) and land use practices (intensive agriculture and farming).

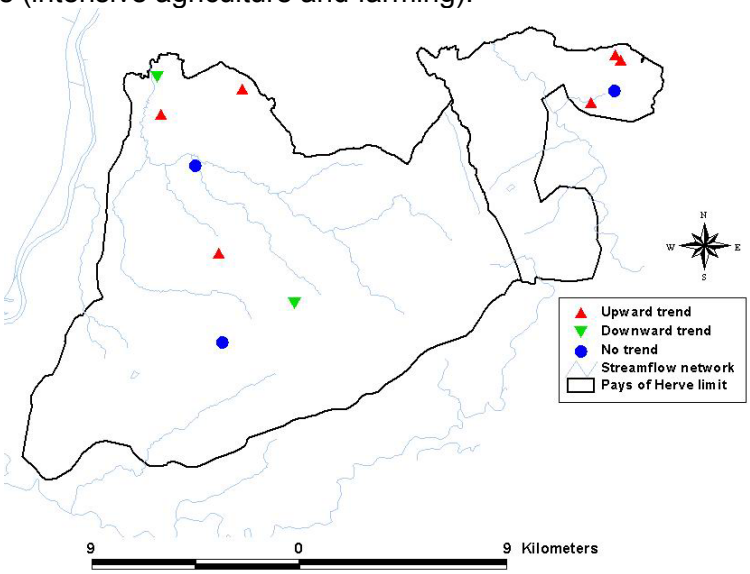

Figure 3.12. Spatial trend distribution in the Pays of Herve groundwater body.

Figure 3.13 presents the distribution of nitrate trends in the Néblon basin. The sampling network is very limited but among these points, 4 of them are very integrative because they correspond to major drainage galleries owned by a water distribution company. These 4 points are characterized by upward nitrate trends. This confirms that the groundwater body is at risk, even if the nitrate pressure is less pronounced in that basin.

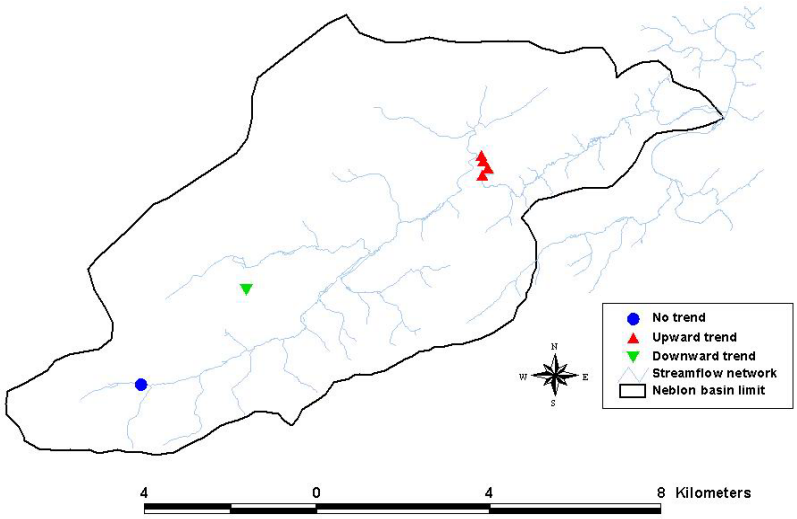

Figure 3.13. Spatial trend distribution in the Néblon basin.

Figure 3.14 presents the trend tests results for the alluvial plain. Most sampling locations do not exhibit trend or even downward trends in nitrates. In the alluvial plain however, land use mainly consists in urbanized and industrialized areas. Agriculture does not constitute a major source of contamination risk there. Furthermore, it is likely that the groundwater quality in the alluvial plain is strongly influenced by the interactions with the Meuse River. Groundwater – surface water interactions are influenced by the existence of dams regulating the level of water in the Meuse for navigation and by water supply wells in the alluvial aquifer. It could probably be interesting to consider these elements in a more detailed analysis of the results.

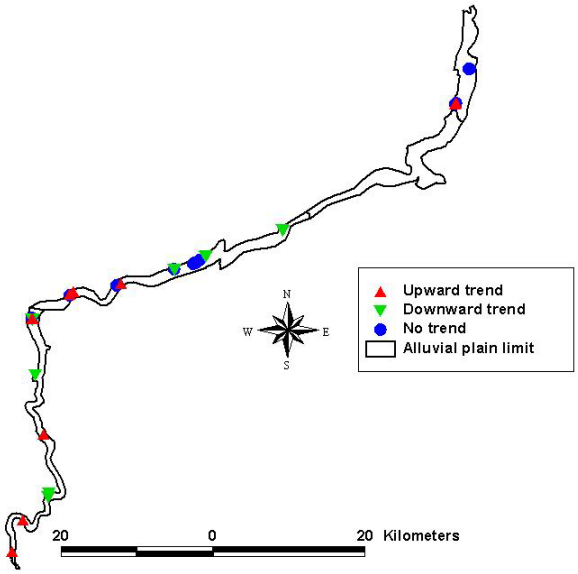

Figure 3.14. Spatial trend distribution in the alluvial plain groundwater body.

3.4 General conclusions and perspectives

3.4.1 Statistical trend analysis

In this deliverable, a consistent and rigorous approach has been proposed and applied for trend detection and quantification in groundwater quality (nitrate) datasets, based on statistical techniques.

Some general observations can be drawn from the point-by-point results obtained for the four groundwater bodies selected in the Walloon part of the Meuse basin. The statistical approach seems robust and able to discriminate between "clear" and "weak" trends. This is related to the two-step procedure: first trend detection, then trend quantification.

For some datasets, the conclusions of the normality tests were not univocal. However, whatever the trend detection and quantification method applied to these datasets, conclusions were very similar. Even if, from a pure statistical point of view, the normality of the dataset is a factor to be considered for selecting one or another trend analysis technique, from a practical point of view, the result of the analysis is not so sensitive to the distribution of the dataset.

3.4.2 Extrapolating trends

The statistical analysis has provided point-by-point estimations of nitrate trends, in the form of a slope expressed in mg NO_3/year (increase or decrease). This result might be enough and appropriate to estimate the short term evolution of groundwater quality in the selected basins (few years), particularly for those groundwater bodies overlain by a thick unsaturated zone that lead to important buffer effects in the evolution of nitrate concentrations in the aquifers (Geer basin, Pays de Herve).

However, end-users and decision makers such as water companies and regional authorities are more interested in the long term evolution of groundwater quality (tens of years) and geological and hydrogeological factors are not the only drivers of nitrate trends in groundwater: land use is also a key factor. The major disadvantage of using a "pure" statistical trend analysis is thus that it is not able to consider variations in land use and functional relations between land use and groundwater quality. For long term evaluation of nitrate trends, more advanced techniques are thus required, such as transfer functions or mechanistic modelling relating land use and groundwater quality.

From a spatial point of view, advances are also still needed in order to produce reliable global estimates of groundwater quality indicators at the scale of the groundwater body, as requested by the EU Water Directive.

3.4.3 Future work

Future work of HGULg in TREND T2 will be focused on the Geer basin where the nitrate dataset is dense and relatively uniformly distributed in the basin. Furthermore, this basin has been the topic of many previous geological and hydrogeological investigations, making it a very interesting case study for integrated research such as within AQUATERRA.

Between March and May 2005, a sampling campaign was organized in the Geer basin (both in the Walloon part and in the Flemish region) for nitrate and tritium measurements. Water samples were sent to Dr P. Maloszewski and Dr. W. Stichler at GSF Münich for tritium analysis. It is expected that such measurements will contribute to a better understanding of spatial variations of nitrate concentrations in the chalk aquifer. Particularly, these results will contribute to explaining the absence of nitrate in confined part of the aquifer. Results have been obtained recently but time was too short to process them for this deliverable. A second sampling campaign is planned in the future.

In the scope of BASIN R3 (Meuse) research activities, HGULg will develop a groundwater flow and transport model for the Geer basin in cooperation with COMPUTE C2. This model will be used in the scope of collaboration with workpackages HYDRO H1 (assessment of the impact of climate change on groundwater resources) and for nitrate trend analysis and forecasting in TREND T2.

For this purpose, it will also be investigated how nitrate trend results obtained in the Geer basin (presented in this deliverable) can be aggregated and used as calibration and validation datasets for the groundwater flow and transport model.

3.5 Appendix

The 97 time-plots are included in the Appendix. These graphs correspond to 97 nitrate sites selected for the four groundwater bodies.

4. Conventional and innovative approaches to trends analysis: a case study for the Brévilles catchment (BRGM)

Pinault J.-L., Guyonnet D., Dubus I.G., Baran N., Gutierrez A. & Mouvet C
BRGM

BRGM
Avenue C. Guillemin
BP 6009
45060 Orléans Cedex 2 France
T: +33 (0)2 38 64 47 50
F: +33 (0)2 38 64 34 46
i.dubus@brgm.fr

4.1 Introduction

Crop protection products are known to represent a potential risk for human and the environment and the presence of pesticides is therefore routinely monitored in environmental media such as groundwater, surface water, and, to a lesser extent, the atmosphere. Surveillance programs for pesticides have different objectives. While some monitoring networks are specifically designed to ascertain whether there is any excess of legal threshold concentrations, most surveillance efforts are targeted towards investigating the spatial spread of the contamination of water resources by pesticides and/or detecting any positive or negative temporal tendency in concentrations. Designing a monitoring study to investigate trends in pesticide concentrations represents a significant investment given i) the costs involved in analysing organic compounds with accuracy; and, ii) the fact that the fate of pesticides is heavily influenced by weather conditions, which means that concentrations need to be monitored over a number of years sufficient to differentiate between variations due to climatic variability and those that can be attributed to measures taken to reduce pesticide contamination.

The major contributing factors to the explanation of temporal variations in pesticide concentrations at a given groundwater point are likely to be:

i) variations in transport properties (essentially governed by the effective rainfall, i.e. the part of the rainfall that effectively contributes to groundwater recharge);
ii) spatial and temporal variations in annual applications of the pesticides; and,
iii) possible variations in the potential for pesticide degradation. The limited number of factors involved and the strong influence of hydrology in the determination of pesticide trends in groundwater means that statistically-based approaches establishing a direct relationship between pesticide concentrations and water inputs to groundwater systems, such as transfer function, Bayesian-based or neural-network-based approaches are well suited to the reconstruction or prediction of past or future changes in groundwater concentrations. In contrast to more deterministic approaches, data requirements are generally low, ensuring their cost effectiveness.

The present document reports on the comparative application of three different approaches to trends analysis for concentrations of pesticides in water resources. A total of three approaches were investigated:
A 'conventional' statistical method referred to as the 'Holt's two parameter exponential smoothing' was first applied to the data for benchmarking purposes. The methodology is only based on the analysis of trends analysis data without recurring to additional information on e.g. input fluxes to the system.
The time series data were also analysed using a method based on the iterative calibration of transfer functions through inverse modelling procedures. The approach was deployed

through the TEMPO computer tool which facilitates the application of the methodology to experimental datasets.
Finally, methodological developments were undertaken to investigate how the combination of possibilistic concepts and neural network approaches could potentially benefit time series analysis.

The supporting data which were used in the present exercise are presented in the earlier TREND2 deliverable T2.1 ('Documented spatial data set containing the subdivision of the basins into groundwater systems and subsystems, the selected locations per subsystem and a description of these sites, available data and projected additional measurements and equipment'). The approaches were evaluated for their ability to predict concentrations of atrazine and its first metabolite deethylatrazine (DEA) in the Brévilles spring and in various piezometers across the Brévilles catchment.

4.2 Time series analysis using 'classical' statistics

4.2.1 The Holt's two parameter method

A simple and pragmatic model for a time series would be to consider each observation as consisting of a constant b and an error component ε, that is: $X_t = b + \varepsilon_t$. The constant b is relatively stable in each segment of the series, but may change slowly over time. If appropriate, then one way to isolate the true value of b, and thus the systematic or predictable part of the series, is to compute a kind of moving average, where the current and immediately preceding ("younger") observations are assigned greater weight than the respective older observations. Simple exponential smoothing accomplishes such weighting, where exponentially smaller weights are assigned to older observations. The specific formula for simple exponential smoothing is:

$$S_t = \alpha . X_t + (1-\alpha) . S_{t-1}$$

When applied recursively to each successive observation in the series, each new smoothed value (forecast) is computed as the weighted average of the current observation and the previous smoothed observation; the previous smoothed observation was computed in turn from the previous observed value and the smoothed value before the previous observation, and so on. Thus, in effect, each smoothed value is the weighted average of the previous observations, where the weights decrease exponentially depending on the value of parameter α. If α is equal to 1 then the previous observations are ignored entirely; if α is equal to 0, then the current observation is ignored entirely, and the smoothed value consists entirely of the previous smoothed value (which in turn is computed from the smoothed observation before it, and so on; thus all smoothed values will be equal to the initial smoothed value S_0). Values of α in-between will produce intermediate results.

In the time series model which was used in the present case, the simple exponential smoothing forecasts are "enhanced" by a linear trend component that is smoothed independently via the γ parameter. This model is also referred to as *Holt's two parameter method*. In order to compute the smoothed value (forecast) for the first observation in the series, both estimates of S_0 and T_0 (initial trend) are necessary. By default, these values are computed as $T_0 = (X_n - X_1)/(N-1)$ where N is the length of the series and $S_0 = X_1 - T_0 / 2$.

So, when a trend component is included in the exponential smoothing process, an independent trend component is computed for each time, and modified as a function of the forecast error and the respective parameter. If the γ parameter is 0, than the trend component is constant across all values of the time series (and for all forecasts). If the parameter is 1, then the trend component is modified "maximally" from observation to observation by the respective forecast error. Parameter values that fall in-between represent mixtures of those two extremes.

4.2.2 Application to the Brévilles data

Time series analysis with a linear trend was applied to the forecasting of atrazine, deethylatrazine, calcium and nitrate fluxes in spring water (Figure 4.1 to Figure 4.4) at the Brévilles site. A 15-day time rate was used in calculations. In all cases the forecast was performed from 16/5/2005, the first step after the last observation on 1/5/2005, to 28/9/2005, i.e. over a total of 10 time steps.

Although the exponential smoothing process is a predictive technique which is used widely, its use to forecast fluxes in spring water is an ill-posed problem, i.e. an error on the estimation of parameter γ may induce very different forecasts, without being able to certify a value is more likely than another.

In all cases, the forecast strongly depends on the parameter γ whose incidence on the fitting of the model is very low, which is a typical characteristic of ill-posed problems. This drawback is inherent in the time series analysis whatever the predictive method that is used. Clearly, in the case of the Brévilles spring data, more information has to be taken into account into the model to produce a reliable forecast. Moreover, the uncertainty of predicted fluxes and concentrations has to be estimated according to the external conditions responsible for the transfer from the soils to the spring. For these reasons, it is believed that conventional statistics are somewhat limited and that more advanced techniques such as those which are presented in section ** and ** should be preferred. The use of such techniques enables the drawing of a relationship between multiple inputs and an output variable, the use of non-linear transfer functions, the inclusion of a transport delay between the soils and the spring and the accounting of dispersion processes during transport in the unsaturated zone.

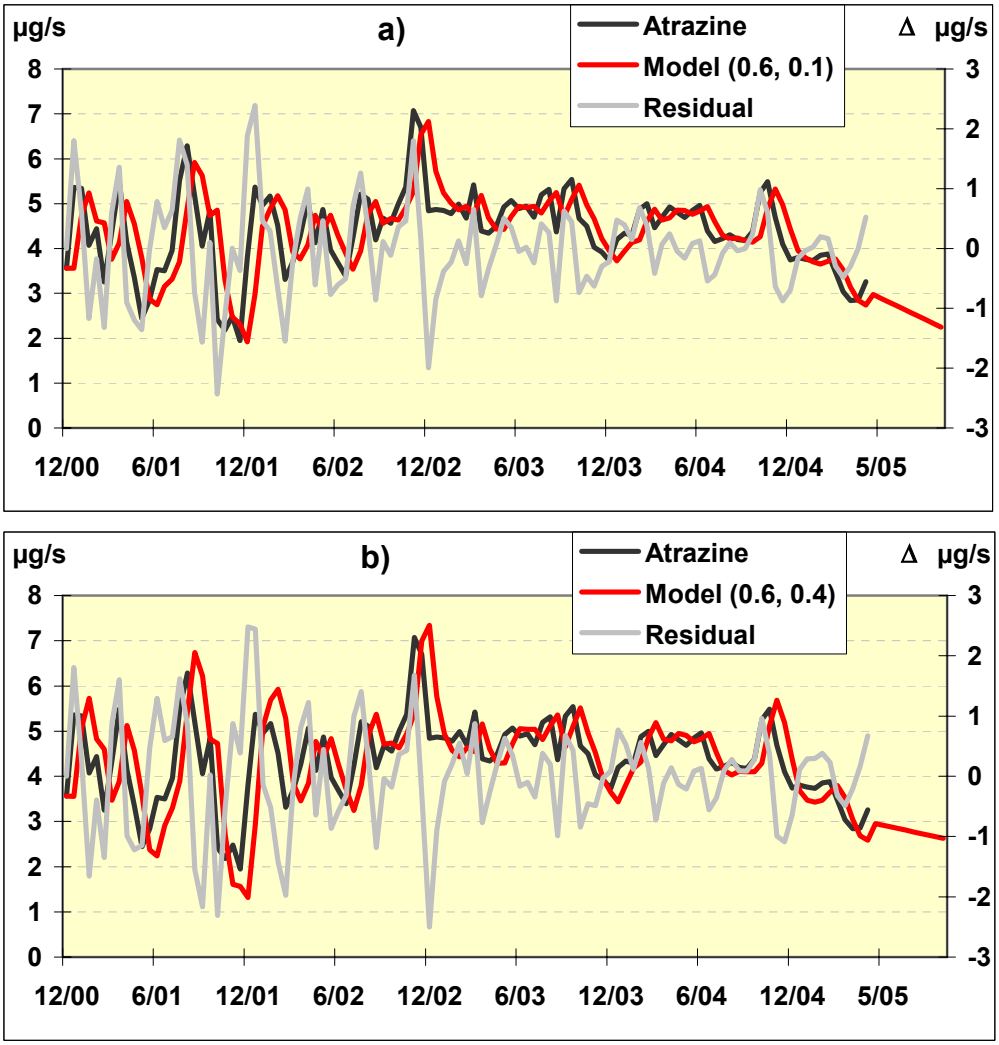

Figure 4.1. Forecasting of atrazine fluxes in spring water at Brévilles. Fluxes of atrazine are expressed in microg/s to facilitate comparison with measured fluxes at Brévilles. The y axis to the left of the figure corresponds to atrazine fluxes while that to the right correspond to the residuals

$S_0 = 3.561$	a) $\alpha = 0.6, \gamma = 0.1$
$T_0 = -0.003$	b) $\alpha = 0.6, \gamma = 0.4$

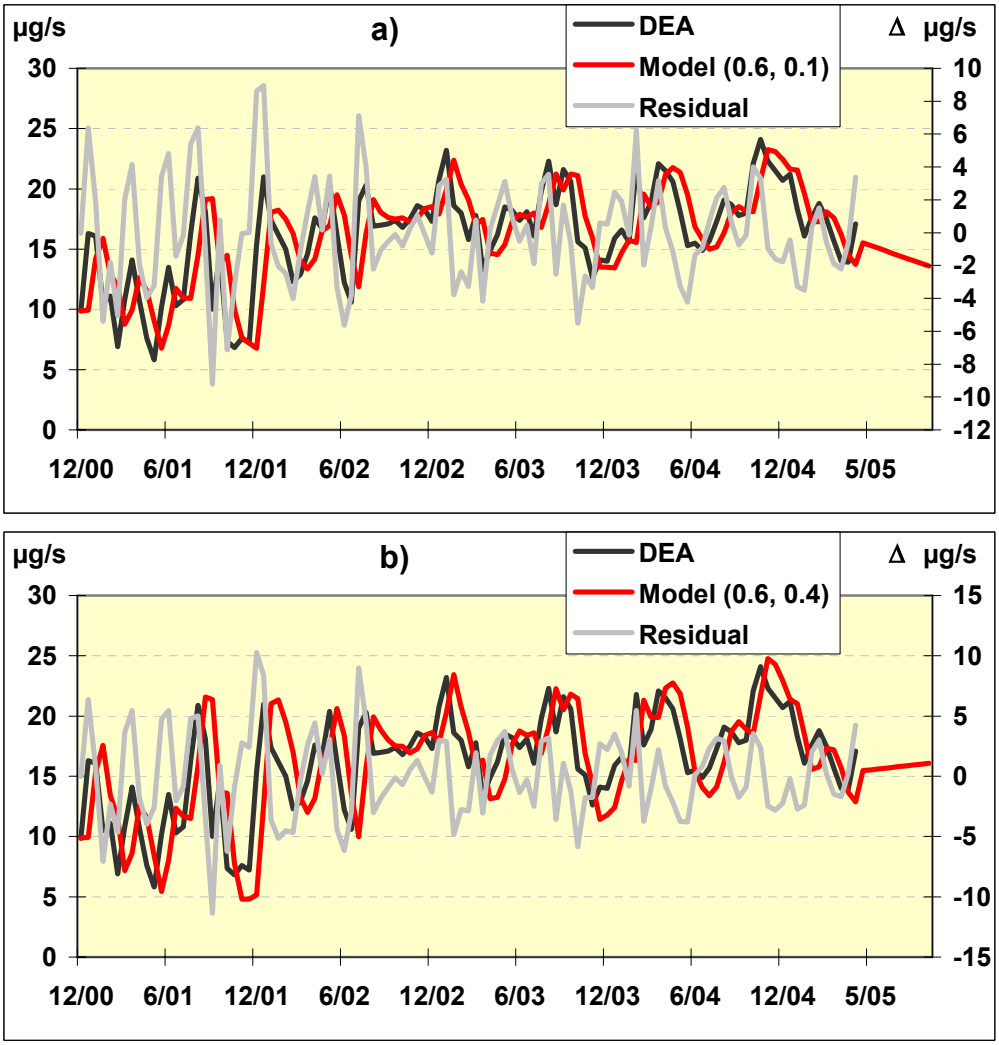

Figure 4.2. Forecasting of deethylatrazine fluxes in spring water at Brévilles. Fluxes of DEA are expressed in microg/s to facilitate comparison with measured fluxes at Brévilles. The y axis to the left of the figure corresponds to DEA fluxes while that to the right correspond to the residuals

$S_0 = 9.816$

$T_0 = 0.0684$

a) $\alpha = 0.6, \gamma = 0.1$

b) $\alpha = 0.6, \gamma = 0.4$

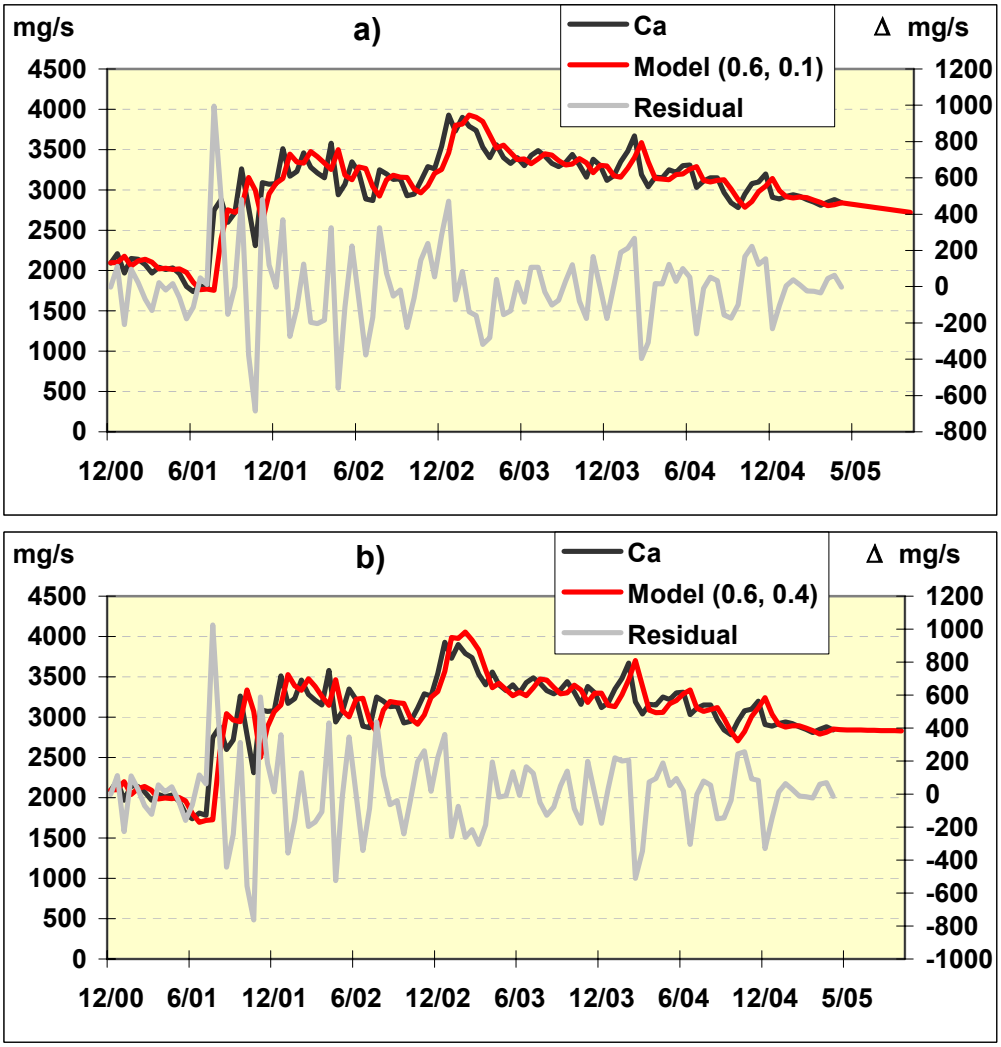

Figure 4.3. Forecasting of calcium fluxes in spring water at Brévilles. Fluxes of calcium are expressed in mg/s to facilitate comparison with measured fluxes at Brévilles. The y axis to the left of the figure corresponds to calcium fluxes while that to the right correspond to the residuals

$S_0 = 2086$

$T_0 = 7.075$

a) $\alpha = 0.6, \gamma = 0.1$

b) $\alpha = 0.6, \gamma = 0.4$

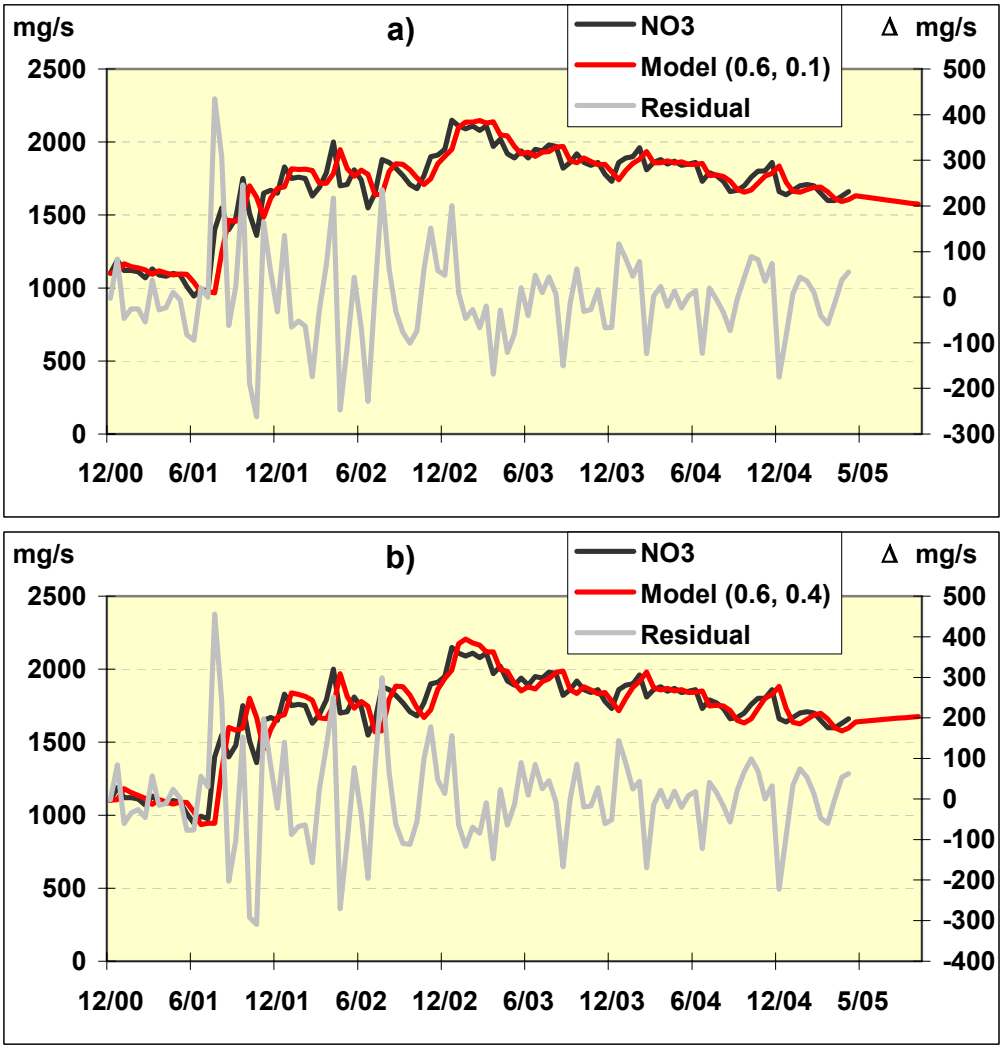

Figure 4.4. Forecasting of nitrate fluxes in spring water at Brévilles. Fluxes of nitrate are expressed in mg/s to facilitate comparison with measured fluxes at Brévilles. The y axis to the left of the figure corresponds to nitrate fluxes while that to the right correspond to the residuals

$S_0 = 1097$

$T_0 = 5.283$

a) $\alpha = 0.6, \gamma = 0.1$

b) $\alpha = 0.6, \gamma = 0.4$

4.3 Time series analysis using TEMPO

4.3.1 Data processing and numerical analysis

General concepts
The processing of the data was undertaken using the TEMPO package [*Pinault*, 2001]. TEMPO is a Windows-based tool which facilitates groundwater data analysis and enables the modelling of time series through iterative calibrations of combinations of transfer functions ('inverse modelling' approach). Although the package has been extensively used to analyse and simulate groundwater flows, it is also suited to analysing water quality data. The tool includes data pre-and post-processing features and a rainfall stochastic generator.

The inverse model which was built within TEMPO to analyse the Brévilles data uses rainfall-hydraulic head or rainfall-flux data to calculate unit hydrographs and impulse responses of fluxes. Fluxes were defined as the product of hydraulic heads (in relation to a reference level) and chemical concentrations. In order to keep the dimension of the pressure head expressed in meters, the calculation of fluxes was carried out with concentration values divided by their mean value (unit standardisation).

The rainfall inputed in the model is defined as the weighted sum of observed precipitations at meteorological stations. The weighted sum is optimized from the cross-correlogram of rainfall and spring flow [Pinault et al., 2005]. It should be noted that the short term correlation between rainfall height and the spring flow at a 10-day time rate is used in the model and that the model does not rely on initial precipitation data. Hence, the best linear combination of rainfall is not necessarily constructed from the meteorological stations closest to the study, but from the stations whose rainfall series are best correlated with the spring flow.
For the Brévilles dataset, the best linear combination was obtained from the Chartres and Senlis meteorological stations (120 and 70 km of the Brévilles catchment, respectively):

$$R(t_i) = 0.57 \times R_{Chartres} + 0.43 \times R_{Senlis} \quad (6)$$

The hydraulic head $\Delta \mathrm{H}(t_i)$, measured at piezometers and expressed in relation to a reference level, was considered to be the result of rainwater infiltration:

$$\Delta \mathbf{H} = 1/\eta . \mathbf{\Gamma} * \mathbf{R}_{eff} \quad (1)$$

Where:
η is a constant related to the effective porosity ω_e of the aquifer: $\omega_e = \eta / \max(\Gamma(t_i))$
$\mathbf{R}_{eff}$ the effective rainfall
$\mathbf{\Gamma}$ the normalized impulse response of the hydraulic head $\Delta \mathrm{H}(t_i)$ to effective rainfall,
and $*$ represents the discrete convolution product.

In the present application, the impulse response $\mathbf{\Gamma}$ was defined on the interval $[0, \tau]$ so that:

$$\begin{cases} \Gamma(t_i) = A.\exp(-\ln(2)((t_i - T)/D)^2 * \exp(-t_i.\ln(2)/L) & \text{if } 0 \le t_i \le \tau \\ \Gamma(t_i) = 0 \quad \text{elsewhere} \end{cases} \quad (2)$$

Where:
T represents the delay of the transfer process after a given impulse to be transferred
D represents the duration of the transfer
L characterizes the dispersion process
And, A is the normalization constant

Equations (2) are the expression of a general dispersive transfer model represented by the Gaussian $\exp(-\ln(2)((t_i - T)/D)^2$ for transfer and the exponential law $\exp(-t_i.\ln(2)/L)$ for

dispersion. The succession of these two phenomena is the convolution product of both laws [*Pinault et al.*, 2005].

Through averaging of the two parts of equation (1), the following constraint for water mass conservation can be obtained:

$$\overline{\Delta \mathrm{H}} = 1/\eta.\overline{\mathrm{R}}_{eff} = \gamma/\eta.\overline{\mathrm{R}} \quad (3)$$

Where:

γ is the proportion of rainwater lost by evapotranspiration, *i.e.* the mean contribution of rainfall to effective rainfall.

The effective rainfall $\mathrm{R}_{eff}(t_i)$ is calculated from the rainfall $\mathrm{R}(t_i)$ and the effective rainfall threshold $\Omega(t_i)$ such that:

$$\mathrm{R}_{eff}(t_i) = \begin{cases} \mathrm{R}(t_i) - \Omega(t_i) & \text{if } \mathrm{R}(t_i) \geq \Omega(t_i) \\ 0 & \text{if } \mathrm{R}(t_i) < \Omega(t_i) \end{cases} \quad (4)$$

$\boldsymbol{\Omega}$ can be interpreted here as the available soil-storage deficit is related to both rainfall and potential evapotranspiration:

$$\boldsymbol{\Omega} = [\boldsymbol{\Gamma}_{\Omega,PET} * \mathbf{PET} + \boldsymbol{\Gamma}_{\Omega,R} * \mathbf{R} + \mathrm{C}^{\mathrm{st}}] \quad (5)$$

where PET is the potential evapotranspiration
R is the rainfall
Cst is a constant

and, $\boldsymbol{\Gamma}_{\Omega,PET}$ and $\boldsymbol{\Gamma}_{\Omega,R}$ are impulse responses of $\boldsymbol{\Omega}$ to $\mathbf{PET}$ and $\mathbf{R}$, respectively.

These impulse responses $\boldsymbol{\Gamma}_{\Omega,PET}$ and $\boldsymbol{\Gamma}_{\Omega,R}$ are represented by trapezoids with four degrees of freedom, with $\boldsymbol{\Gamma}_{\Omega,PET}$ being positive and $\boldsymbol{\Gamma}_{\Omega,R}$ being negative, i.e. the rainfall results in a decrease in $\Omega(t_i)$ whereas the potential evapotranspiration causes an increase in $\Omega(t_i)$ [*Pinault et al.*, 2001 a].

The modelling consists in optimising the impulse responses $\boldsymbol{\Gamma}$, $\boldsymbol{\Gamma}_{\Omega,\mathrm{PET}}$, $\boldsymbol{\Gamma}_{\Omega,\mathrm{R}}$, and the constant C^{st} through an iterative process so as to get the best fit between predicted and observed hydraulic heads.

The approach described above for hydraulic heads is universal and was applied to mass transfers and spring flow in the present work. For applications involving mass transfers, relationships (4) and (5) refer to the effective input flux, i.e. the effective rainfall is no longer considered as a water resource but as a flux when rainwater dissolves ions in the soils and in the vadose zone that is considered as the input of the model. Processing of spring flow was performed exactly in the same way except for the flow $\mathrm{Q}(t_i)$ which replaces the piezometric level variations $\Delta \mathrm{H}(t_i)$, as shown in (7) where S is the catchment area:

$$\mathbf{Q} = S.\boldsymbol{\Gamma} * \mathbf{R}_{eff} \quad (7)$$

Identification of individual contributions to water and chemical fluxes at the spring and in piezometers

This inverse approach may be extended so as to express the output in relation with several inputs $\mathbf{Q}_1$ ... $\mathbf{Q}_p$:

$$\mathbf{Q} = S.\left[\lambda.\boldsymbol{\Gamma} * \mathbf{R}_{eff} + \lambda_1.\boldsymbol{\Gamma}_1 * \mathbf{Q}_1 + \cdots + \lambda_p.\boldsymbol{\Gamma}_p * \mathbf{Q}_p\right] + \boldsymbol{\varepsilon} \quad (8)$$

in order to separate the output $\mathbf{Q}$ into $p+1$ components $S.\lambda.\Gamma * R_{eff}$, $S.\lambda_1.\Gamma_1 * Q_1$,...whose contribution is given by the corresponding weighting factors $S.\lambda.\|R_{eff}\|/\|Q\|$, $S.\lambda_1.\|Q_1\|/\|Q\|$,... $\|F\|$ is the l_2 norm of the discrete function $F=\{F_1,\cdots\}$, i.e. $\|F\|=\sqrt{\sum F_i^2}$.

The separation is all the more reliable as the pairs of cross-correlograms obtained from the inputs have their absolute value lower than 1 for the lags i so that $-m \le i \le m$ where m is the length of the impulse responses $\Gamma_k = 0 \quad k > m$. In effect, the constraints applied on the positive weighting factors whose sum is 1 give the inverse problem a sense in a wide scope of applications without the requirement of any regularization technique.

This method is applied for separating the calcium flux measured at the spring. The calcium may be used as a tracer for mass transfer from the groundwater to the spring, the dissolution of carbonates occurring at the catchment scale. The calcium flux measured at piezometers may be used as inputs of a transfer model the output of which is the calcium flux at the spring. Nevertheless, the signatures of the calcium fluxes at piezometers are correlated and only two piezometers can be used as inputs (Figure 4.5). The contributions of calcium fluxes from piezometers PZ2 and PZ6 to the calcium flux at the spring may be separated since the behaviours of PZ2 and PZ6 fluxes are clearly differentiated for the observation period, the PZ2 flux remaining almost steady after 2002 whereas the PZ6 flux decreases slowly (Figure 4.5). So, the calcium flux at the spring can be separated into three components related to rainfall, i.e. runoff and two components groundwater from both hillside of the catchment.

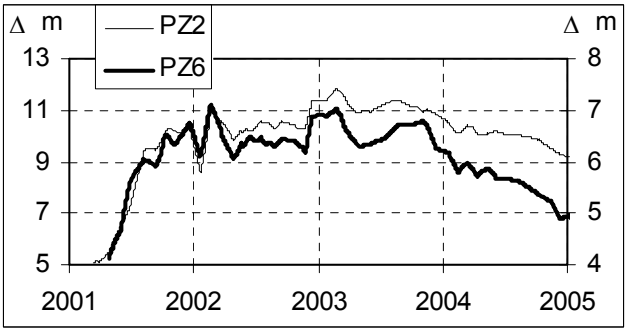

Figure 4.5: Calcium fluxes observed in the PZ2 and PZ6 piezometers

Flux separation is shown in Figure 4.6. Impulse responses are relatively short (Figure 4.6b). The mean transit times (the mean lags) are 33 days for runoff, 73 days for PZ2 and 44 days for PZ6. As for the two piezometers, the transit time reflects the distance of the piezometer to the spring. The contribution of every component is 4.5% for runoff, 54% for PZ2 and 41.5% for PZ6. The model reproduces accurately the long term variations of the calcium flux measured at the spring (Figure 4.6a), which means that the two piezometers PZ2 and PZ6 are exhaustive for representing mass transfer from groundwater to the spring. The catchment may be split therefore into two sub-catchments whose areas are proportional to the contribution of both piezometers. The ratio of PZ2 and PZ6 contributions is 1.3, which corresponds closely to the ratio of both hillsides (Figure 4.7). Thus the components of the calcium flux at the spring are representative of mass transfer from runoff and from groundwater discharge issuing both hillsides (Figure 4.6d).

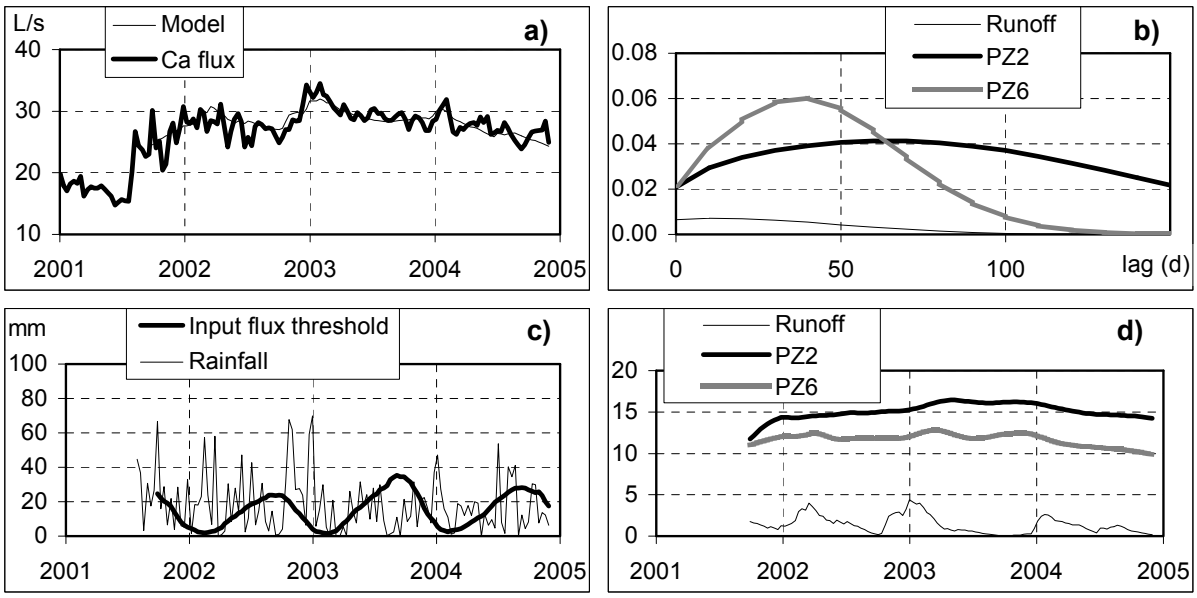

Figure 4.6. Separation of Ca flux at the spring. The raw data are aggregated to create a continuous 10-day sampling period. – a) Comparison between the observed and the computed calcium flux – b) The impulse responses – c) The input flux threshold used to calculate the input flux from rainfall – d) The separation of the Ca flux at the spring into 3 components related to runoff and groundwater discharge.

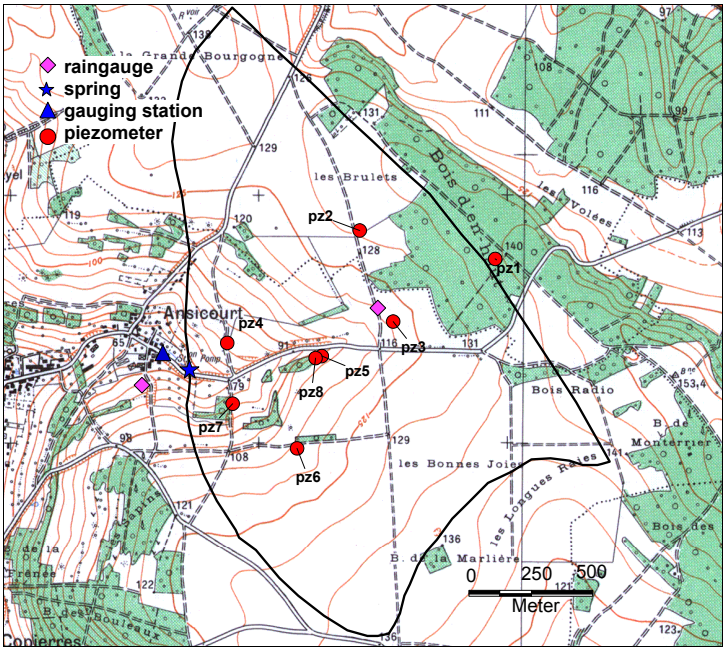

Figure 4.7. Location of the various monitoring devices on the Brévilles catchment

Expressing concentrations in the vadose zone

Another aspect of inverse modeling of mass transfer concerns the reconstruction of concentration $\Delta\beta(t_i)$ of dissolved species at the input of the model. This method is applied for separating the calcium, nitrate, atrazine and deethylatrazine fluxes measured at piezometers and at the spring, the inputs of the models being the corresponding fluxes through the soils and the unsaturated zone. For pressure head variations the output flux $\mathrm{F}(t_i)$ can therefore be written as a piezometric level of groundwater whose constant concentration is $\overline{\Delta\mu}$:

$$\mathrm{F}(t_i) = \Delta \mathrm{H}(t_i) \cdot \Delta\mu(t_i) / \overline{\Delta\mu} = 1/\eta \cdot \Gamma_{flux}(t_i) * \left(\mathrm{R}_{eff}(t_i) \cdot \Delta\beta(t_i) / \overline{\Delta\mu}\right) \quad (9)$$

where $\Delta\mu(t_i)$ is the concentration measured at piezometers, and $\mathbf{\Gamma}_{flux}$ is again a normalized impulse response. In this way, the following relationship holds $\overline{\mathrm{F}} = \overline{\Delta \mathrm{H}} = 1/\eta \cdot \overline{\mathrm{R}_{eff}}$ according to (3). The term $\Delta\beta(t_i)/\overline{\Delta\mu}$ is a calculated function of time, which represents the relative variations of the concentration at the input of the model, i.e. in the vadose zone.

To solve equation (9) relative to mass transfer, a model is required for the concentration in the vadose zone $\Delta\beta(t_i)$, which may be represented by its trigonometric series whose Fourier coefficients are $\hat{c}_n$, $n = 0, N$, due to their pseudo-periodic behaviour from year to year; N is the number of years in the observation period. Thus, the resolution of equation (9) amounts to the estimation of the set of functions $(\mathbf{\Gamma}_{flux}, \hat{\mathbf{c}})$.

Data processing of series related to the piezometer PZ8 are presented in Figure 4.8. The model referring to $\Delta \mathrm{H}(t_i)$ shown in Figure 4.8a is computed from (1). The impulse response $\mathbf{\Gamma}$ is represented in Figure 4.8b. The observed and computed fluxes of calcium, nitrate, atrazine and deethylatrazine calculated from (9) are shown in Figure 4.8c, e, g, i. The corresponding computed concentrations in the vadose zone $\Delta\beta(t_i)$ are represented in Figure 4.8d, f, h, j. For every flux, the model fairly reproduces the long term variations of observed values. The impulse responses $\mathbf{\Gamma}_{flux}$ relative to fluxes are not represented since there are very similar to the impulse response of the piezometric level to effective rainfall shown in Figure 4.8b.

As for the spring fluxes $\mathrm{F}(t_i)$, they are the product of the spring flow $\mathrm{Q}(t_i)$ by the relative concentration of the corresponding dissolved specie in spring water:

$$\mathrm{F}(t_i) = \mathrm{Q}(t_i) \cdot \Delta\mu(t_i) / \overline{\Delta\mu} = S \cdot \Gamma_{flux}(t_i) * \left(\mathrm{R}_{eff}(t_i) \cdot \Delta\beta(t_i) / \overline{\Delta\mu} \right) \qquad (10)$$

The method is used for processing pressure head variations of the piezometer PZ8 as well as the fluxes of calcium, nitrate, atrazine and DEA (deethylatrazine) observed at the same location. (Figure 4.8). The impulse responses relative to the pressure head variations and to the fluxes being very similar, only that referring to pressure head variations is represented (Figure 4.8b). For every flux, the model fairly reproduces the long term variations of observed values. The computed concentrations $\Delta\beta(t_i)$ in water in the vadose zone are represented in Figure 4.8d, f, h, j. The same processing is applied to the data referring to the spring (Figure 4.9).

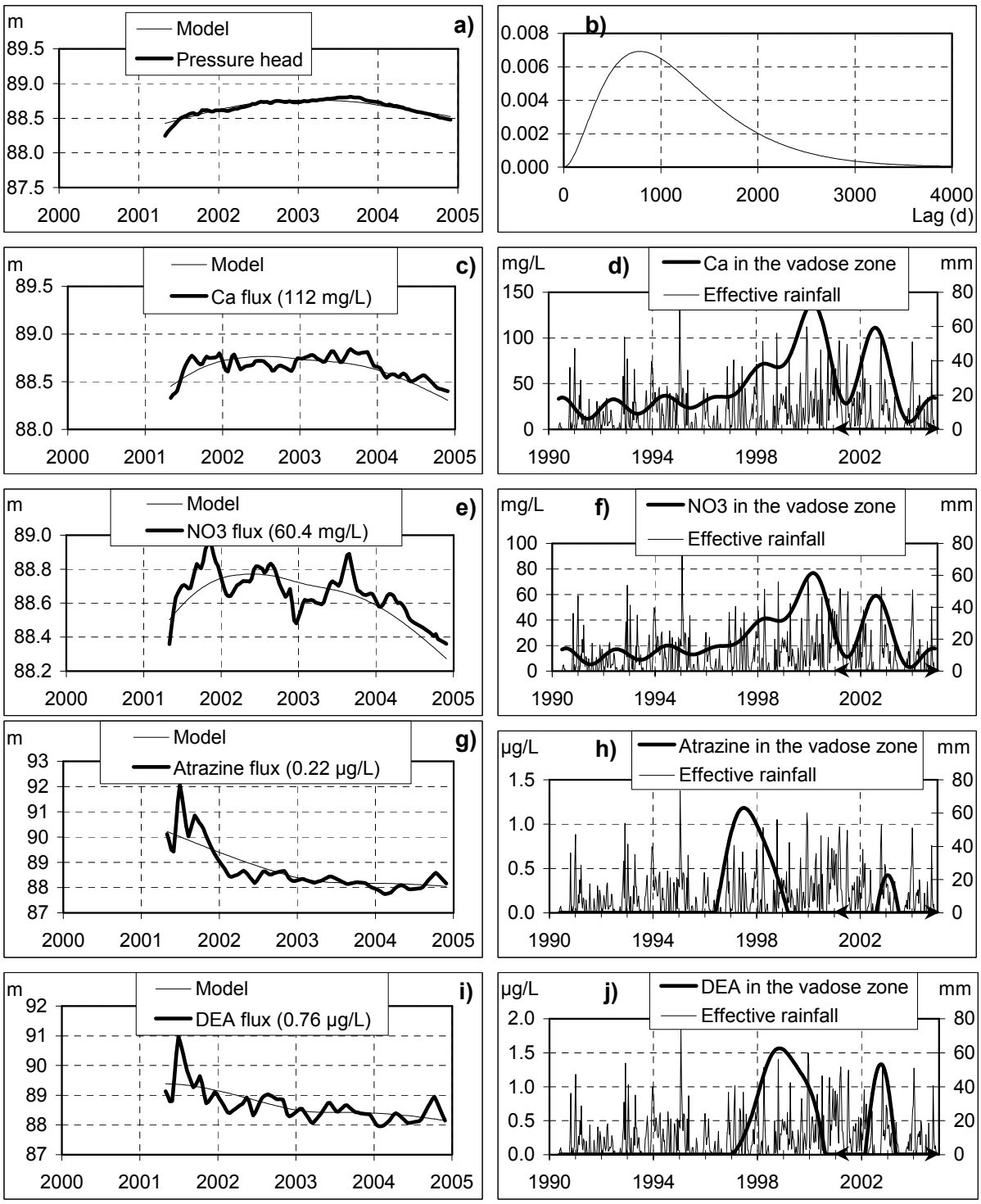

Figure 4.8. Processing of pressure head and fluxes of piezometer PZ8. A 10-day sampling rate is used (the observation period is symbolized by arrows on the time axis) – a) Comparison between the observed and the computed piezometric level – b) The impulse response – c) Comparison of the observed and the computed calcium flux – d) The computed calcium concentration in the vadose zone e) Comparison of the observed and the computed nitrate flux – f) The computed nitrate concentration in the vadose zone – g) Comparison of the observed and the computed atrazine flux – h) The computed atrazine concentration in the vadose zone – i) Comparison of the observed and the computed deethylatrazine flux – j) The computed deethylatrazine concentration in the vadose zone.

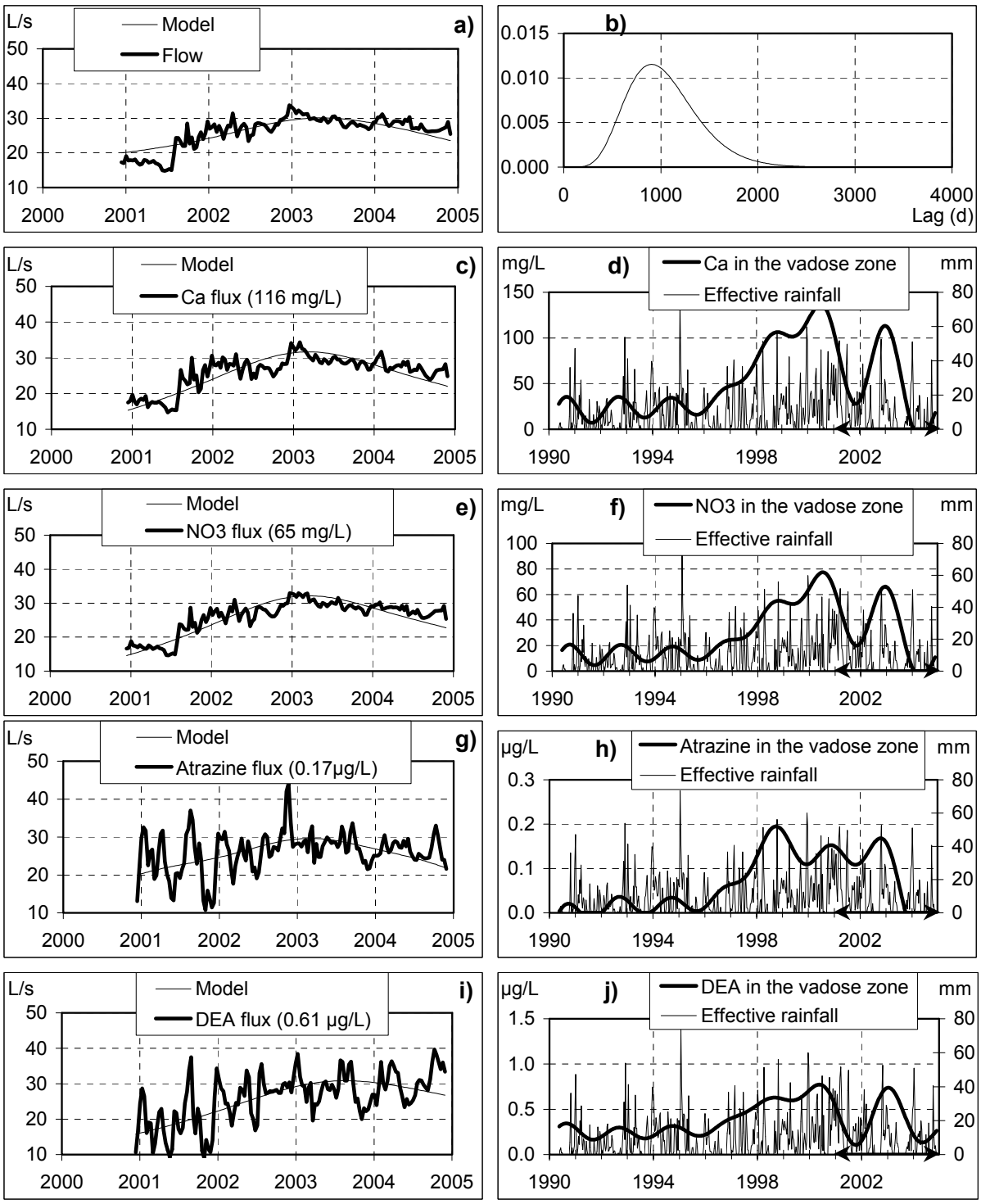

Figure 4.9. Processing of pressure head and fluxes of the spring. A 10-day sampling rate is used. – a) Comparison between the observed and the computed flow – b) The impulse response – c) Comparison of the observed and the computed calcium flux – d) The computed calcium concentration in the vadose zone at the catchment scale – e) Comparison of the observed and the computed nitrate flux – f) The computed nitrate concentration in the vadose zone at the catchment scale – g) Comparison of the observed and the computed atrazine flux – h) The computed atrazine concentration in the vadose zone at the catchment scale – i) Comparison of the observed and the computed deethylatrazine flux – j) The computed deethylatrazine concentration in the vadose zone at the catchment scale.

4.3.2 Results

Functioning of the Brévilles catchment

The computed concentrations of dissolved species in the vadose zone typically disclose strong variations for all species. These variations at the input of the models are due to both concentration variations in water in the vadose zone or to water content. The calcium flux through the vadose zone is tightly related to effective rainfall since calcium dissolution of calcareous formations mainly occurs for wet periods, if not it is only slightly transported towards the groundwater. The other dissolved species are also strongly influenced by the precipitation amount for migrating from the vadose zone to the groundwater and from the groundwater to the spring. To isolate the input concentrations from variations related to the climatic conditions and to put in a prominence the anthropogenic contributions to transfers, the concentrations of nitrate, atrazine and DEA in the vadose zone were divided by the relative calcium concentration. Indeed, the calcium source that comes from the dissolution of carbonates is evenly distributed onto the catchment and its concentration calculated in Figure 4.8d and Figure 4.9d is entirely controlled by climatic conditions. Thus:

$$[NO_3]_{Ca} = [NO_3] \times [\overline{Ca}]/[Ca] \quad (11)$$

$$[\text{atrazine}]_{Ca} = [\text{atrazine}] \times [\overline{Ca}]/[Ca] \quad (12)$$

$$[DEA]_{Ca} = [DEA] \times [\overline{Ca}]/[Ca] \quad (13)$$

The long duration of transfers allows the reconstruction of concentrations in the vadose zone prior to the observation period; the mean transit time of fluxes through the vadose zone is close to 1150 days for every piezometer, which enables to reconstruct the fluxes since the early 1990. The larger the concentration reconstruction the lower its contribution to groundwater transfers within the observation period that starts at the beginning of 2001. The standardization of fluxes according to (11-13) enables expressing the concentrations in stationary conditions.

Concentrations defined in (11-13) are represented for every piezometer and for the spring in Figure 4.10 for nitrate, Figure 4.11 for atrazine and Figure 4.12 for DEA. These reconstructed series of concentrations can be compared to information on land use and atrazine inputs to the system for the year 1994 to 1999 using maps produced as part of the TREND2 deliverable T2.2.

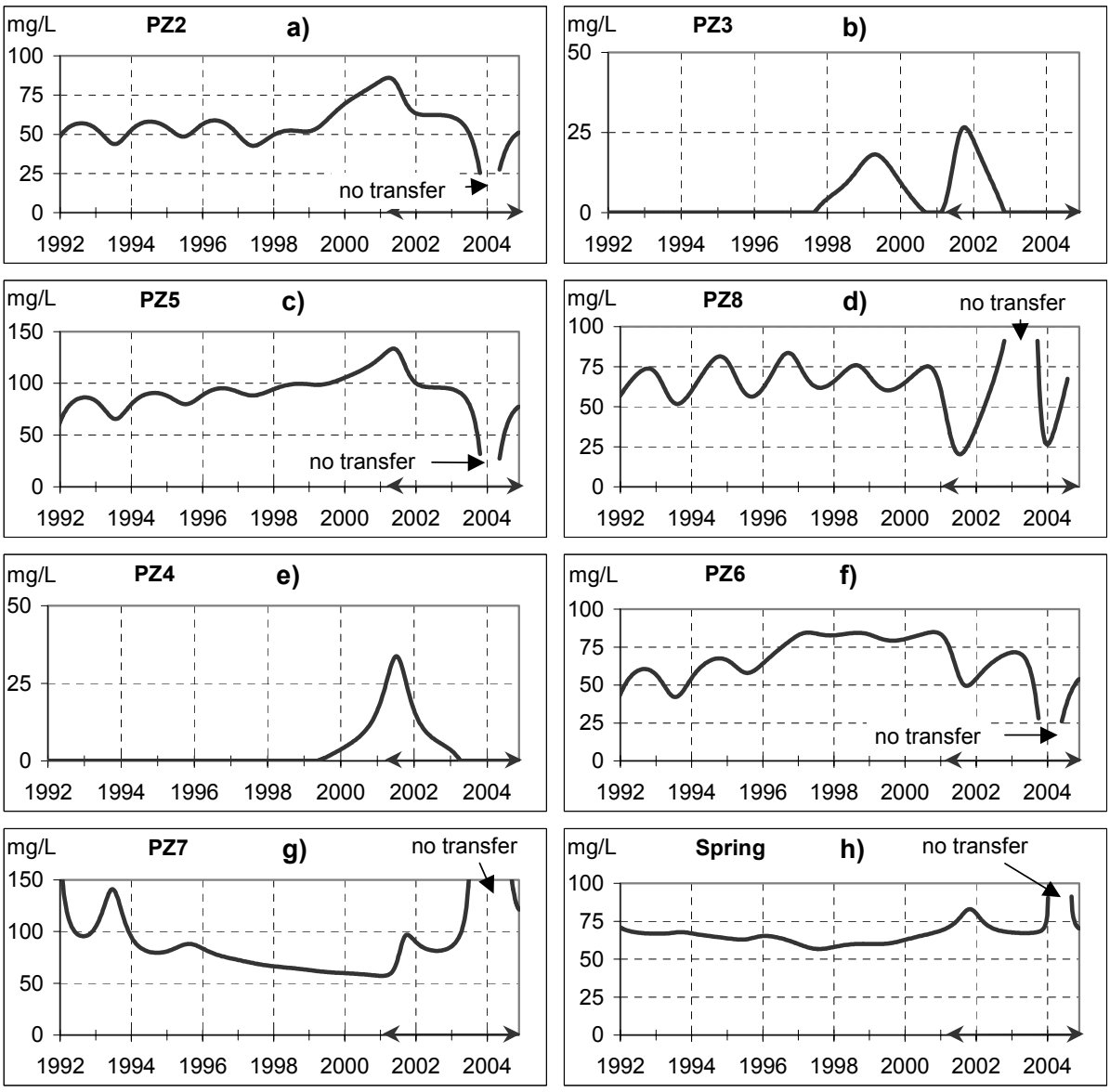

Figure 4.10. Reconstructed nitrate concentration in the vadose zone according to (10)

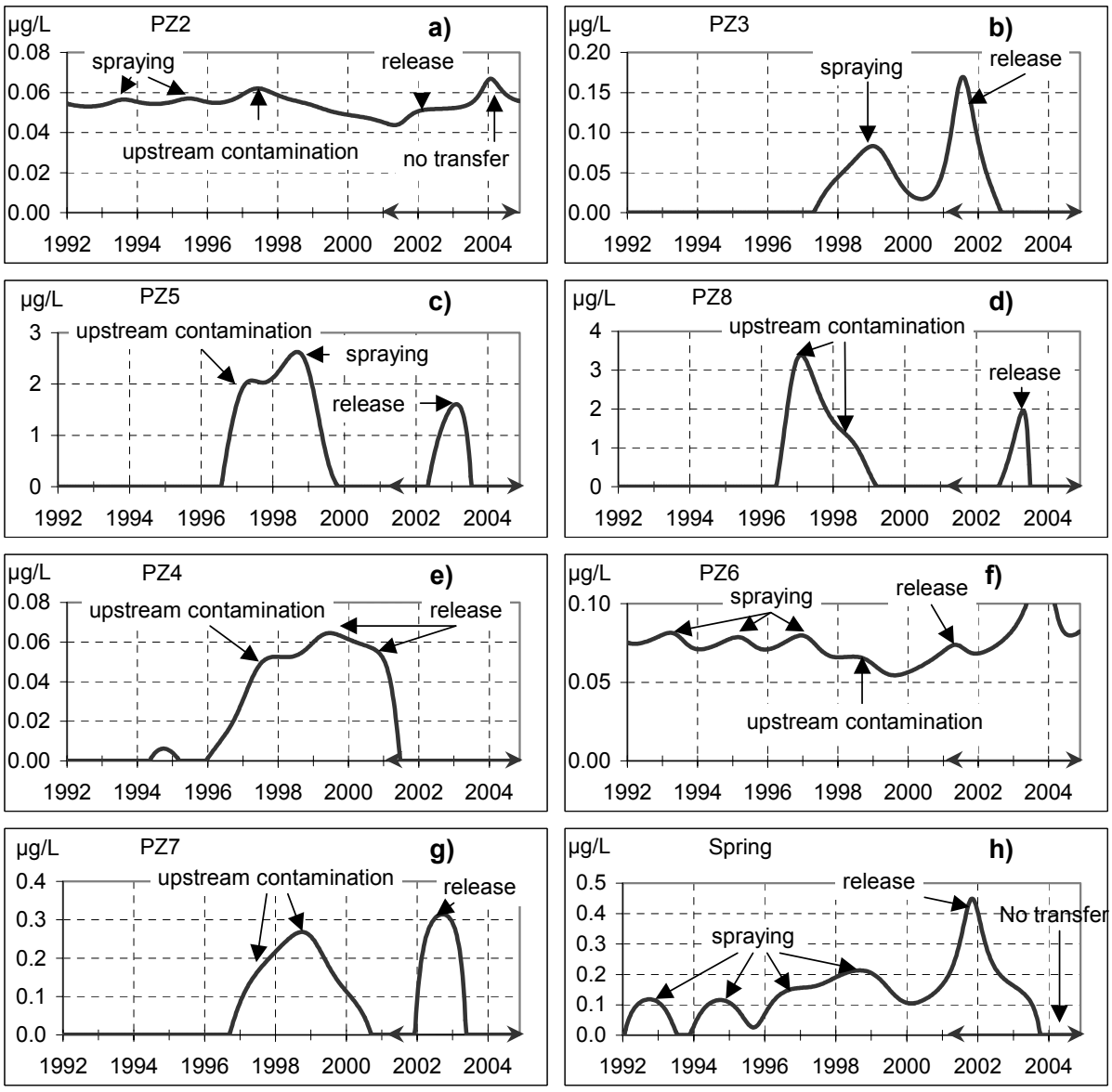

Figure 4.11. Reconstructed atrazine concentrations in the vadose zone according to (11)

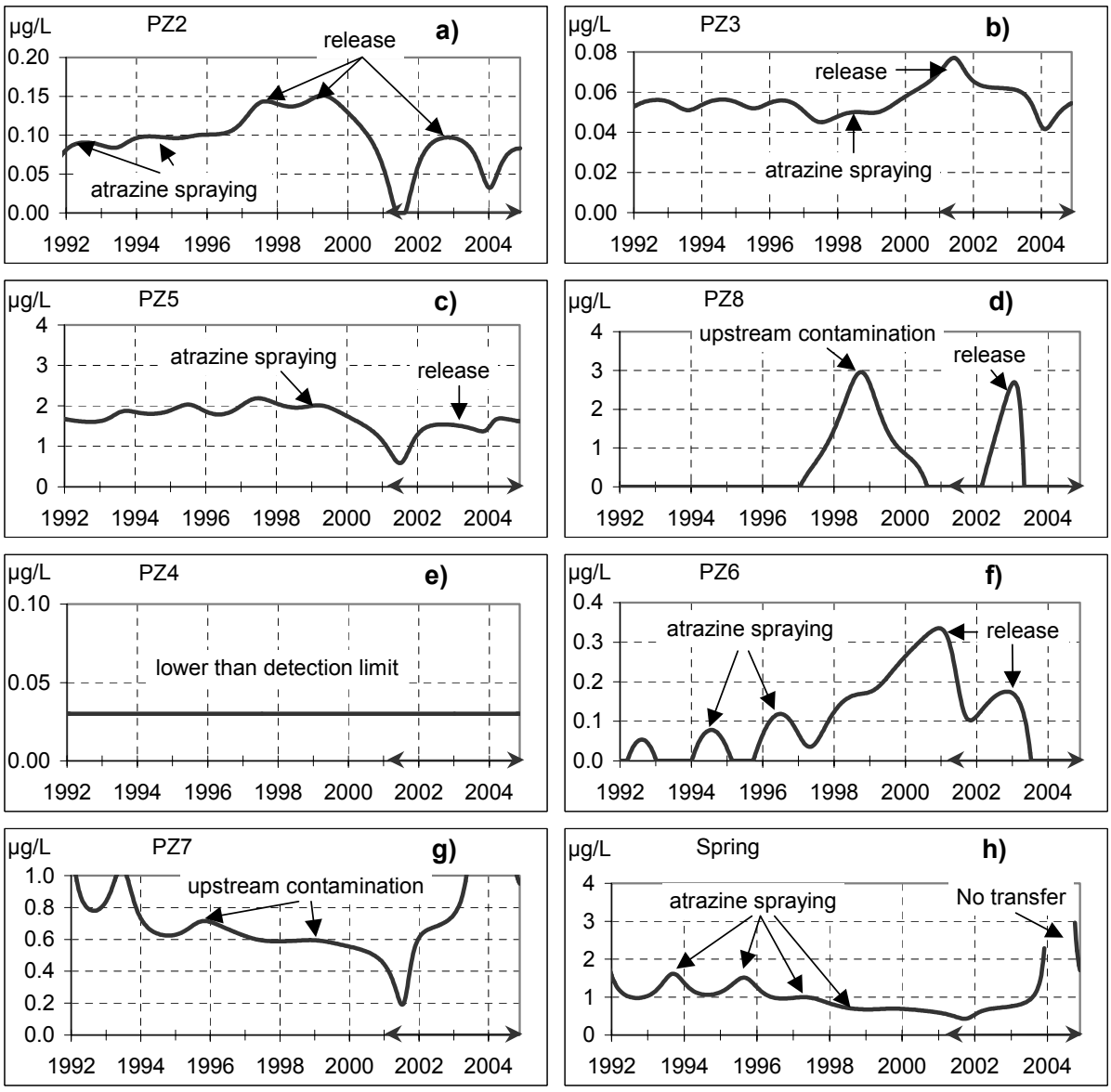

Figure 4.12. Reconstructed deethylatrazine concentration in the vadose zone according to (12)

Nitrate concentration in the vadose zone calculated from the nitrate flux observed at the spring is nearly constant, close to 60 mg/L, for the years during which the transfer through the unsaturated zone is effective (Figure 4.10h). Since the spring water is representative of the groundwater quality at the catchment scale, the nitrate in the vadose zone effectively behaves as if it was being issued from a stock that is restored each year. Nitrate concentrations disclose smooth variations at piezometers, except for piezometers PZ3 and PZ4 which both show a low contamination. The piezometer PZ3 is located downstream of a grove close to the upper limit of the catchment. As for piezometer PZ4, its peculiar behaviour suggests that it is not in relation with the main aquifer, which has been confirmed by recent tracer studies.

Atrazine concentration in the vadose zone reconstructed from fluxes observed at piezometers (Figure 4.11) relates sprayings and upstream contamination both being testified by land use although it should be noted that the concentration ranges are extremely variable from one piezometer to the other. Spraying of a plot upright a piezometer was found to produce a concentration peak that may generally be clearly identified (Figure 4.11a, b, c, f). Upstream contamination occurs when a piezometer intercepts the atrazine plume which was issued from a sprayed plot located upstream of that piezometer (Figure 4.11a, c, d, e, f, g). The responses of the piezometers PZ5 and PZ8 which are located 20 meters away are of particular interest. Both piezometers were highly contaminated in 1997 and 1998. The upstream contamination for 1997 could be confirmed by the land use at the time. This allows contamination to be identified. It can be inferred that the sprayed field close to the upper limit of the catchment is upstream of both piezometers and the plume followed the valley downwards to the spring. The mean mass transfer time through the vadose zone being about twenty times higher than that from piezometers to the spring, the location of piezometers has no influence on the delayed response of groundwater to agricultural practices. In 1998, the field located upright to the piezometer PZ5 was sprayed and concentration peaks can be clearly identified at piezometer PZ5 due to the migration of atrazine through the vadose zone and at piezometer PZ8 that intercepted the atrazine plume, being located downstream of the field. It is interesting to note that Figure 4.11 shows the release of atrazine after 1999 while the compound was no longer being used on this catchment. It appears that two types of atrazine should be considered: a mobile atrazine that follows water migration in the vadose zone and an atrazine that is retained in the pores of soil and subsoil material, the mobility of which strongly depends on the water flux through the unsaturated zone. The release of atrazine mainly occurred in 2001, which was a particularly wet year. The reconstructed atrazine concentration in the vadose zone from the flux observed at the spring (Figure 4.11) integrates the whole catchment. The series clearly allows the identification of successive years of application and also of the significant release of bound atrazine in 2001. Overall, climatic conditions appear to play an important role in the determination of atrazine transport to groundwater.

Trend extrapolation of atrazine concentrations at the spring

The forecast of atrazine concentrations at the spring requires two transfer functions to be used in order to simulate spring flow and the atrazine flux (atrazine concentrations are calculated as the ratio between the atrazine flux in spring water and the spring flow). The transfer model for the atrazine flux accounts for both the mobile atrazine which results from a recent application and that being slowly released in response to significant rainfall events. The input related to the mobile atrazine is simply the mass of atrazine sprayed every year on the catchment weighted by the effective rainfall (Figure 4.13c). The input related to the atrazine which is being slowly released is represented by the effective rainfall, which assumes there is a stock of atrazine in the soils and in the unsaturated zone, i.e. only rainfall can explain the atrazine releases from the vadose zone to the groundwater. The release of atrazine is a non-linear process since it occurs during wet years only.

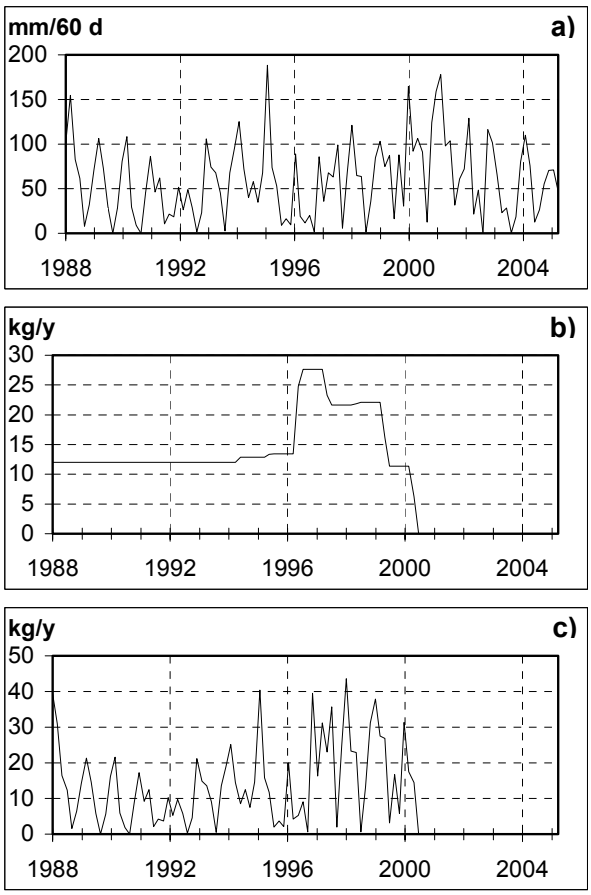

Figure 4.13. The inputs of the transfer model of the atrazine flux to the spring. A 60-day sampling rate is used – a) effective rainfall – b) The mass of atrazine sprayed every year on the catchment – c) The mass of atrazine sprayed every year on the catchment weighted by the effective rainfall.

The atrazine stock undergoes biodegradation processes and the atrazine mass $m(t)$ available since the beginning of the forecast period is weighted so that:

$$m(t) = m_0 \exp(-\lambda.t) \quad (14)$$

where m_0 is the initial stock; t is the elapsed time since the beginning of forecast and $T_{1/2} = \ln(2)/\lambda$ is the half-life of atrazine in the system. The mass balance does not take into account the export of atrazine to the spring because it is lower than 1 % every year, which can be neglected.

The shortness of the observation period in comparison with the transfer times at the catchment scale does not allow non-linearities to be taken into account. Moreover, neither the percentage w of mobile atrazine in the vadose zone, nor the half life of atrazine can be estimated as this would require an observation period of at least 4 times the mean mass transfer time from the vadose zone to the spring, i.e. ca. 12 years. So, both the weighting factor w and the half life $T_{1/2}$ of atrazine are subsequently used as uncertain parameters in the transfer models.

Different scenarios were considered using different half-lifes for atrazine (5, 25 and 100 years), different release rates (release of bound atrazine or not) and different weighting factors for the proportion of mobile atrazine in the vadose zone ($w = 30\ \%$ and $w = 60\ \%$) to try to account for uncertainties in the modelling. Models represented in Figure 4.14a and 14b (i.e. for different values of w) were found to be very similar as the estimation of w is an ill-posed problem from a numerical point of view. The two components of the atrazine flux are represented in Figure 4.14c, d based on equation (8). Here the input flux R_{eff} represents the

released atrazine flux through the vadose zone and Q_1 is the mass of atrazine sprayed every year weighted by the effective rainfall to represent the mobile atrazine flux through the vadose zone. Atrazine release at the spring is therefore effectively approximated by a linear transfer model.

Predicted concentrations for atrazine at the spring for the various scenarios considered are presented in Figure 4.15. Synthetic rainfall data were generated within TEMPO on the basis of the rainfall characteristics for previous years. The release of atrazine was found to occur for wet years, which is consistent with earlier observations made for the year 2001. The upper limit of predicted atrazine concentrations corresponds to wet years for which the return period is 10 years. The lower limit decreases to zero because the atrazine is assumed to be strongly bound to soil and subsoil material and no release is assumed to occur. The actual future values for atrazine concentrations in the Brévilles spring will be somewhere within those two limits depending on the precipitation amount and the actual release and degradation rates. The higher the percentage w of mobile atrazine, the steeper the decrease of atrazine concentration in 2005 and 2006 when the mobile atrazine flux issuing from rainfall prior to 1999 is transferred to the spring. The overall duration of the spring contamination is strongly determined by hypotheses made on the half-life of atrazine.

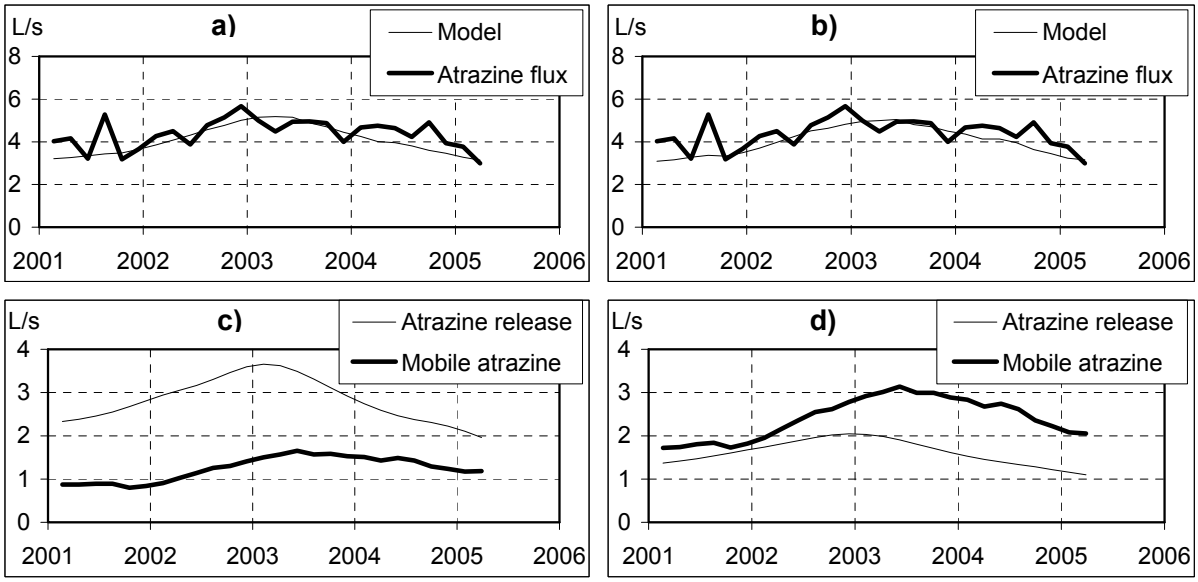

Figure 4.14. Separation of the atrazine flux at the spring into two fluxes representing mobile atrazine and the atrazine release. A 60-day sampling rate is used – a and b) comparison of the atrazine flux and the model (30% mobile atrazine in a and 60% mobile atrazine in b) – c and d) the atrazine fluxes (30% mobile atrazine in a and 60% mobile atrazine in b)

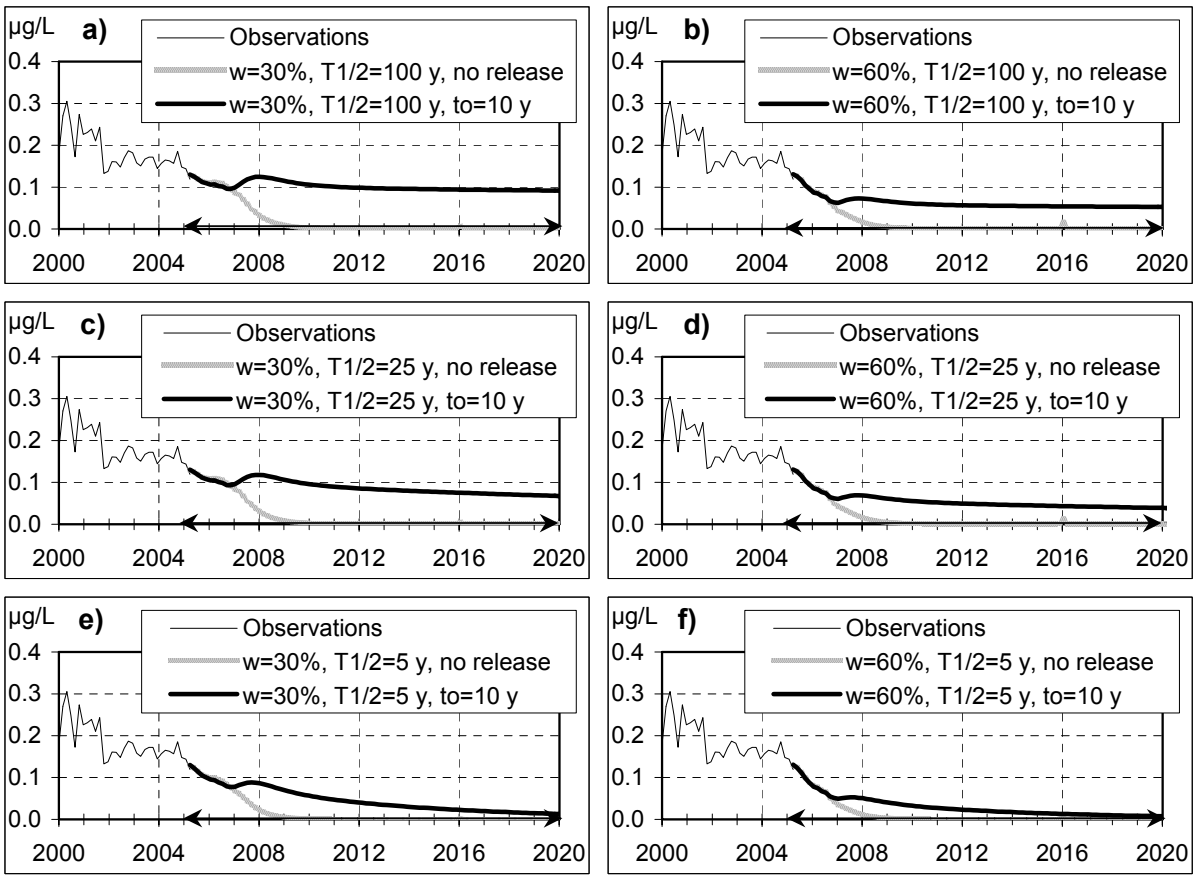

Figure 4.15. Predicted atrazine concentrations in the spring (the forecast period is symbolized by arrows on the time axis). A 60-day sampling rate is used. The upper limit of the expected atrazine concentration corresponds to wet conditions defined from rainfall height whose return period t_0 is 10-years, i.e. 115 mm per 60 days. The lower limit corresponds to dry years during which no release occurs; w is the percentage of mobile atrazine and $T_{1/2}$ is the half life of atrazine.

4.3.3 Conclusions and perspectives

We demonstrated the use of a transfer function approach to reconstruct and predict time series of nitrate and pesticides in the Brévilles spring. Time series of pesticide concentrations at the spring and in a number of piezometers on the catchment were used to infer characteristics of transfer functions using an inverse modelling procedure and information on rainfall at the site. Pesticide inputs which were reconstructed through the methodology were found to be in agreement with detailed knowledge of pesticide applications on maize fields in the catchment.

The question of whether the limited period for which pesticide concentrations data were available (4 years) would support a robust deployment of the methodology was asked at the start at the study. The fact that the pesticide inputs to the system prior to the observation period were successfully reconstructed demonstrated that the methodology can be deployed even with short time series. A current limitation of the approach is that it is not possible to differentiate between pesticide inputs resulting from a direct application of pesticides to a field and those resulting from the release of an existing stock of pesticides in the soil and/or subsoil in response to significant rainfall events. This limitation is however of little relevance in the case of Brévilles where the pesticide under study had not been used since 1999, or more generally speaking, in the case of nitrate where there is usually very small annual variations in nitrate loadings at a few meters below the soil surface.

The calibrated transfer functions were used to make predictions on the future variations of pesticide concentrations at the Brévilles spring using synthetically-produced rainfall series. Although we tried to account for imperfect knowledge in a number of processes through the

use of different scenarios, the predictions for atrazine concentrations remain clearly uncertain given that there are uncertainties on i) the future rainfall; ii) the proportion of atrazine which is being released from existing stocks in the soil/subsoil; iii) degradation rates for the compound. The uncertainty in the predictions could be reduced by acquiring longer time series of pesticide concentrations and/or generating field or laboratory information on the degradation of atrazine in groundwater systems.

The methodology presented above is general in essence, does not require detailed information on the physico-chemical properties of the system under study and can therefore be applied to all kinds of pollutants and surface water / groundwater systems. Hence, while the conclusions of the present study are provisional, the TEMPO package has proven a useful tool for analysing, understanding and predicting trends in water quality data.

4.4 Time series analysis using possibilistic regression

4.4.1 Introduction to possibilistic («fuzzy») regression

Introduction
The main objective of the TREND2 Work Package is to provide methods for i) identifying trends in water quality time series; and, ii) extrapolating such trends into the future for the purpose of early warning with respect to water quality. There is a variety of approaches that can be applied to this general objective. A basic criterion that will guide the choice of the methodology is the level of knowledge concerning the behaviour of the system at hand (in our case the soil-water system). In the ideal case, investigators will dispose of a mechanistic model that reproduces available information. By mechanistic we mean a model that accounts for physical and chemical phenomena such as the physical structure of the system (and heterogeneity thereof), flow of water in the sub-surface, transport and fate of potentially harmful substances. In the event that such a model should be available, the general procedure consists in calibrating the model with respect to available information on water quality and then extrapolating model calculations in order to calculate concentrations expected in the future. Unfortunately, in real situations, the availability of such a mechanistic model will rather be the exception than the rule. Therefore, methods are needed that are suited to "poorer" levels of knowledge of the system's behaviour. If a significant number of water quality data are available, and if the available time window is characteristic of the system's behaviour, then this data can be used to "learn" about the system's behaviour (without a mechanistic model) and therefore project this behaviour into the future.

The previous chapter presents the application of signal analysis methods to data modelling (using generic transfer functions), trend identification and trend extrapolation. In this section we propose an exploratory investigation of another method: possibilistic regression using neural networks. The proposed method makes use of neural network (NN) analysis to "learn" a "model" of the input-output relationship, but in addition it calculates the amount of imprecision about this trend. It is expected to be of particular interest in a risk–based framework by providing an upper bound on expected groundwater concentrations.

Basic notions in possibility theory
While probability distributions are mathematical tools that allow a description of random variability, possibility distributions (also called fuzzy sets or fuzzy numbers) are mathematical tools that describe information that is incomplete or imprecise (Zadeh, 1978; Dubois & Prade, 1988).

For a variable *X* that is imprecisely known, a possibility distribution representing this variable is characterized by its membership function (denoted μ) such that $\mu(x^*) = 1$ for some value x^* of X. This function, the values of which lie between zero and one, describes the level of likelihood (possibility) that variable *X* may take a certain value *x*. The term "possibility" refers to the idea of lack of surprise; the more possible a value, the less surprising it is.

A possibility distribution (or fuzzy number) can be thought of as a "refined interval": a series of nested min-max intervals, each interval having its own level of likelihood. The interval of values judged most likely is called the "core" of the distribution, while the interval outside of which values are judged not possible is called the "support" of the distribution. The example in Figure 4.16 conveys the following information:
The porosity of this soil is considered most likely to lie between 25 and 45%. This interval is assigned a possibility of unity.
Values outside the range 15% - 50% are considered not possible.

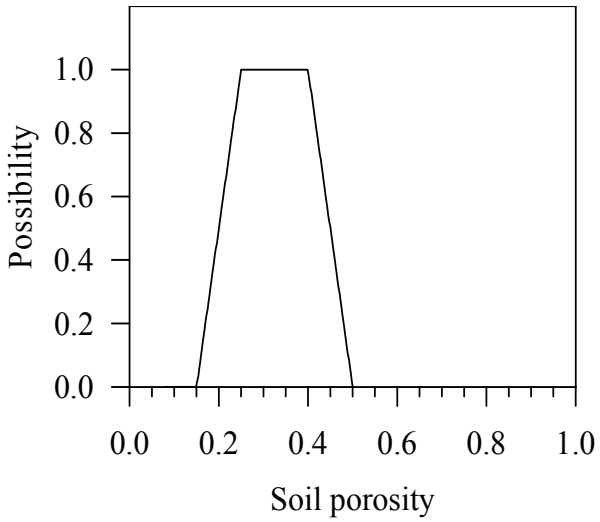

Figure 4.16. Example of a possibility distribution for the porosity of a soil

It is worth noting that this sort of incomplete information is quite typical of real-world situations. Possibility distributions are therefore useful in such situations where available information concerning a variable is incomplete or imprecise (situations of partial ignorance) and therefore the selection of a single probability distribution cannot be justified on the basis of available information.

There is, however, a direct link between possibility theory and probability theory (see Dubois & Prade, 1992): a possibility distribution encodes a "family" of probability distributions. In the case of Figure 4.16, the corresponding family of probability distributions is depicted in Figure 4.17: it is the family of all the probability distributions that lie between the upper probability bound represented by the distribution on the left (full line) and the lower probability bound represented by the distribution on the right (dashed line). This lower bound is symmetrical with respect to the right branch of the possibility distribution indicated as a dotted line. The distance between the upper and lower probability distributions is a consequence of imprecision in the available information. If there is no imprecision, the two distributions coincide into a single probability distribution and express pure random variability (classical probability theory). If there is no imprecision and also no random variability, then the variable is referred to as "crisp" (precise).

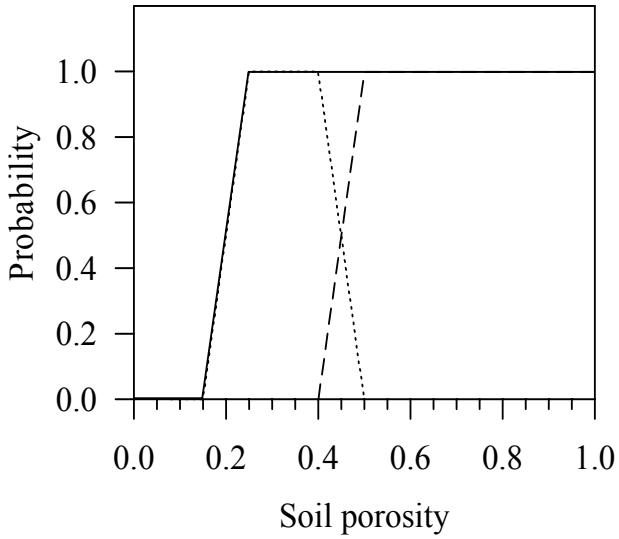

Figure 4.17. Left and right limits of the family of probability distributions encoded by the possibility distribution of Figure 4.16

4.4.2 Possibilistic regression

Introduction
There exists two different types of possibilistic (fuzzy) based extensions of regression methods in data analysis (Kacprzyk and Fedrizzi, 1992; Tanaka and Guo, 1999, Bandemer and Naether, 1992; Diamond and Tanaka, 1998). The first one deals with fuzzy (imprecise) output data, and possibly also fuzzy inputs, to be described by a fuzzy regression function. This type of method has been proposed for dealing with imprecise and qualitative data by several authors (Celmins, 1987; Diamond, 1988). It is based on linear fuzzy least squares fitting.

The second type of approach is referred to as possibilistic regression and handles ordinary data. A linear model, proposed initially by Tanaka (1987) "learns" a fuzzy regression function from crisp (precise) inputs and crisp or interval outputs. In the first step, a linear regression function that produces an interval from crisp inputs is learned by solving a linear programming problem. Next, a fuzzy interval linear regression function is deduced. This function associates a fuzzy interval to a crisp input. This method has been extended to non linear fuzzy regression by Ishibuchi and Tanaka (1992) and Jenga et al. (2003). The advantage of the method is that it is very efficient in terms of computation time and it can handle noise to some extent.

In the following, possibilistic regression was applied since it applies to crisp (precise) inputs and outputs. In the context of groundwater quality time series (concentration versus time), it is assumed therefore that both time and concentration can be measured with sufficient precision.

Advantages and limitations
The main benefits of possibilistic regression with respect to classical regression is that the former describes both the general tendency of the function (as classical regression does) but also the amount of imprecision around the general tendency. In particular, the non-linear extension of possibilistic regression based on neural networks (Ishibushi and Tanaka, 1992) is used in the experimentations proposed here. This method has several advantages. First, in contrast with standard possibilistic regression (Tanaka, 1987), it allows a more faithful representation of the data through the use of a non-linear function. Moreover, the method proposed by Tanaka (1987) was based on linear programming, which can become very costly when dealing with large amounts of data as is the case here. The neural networks approach is more efficient (Ishibuchi and Tanaka, 1992) in terms of computation time and the users can fix the trade-off between the computation time and the accuracy of the results. Finally, it is known that neural networks perform extrapolations that are statistically meaningful.

Nevertheless, the method has some limitations too. The first one is a limitation of any learning method; namely, the data given in the inputs must be sufficiently informative with respect to describing the outputs. Also, information on relevant parameters must be available for extrapolation. Besides, neural networks have difficulties for learning some types of functions such as periodic ones. Neural networks are also very sensitive to outliers (marginal points of the output). In the applications considered herein, all the data, even that which departs from the general tendency, is taken into consideration. It is worth noting that an extension of the method, based on support vector machine (SVM ; Jenga et al., 2003), has been proposed for dealing with outliers. For reasons of time constraints, it was not possible to explore this alternative for the study presented here.

Neural network based possibilistic regression
Neural networks are a general "learning" scheme that generates a function from pairs of input-output data. The function "learned" can then be used for classification or extrapolation purposes. A neural network is made of several nodes, organized in layers and linked by weights (synapses). Each layer computes a sigmoid function of a weighted sum of outputs from the previous layer. Inputs of the first layer are the inputs of the function to be induced. For the "learning" scheme, a pair of input-output data is chosen randomly and the data output

is compared with the neural network output. Then, the neural network weights are adjusted following the discrepancy between the output data and the network output (Ishibuchi and Tanaka, 1992).

It is worth noting that curve-fitting methods, based on polynomials, would not be appropriate for extrapolation: one could obtain a fit between a polynomial and the measured data, but this fit could not be used for extrapolation because it would not be statistically representative. on the contrary, it is known that neural networks provide a statistically representative regression.

This learning step is repeated a large number of times, the latter being fixed by the user (typically from 10 million to 100 million iterations are performed). Note however that an excessive number of iterations can lead to "over-precise" learning and potentially to extrapolation anomalies.

Let us consider a vector of the form $<\vec{x}_p = (x_{p1}, \ldots x_{pm}), y_p>$ where $(x_{p1}, \ldots, x_{pn})$ are the inputs and y_p is the output. The aim of a neural network is to "learn" a function g that minimizes the discrepancy between measured and calculated output. So we build a neural network that will help us define a function g such that:

$$\sum_{n=1}^{m} \frac{1}{2}(y_p - g(x_{p1},...,x_{pm}))^2$$

is minimal.

This theoretical requires a neural network with only two layers. The first layer is the input unit, the second layer is the hidden unit.

The input unit is defined by n neurons $O_{11}, ..,O_{1n}$. The value of the neurons when a new data vector $\vec{x}_p$ is introduced is:

$$O_{1i}(\overrightarrow{x_p}) = x_{pi}$$

The hidden layer contains n' neurons (n' is a parameter fixed by the user) $O_{21}, \ldots O_{2n}$. Each neuron of the input layers O_{1i} is linked with each neuron of the hidden layer O_{1j} by the synaptic weight w_{ji}. The value of the neurons when a new data vector $\vec{x}_p$ is introduced is:

$$O_{2j}(\vec{x}_p) = sig(net_j(\vec{x}_p))$$

with:

$$sig(x) = \frac{1}{1+\exp(-x)}$$

and:

$$net_j(\vec{x}_p) = \sum_{i=1}^{n} w_{ji} \cdot O_{1i}(\overrightarrow{x_p}) + \theta_j$$

The value of the function g defined by the neural network is given by the output neuron O which is linked with each neuron O_{2j} of the hidden layer by a synaptic weight w_j. The values of the function and the output neuron, when a new data vector $\vec{x}_p$ is introduced are:

$$g(\vec{x}_p) = O(\overrightarrow{x_p}) = sig(net(\vec{x}_p) + \theta$$

At each step of the learning process, a vector is randomly selected from the training data set. Then the error of g is back-propagated in the neural network. The values of the synaptic weights w_{ji}, w_j and the values θ_j and θ are updated in order to minimize the error.

Possibilistic regression with neural network

The classical scheme of neural networks provides standard non-linear regression. The proposed approach, based on Ishibuchi and Tanaka (1992) learns three neural networks: one for the standard linear regression, one for the upper bound regression and another for the lower bound regression. The result can be interpreted as a possibility distribution taking the standard regression result as the core of the distribution while the upper and lower bounds define the support of the distribution.

The upper-bound function is denoted as g*. For learning this function, we learn a neural network that minimizes the value:

$$\sum_{n=1}^{m} \frac{1}{2} \cdot w_p \cdot (y_p - g^*(\vec{x}_p))^2$$

where ω_p is specified depending on whether y_p is less or greater than $g^*(\vec{x}_p)$.

More precisely, we use the following weighting scheme:

$$w_p = \begin{cases} 1 \text{ if } y_p > g^*(\vec{x}_p) \\ w \text{ if } y_p \leq g^*(\vec{x}_p) \end{cases}$$

where ω is a small positive value in the open interval]0, 1[. Thus more weight is given to calculated results that fall above the measured data than to the other results.

If r is the number of learning steps of the algorithm, at step t we have:

$$w(t) = \frac{1}{1 + (\frac{t}{r/20})^3}$$

This weight allows us to have a function that is just greater than the target function.

In the same manner, the lower bound g_* is computed by considering the minimization of:

$$\sum_{n=1}^{m} \frac{1}{2} \cdot w_p \cdot (y_p - g_*(\vec{x}_p))^2$$

where:

$$w_p = \begin{cases} 1 \text{ if } y_p < g_*(\vec{x}_p) \\ w \text{ if } y_p \geq g_*(\vec{x}_p) \end{cases}$$

We thus give more weight to calculated results that fall below the measured data. We thus obtain a lower bound regression. Note that if the same weight is given to all errors, we obtain the classical regression curve.

For the data presented hereafter, 5 hidden neurons were used for the neural network. Tests were also performed with 4 hidden nodes and results were practically identical. Note that one drawback of the neural network approach is that there is no definite rule to define the optimal number of hidden nodes.

Results

The method is applied to time series of atrazine, deethylatrazine and spring discharge data from the Brévilles case study.

Results are presented in appendices and grouped according to the type of information that was used for the "learning" process. Four types of information were used:
Time of measurement (week number).
Measurement month number.
Annual supply of atrazine in the fields (an arbitrary offset of 8 years was applied to account for the fact that there is a delay between the application of atrazine and its apparition in groundwater.
Rainfall.
These sources of information can be used individually or else combined.

The first trials with the possibilistic regression method are performed with time information only (Appendix 4.1). For each output, results are presented for the learning data interval, the learning data interval plus one year, the learning data interval plus five years and the learning data interval plus twenty years.

Results for atrazine are presented in Figure 4.18. The standard neural network-based regression appears in green while the boundary regressions appear in brown. We observe a general trend towards decreasing concentrations. In the long run (learning interval + 20 years) concentrations level out. This levelling is largely influenced by the sigmoid function used in the neural network. If there is no more "learning data", results are increasingly influenced by this function.
The same results are presented in Figure 4.19 as possibility distributions; in red for the learning period and in grey for the extrapolated period. As mentioned previously the cores of these distributions are defined by the classical regression curve (in green in the previous figure) while the supports are defined by the boundary regression curves. The upper limits of the extrapolated supports can be interpreted in terms of probability as concentration values for which the probability of having higher values is zero. It should be noted, however, that this "certainty" of not exceeding the upper bound is only as good as the data: should a new measured concentration show a value higher than the extrapolated upper bound and all the curves would be modified.

Figure 4.20 shows results for deethylatrazine. Here the extrapolation rapidly reaches a plateau.

This is also the case in Figure 4.21 (spring discharge data) while one might have expected ("chi-by-eye") a decreasing trend. Judging by the neural network computation, an extrapolated plateau appears more statistically representative.

The second trial (Appendix 4.2), makes use of information on the measurement week and the measurement month number. As the latter information is correlated to climatic information, one might expect it to be useful in the "learning" process. Results in Figure 4.22 show cyclic peaks in atrazine concentrations that correspond rather well with measured peaks. It would appear that the month number may "explain" part of the observed behaviour.

Results for deethylatrazine in Figure 4.23 suggest problems in the extrapolation : the lower regression curve displays cyclic variations that do not appear in the other two regressions. The results for spring discharge are not very different from those of Appendix 4.1 where the month number was not used.

The third trial (Appendix 4.3) makes use of time information (week number) and also of information on annual supply of atrazine. There is a notable influence on the extrapolated level of atrazine (Figure 4.25) with a "plateau" that is higher than in the case of Appendix 4.2.

Extrapolated values of deethylatrazine (Figure 4.26) show an increase and then level out, the latter being probably an effect of the sigmoid function used in the neural network scheme. Again no significant difference in extrapolated discharge rates is observed.

In the fourth trial (Appendix 4.4), time information is combined with information on rainfall. For the extrapolation period, rainfall simulated with TEMPO was used. The influence on fits to the learning period and on the extrapolation periods (Figure 4.28 to Figure 4.30) is questionable. Abrupt peaks appear as there is no buffering of the rainfall data.

The fifth trial (Appendix 4.5) uses three sources of information: time (week number), month number and annual supply of atrazine. The upper regression of atrazine follows the data quite well (Figure 4.31). The extrapolation of deethylatrazine is difficult. Note that as the classical regression is independent from the other two, it is possible that it may cross over as is the case in Figure 4.32.

The last trial (Appendix 4.6) uses all available sources of information: time (week number), month number, annual supply of atrazine and month number. The results are questionable in particular due to the use of the rainfall information.

4.4.3 Conclusions and perspectives

This chapter presents the results of an exploratory investigation of an innovative methodology for time series trend analysis and extrapolation. This methodology is based on the use of a modified scheme of neural networks from Ishibuchi and Tanaka (1992). The main advantage of this methodology with respect to classical non-linear regression using neural network schemes is that it provides an estimate of the imprecision on the regression. This imprecision is materialized by the distance between the upper and lower regressions. In a context of trend analysis of groundwater quality time series for the purpose of early warning, the upper bound could be used as a conservative indicator of potential threshold excess.

This methodology is similar in philosophy to the TEMPO approach: the data themselves are used to “learn” (through optimisation) a relationship between inputs and outputs and this relationship is used for extrapolation. It differs therefore from the mechanistic approach where a model of pollutant migration and fate is used to predict concentrations. The TEMPO approach uses tools from the field of signal analysis while the approach presented here uses neural networks. It is felt that TEMPO allows for much more expert input and judgement than the neural network approach which is more “brute force”. Nevertheless, the results presented herein suggest that the approach holds promise in a risk management context and it will therefore be the topic of further investigation.

4.4 Discrepancy between the CFC age of interstitial water and the mean transfer time calculated from impulse responses.

The mean transfer time calculated from impulse responses is about 3 years for all piezometers, that that addresses to the migration of water or the mass transport (Ca, nitrate). This mean transfer time is referring to the mobile water that significantly contributes to the observed transfers. The age deduced from CFC or tritium analysis of interstitial water strongly depends on the age of water that is trapped in the small pores and do not contribute significantly to the mass transport.

The discrepancy observed between both methods for water dating is relatively traditional in chalk formations. A dual porosity, interstitial porosity and fracture porosity characterize the chalk. This behavior is specific to the chalk, which shows both a very fine porosity network and a well-organized fracture network on a large scale. Water content in the interstitial porosity is always close to saturation due to both water migration downwards to the water table and the capillary fringe. After significant effective rainfall, an increase in capillary pressure leads to saturation of the conductive fractures, which occurs when the water content exceeds a certain threshold [Wellings, 1984, Peters and Klavetter, 1988, Price et al., 2000, Mahmood-ul-Hassan. and Gregory, 2002, Haria et al., 2003]. Below this threshold,

water is only slightly mobile because it is trapped in the fine pores of the chalk. In such conditions, the velocity of water migration is commonly 50 cm/y and, consequently, the water flux through the unsaturated zone is relatively low.
When water transfer occurs through the fractures, the mean transit time may be more than 10 times lower. So, although the fracture porosity is generally a few percents whereas the matrix porosity may reach 30%, the water flux through the unsaturated zone is strongly enhanced.
The unsaturated zone of the Brevilles catchment that consists of limestone with a dual porosity behaves like a chalk formation as for water migration. It is the reason why the mean transit time given by both methods is different.

4.5 Summary and perspectives

The water and pesticide data from the Brévilles catchment were used to evaluate three approaches to trend analysis. The first approach is based on statistical theory and attempts to analyse trends in pesticide concentrations based on concentrations data only. The approach which was retained in the present work is know as the Holt's two parameter method which includes an exponential smoothing of the data. The methodology does not account for the strong effects environmental factors might have on pesticide concentrations (e.g. the influence of rainfall in determining pesticide transfers). Also, the system was demonstrated to be ill-posed from a calibration point of view, which means that a wide variety of predictions can be made on the basis of the same dataset. The performance of 'classical' approaches to trend analysis are therefore unlikely to be of value to predict pesticide concentrations in the Brévilles spring and alternative approaches were therefore evaluated.

Trends in pesticide concentrations were analysed using a methodology based on the iterative determination of transfer functions which draw a direct relationship between observed pesticide concentrations and other inputs such as an indication of groundwater recharge. The approach was evaluated through the back-derivation of temporal variations in pesticide inputs to the groundwater system using the time series analysis tool TEMPO. The reconstructed pesticide inputs were found to match observed pesticide applications on the catchment and helped to understand the functioning of the groundwater system. Different scenarios were considered with regard to potential influencing factors such as degradation rates of pesticides, the potential release of pesticides from soil and subsoil stocks. The scenarios were combined to stochastically generated weather data to result in predictions of pesticide concentrations in the Brévilles spring over the next 15 years. It should be emphasised that given the uncertainties associated with key fate processes that are poorly known and uncertainty in future weather conditions, predictions made remain uncertain. Still, while the conclusions of the present study are provisional, the TEMPO package has proven a useful tool for analysing, understanding and predicting trends in water quality data.

Methodological developments were also undertaken to investigate the potential usefulness of a methodology combining possibilistic regression and artificial neural networks. The main advantage of this methodology with respect to classical non-linear regression using neural network schemes is that it provides an estimate of the imprecision on the regression. Although TEMPO was found to be more flexible in integrating expert knowledge and judgement on the functioning of the system under study, the results obtained when applying the new methodology to the Brévilles data suggest that the possibility approach could be of interest in a risk management context where the upper bound could be used as a conservative indicator of potential threshold exceedances.

The main advantage of the approaches based on transfer functions and possibilistic regression which were evaluated in the present study is that they require only information on measured data and rainfall inputs to yield results of potential interest. These low data requirements are in sharp contrast with the deterministic approach which will be investigated as part of future work in the TREND2 work package. The approaches are also generic in

their nature and can be easily applied to other environmental contaminants or other groundwater or surface water systems.

5. Discussion

This discussion is meant to briefly summarise the characteristics of the various study areas, to highlight apparent differences between the study sites and to examine the consequences for the work on trend detection.

5.1 Differences between study sites: pumping wells and springs versus observation wells

Results of deliverables T2.3 and T2.4 strongly indicate that a consideration of travel times in the groundwater systems is essential for detection of trends and trend reversal. Quite different approaches have been followed in the TREND subcatchments case studies to deal with variations due to travel times. An important reason for these diverging approaches is the type of monitoring networks that were used for trend detection, in combination with different hydrogeological settings.

Table 5.1 summarizes some main hydrogeological characteristics of the selected sub-basins. It shows that a wide range of hydrogeological situations was selected. This has major consequences for the type of wells used to collect monitoring data (see below). Moreover, a completely different age distribution and chemical reactivity is anticipated between the various types of aquifers.

Table 5.1 Summary of hydrogeological characteristics of the selected sub-basins of T2.3 and T2.4

Sub-basin	Hydrogeological characteristics	Unsaturated zone
Dommel/Brabant	Unconsolidated Plesitocence deposits; fine to medium coarse sands, loam	Shallow (1-5 m)
Wallony-Hesbaye	Cretaceous chalk, fissured, dual porosity aquifer	Thick
Wallony-Pays de Herve	Cretaceous chalk and sands, fissured	Thick
Wallony-Néblon	Carboniferous limestone, folded karstified	Thick
Wallony-Meuse alluvial plain	Unconsolidated deposits; gravels, sands and clays	Shallow (1-5 m)
Brévilles	Lutecian limestone over Cuise sands, limestone fissured	Thick (> 30 m sometimes)

Quite different monitoring systems exist in the selected sub-basins (Table 5.2). The Brabant and Dommel sub-basins have nested observation wells at specific depths which are dedicated to groundwater quality monitoring. Monitoring data in the Wallonian catchment originate from the Wallonian nitrate survey network. Both pumping wells, springs and galleries are used for nitrate monitoring. Monitoring in the Brévilles catchment is done in piezometers and in the Brévilles spring itself, and is seven piezometers.

Table 5.2 Summary of monitoring systems in the selected sub-basins in deliverables T2.3 and T2.4

Sub-basin	Observation wells	Pumping wells	Others	Typical screen lengths	Typical monitoring depths - SL
NL Dommel	X	X [b]		2 m	10, 25 m
NL Brabant	X				
Wallony-Hesbaye	X	X	Galleries	10-30 m	20-40 m [a]
Wallony-Pays de Herve	X	X	Galleries, springs	10-30 m	20-40 m [a]
Wallony-Néblon	X		Galleries, springs	10-30 m	20-40 m [a]
Wallony-Meuse alluvial plain	X	X		5-15 m	5-15 m
Brévilles	X		Spring	10-20 m	14-42 m

. SL = Surface Level, [a] = exact lengths and depths not yet known, [b] = not yet certain

There are important differences between the monitoring systems used that are relevant for trend analysis. Probably the most important aspect is the difference in travel time (groundwater age) for samples which are taken from a pumping well, spring or gallery and for samples which are taken from monitoring screens which are not pumped.

For *pumping wells, springs and galleries* the groundwater sample reflects a mixture of travel times which could best be described using the complete travel time frequency distribution. Young and very old groundwater are mixed because of the converging flow field. The average travel time, or characteristic time, is often counted in decades (see Figure 5.1)

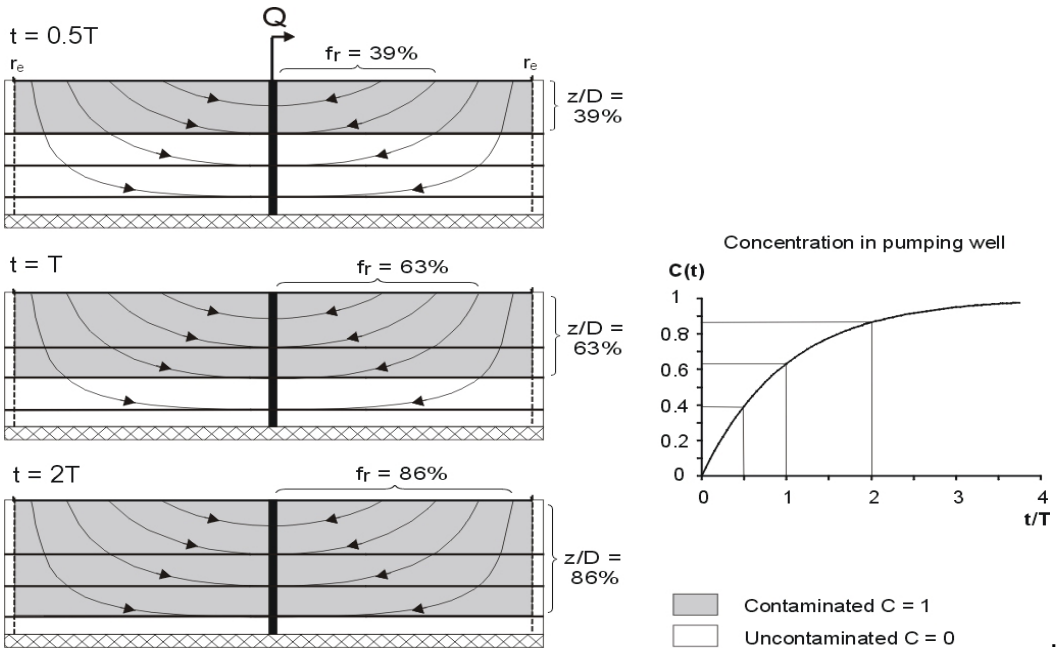

Figure 5.1: Pumping wells typically attract groundwater with a mixture of travel times; young water with short flow paths and old water with long flow paths. Consequently, the resulting concenration time series in pumping wells are both influenced by recent antropogenical contamination (gray color in the graphs) aand the simultaneous attraction of old, uncontaminated water (white color in the graphs)

The presented results of the Brévilles and Wallonian cases mainly deal with these kind of monitoring types. Transfer times in the thick unsaturated zone of the Brévilles and Wallonian subcatchments appeared to be considerable and need to be integrated in the trend analysis concept. Both the Brévilles spring and the Wallonian catchment show concentration fluctuations with time, due to reaction of the fast part of the groundwater system to climatological variations.

Samples from *multi-level or single-level observation wells* have more or less fixed travel time from the earth surface to the screen. Deeper screens generally exhibit older water than shallow screens, due to the slow vertical groundwater flow component. When short screens are applied, only limited mixing is anticipated. Observation wells with large screen length take an intermediate position relative to short screened wells and pumping wells.

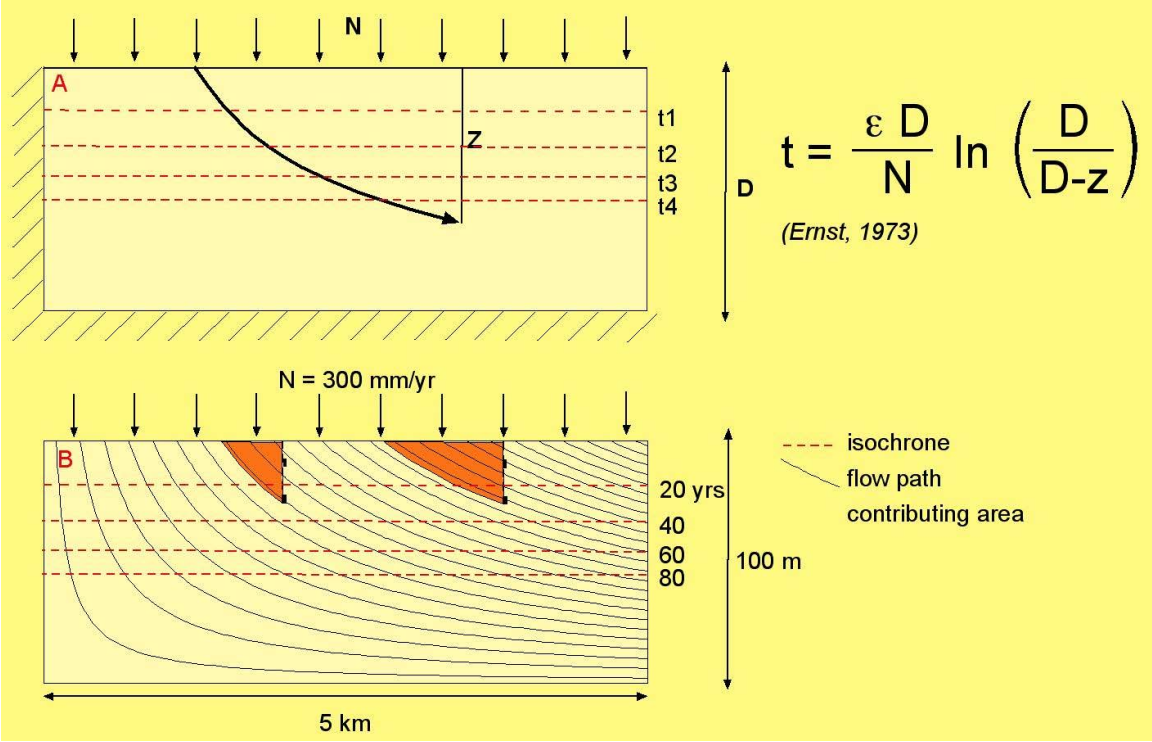

Figure 5.2 Observation wells typically have a narrow range of travel time associated, especially when applied in granular aquifers. In a simple hydrogeological setting as above, a simple pattern of increasing groundwater age with depth is observed (see also Broers 2004)

The Dutch Meuse case is based on this kind of monitoring systems and a general increase of groundwater age with depth was observed using tritium-helium, CFC and SF6 dating. Here, variations in groundwater age still impedes trend analysis. Age scaling effectively removes these kind of variations, and trend reversal could be demonstrated. Age dating appeared to be crucial to establish this objective.

Overall, we might conclude that differente monitoring types need different approaches for trend analysis. The deliverables T2.3 and T2.4 focused on statistical methods for trend detection. Future deliverables of the TREND 2 work package will also concentrate on deterministic and modelling approaches.

5.2 Specific results

5.2.1 Meuse (NL)

In the Dutch Meuse basin, groundwater age dating has proven to be very helpful when researching trends in groundwater quality. The trend reversal and subsequent downward trend have been observed in conservative chemical indicators (oxidation capacity and sum of cations) and are consistent with the estimateds of historical input of solutes which was extensively described in Deliverable T2.2.
Using the groundwater ages and the extrapolated time trends to predict future groundwater quality shows that shallow groundwater quality will improve, but deeper water quality may deteriorate as a result of the peak reaching these depths. Regional improvements of groundwater quality will be very slow because of the variation in groundwater ages.

5.2.2 Meuse (BE)

For the Walloon part of the Meuse basin, a consistent and rigorous approach has been proposed and applied for trend detection and quantification in groundwater quality (nitrate) datasets, based on statistical techniques that is robust and able to discriminate between "clear" and "weak" trends. This is related to the two-step procedure: first trend detection, then trend quantification.

The statistical analysis has provided point-by-point estimations of nitrate trends, in the form of a slope expressed in mg NO_3/year (increase or decrease). This result might be enough and appropriate to estimate the short term evolution of groundwater quality in the selected basins (few years), particularly for those groundwater bodies overlain by a thick unsaturated zone that lead to important buffer effects in the evolution of nitrate concentrations in the aquifers (Geer basin, Pays de Herve).

The major disadvantage of using a "pure" statistical trend analysis is thus that it is not able to consider variations in land use and functional relations between land use and groundwater quality. For long term evaluation of nitrate trends, more advanced techniques are thus required, such as transfer functions or mechanistic modelling relating land use and groundwater quality. From a spatial point of view, advances are also still needed in order to produce reliable global estimates of groundwater quality indicators at the scale of the groundwater body, as requested by the EU Water Directive.

5.2.3 Brévilles (F)

The water and pesticide data from the Brévilles catchment were used to evaluate three approaches to trend analysis. The first approach is based on statistical theory and attempts to analyse trends in pesticide concentrations based on concentrations data only. The methodology does not account for the strong effects environmental factors might have on pesticide concentrations and was demonstrated to be ill-posed from a calibration point of view. The performance of 'classical' approaches to trend analysis are therefore unlikely to be of value to predict pesticide concentrations in the Brévilles spring and alternative approaches were therefore evaluated.

Trends in pesticide concentrations were also analysed using a methodology based on the iterative determination of transfer functions which draw a direct relationship between observed pesticide concentrations and other inputs such as an indication of groundwater recharge. While the conclusions of the present study are provisional, the TEMPO package has proven a useful tool for analysing, understanding and predicting trends in water quality data.

Thirdly, a methodology combining possibilistic regression and artificial neural networks was developed. The main advantage of this methodology with respect to classical non-linear regression using neural network schemes is that it provides an estimate of the imprecision on the regression. Applying the new methodology to the Brévilles data suggest that the possibility approach could be of interest in a risk management context where the upper bound could be used as a conservative indicator of potential threshold exceedances.

The main advantage of the approaches based on transfer functions and possibilistic regression which were evaluated in the present study is that they require only information on measured data and rainfall inputs to yield results of potential interest.

In the complex Brévilles catchment, the unsaturated zone and fractured behaviour complicate the interpretation of modern age dating techniques. The study of environmental tracers shows a dual velocity system, where water is able to infiltrate at high rates through cracks and fractures, and through the porous medium at low rates. CFC ages point to relatively old water and slow transport (deliverable T2.3), whereas transfer times derived from time series analysis (this Deliverabele) point to relatively fast transport. Which of the two transport rates is most important for trend analysis and trend understanding is subject for future research.

6. References

Bandemern H., Naether, W. (1992) - Fuzzy Data Analysis. Kluwer Academic Publishers, Dordrecht, Boston, London 1992.

Birardar, D.P., and A.L. Rayburn. 1995. Chromosomal damage induced by herbicide contamination at concentrations observed in public water supplies. J. Environ. Qual. 24:1222–1225.

Broers, H.P. (2004) The spatial distribution of groundwater age for different geohydrological situations in The Netherlands: implications for groundwater quality monitoring at the regional scale. Journal of Hydrology 299: 84-106

Broers, H.P. and Van der Gift, B, (2004) Regional monitoring of temporal changes in groundwater quality. Journal of Hydrology: 296: 192-220.

Broers, H.P. (2004) Nitrate Reduction and Pyrite Oxidation in the Netherlands. Chapter 14 in: Nitrate in groundwaters IAH Selected papers on hydrogeology., Eds. L.Razowska-Jaworek & A. Sadurski. p. 141-149. Balkema Publishers, Leiden, The Netherlands.

Brouyère, S. *et al.,* (2004). "Migration of contaminants through the unsaturated zone overlying the Hesbaye chalky aquifer in Belgium: a field investigation." Journal of Contaminant Hydrology **72**: 135-164.

Carr, J. R. (1995). Numerical analysis for the geological sciences. Penitence-Hall, Inc., Englewood Cliffs, New Jersey, EUA, pp. 592.

Celis, R., J. Cornejo, M.C. Hermosin, and W.C. Koskinen 1998. Sorption of atrazine and simazine by model associations of soil colloids. Soil Sci. Soc. Am. J. 62:165–171.

Celis, R., J. Cornejo, M.C. Hermosin, and W.C. Koskinen. 1997. Sorption–desorption of atrazine and simazine by model soil colloidal components. Soil Sci. Soc. Am. J. 61:436–443.

Celmins, A. (1987) - Least squares model fitting to fuzzy vector data. Fuzzy Sets Syst., 22(3):245–269.

Clark, G.M., D.A. Goolsby, and W.A. Battaglin. 1999. Seasonal and annual load of herbicides from the Mississippi River basin to the Gulf of Mexico. Environ. Sci. Technol. 33:981–986.

Clay, S.A., and W.C. Koskinen. 1990. Adsorption and desorption of atrazine, hydroxyatrazine, and S-glutathiane atrazine on two soils. Weed Sci. 38:262–266.

Cleveland, W.S., Devlin, S.J., 1988. Locally weighted regression; an approach to regression analysis by local fitting. Journal of American Statistics Association 83, 596–610.

Dassargues, A. and A. Monjoie (1993). The chalk in Belgium. The hydrogeology of the chalk of the North-West Europe. R. A. Downing, M. Price and G. P. Jones. Oxford Science Publication, Clarendon Press. Oxford, UK, pp. 153 - 269.

Diamond, P. (1988) - Fuzzy least squares. Inf. Sci., 46(3):141-157.

Diamond, P., Tanaka, H. (1998) - Fuzzy regression analysis. Fuzzy Sets in Decision Analysis, Operations Research and Statistics. The Handbooks of Fuzzy Sets Series. Kluwer Academic Publishers, pages 349-387.

Dubois, D., and Prade, H. (1988). Possibility theory. New York Plenum Press, 263 pp.

Dubois, D., and Prade, H. (1992). “When upper probabilities are possibility measures.” Fuzzy Sets and Systems, 49, 95-74.

Evangelou, V.P., and J. Wang. 1993. Differences between infrared spectra of atrazine obtained under transmittance and diffuse reflectance modes. Spectrochim. Acta 49A:291–295.

Gamble, D.S., C.H. Langford, and G.R. Barrie-Webster. 1994. Interactions of pesticides and metal ions with soils. Rev. Environ. Contam. Toxicol. 135:63–90.

Goode, D. J. (1996) Direct simulation of groundwater age. Water Resources Research 32, 289-296.

Goolsby, D.A., E.M. Thurman, M.L. Pomes, M.T. Meyer, and W.A. Battaglin. 1997. Herbicides and their metabolites in rainfall. Environ. Sci. Technol. 31:1325–1333.

Hanson, C. R. (2002). Nitrate concentration in Canterbury groundwater -a review of existing data. Christchurch, Environment Canterbury.R02/17 ISBN 1-86937-457-6. pp. 87

Haria A. H., M. G. Hodnett and A. C. Johnson, Mechanisms of groundwater recharge and pesticide penetration to a chalk aquifer in southern England, Journal of Hydrology, 275, 122-137, 2003.

Helsel, D. R. and R. M. Hirsch (1995). Statistical Methods in Water Resources. USGS, pp. 510.

Hirsch, R. M. *et al.,* (1991). "Selection of methods for the detection and estimation of trends in water quality." Water Resources Research **27**(5): 803-813.

Hirsch, R. M. *et al.,* (1982). "Techniques of trend analysis for monthly water quality data." Water Resources Research **18**(1): 107-121.

Ishibuchi, H. and Tanaka, H. (1992) - Fuzzy regression analysis using neural networks. Fuzzy Sets and Systems, 50:5765.

Jenga, J., Chuang, C. and Su, S. F. (2003) - Support vector interval regression networks for interval regression analysis. Fuzzy Sets and Systems, 138 (2):283-300.

Kacprzyk, J. and Fedrizzi, M. (Eds.) (1992) - Fuzzy Regression Analysis. Omnitech Press, Dordrecht, Boston, London.

Kolpin, D.W., J.E. Barbash, and R.J. Gilliom. 1998. Occurrence of pesticides in shallow groundwater of the United States. Environ. Sci. Technol. 32:558–566.

Koskinen, W.C., and S.A. Clay. 1997. Factors affecting atrazine fate in north central U.S. soils. Rev. Environ. Contam. Toxicol. 151: 117–165.

Kruger, E.L., P.J. Rice, J.C. Anhalt, T.A. Anderson, and J.R. Coats. 1997. Comparative fates of atrazine and deethylatrazine in sterile and nonsterile soils. J. Environ. Qual. 26:95–101.

Lettenmaier, D. P. *et al.,* (1991). "Trends in stream quality in the continental United States, 1978-1987." Water Resources Research **27**(3): 327-339.

Libiseller, C. and A. Grimvall (2002). "Performance of partial Mann-Kendall tests for trend detection in the presence of covariates." Environmetrics **13**: 71-84.

Loftis, J. C. *et al.,* (1991). "Multivariate tests for trend in water quality." Water Resources Research **27**(7): 1419-1429.

Mahmood-ul-Hassan M. and P. J. Gregory, Dynamics of water movement on Chalkland, Journal of Hydrology, 257, 27-41, 2002.

Martin-Neto L., Traghetta D. G., Vaz C.M.P, Crestana S., and Sposito G., On the Interaction Mechanisms of Atrazine and Hydroxyatrazine with Humic Substances, J. Environ. Qual. 2001 30: 520-525.

Meinardi, C.R., 1994. Groundwater recharge and travel times in the sandy regions of the Netherlands. PhD Thesis, Free University of Amsterdam, 211 pp.

Moreau, C., and C. Mouvet. 1997. Sorption and desorption of atrazine, deethylatrazine, and hydroxyatrazine by soil and aquifer solids. J. Environ. Qual. 26:416–424.

Peters R.R. and E.A. Klavetter, A continuum model for water movement in a unsaturated fractured rock mass, Water Resour. Res, 24, 416-430, 1988.

Pignatello, J.J., and L.Q. Huang. 1991. Sorptive reversibility of atrazine and metalachlor residues in field soil samples. J. Environ. Qual. 20:222–228.

Pinault J.-L., H. Pauwels and C. Cann, Inverse modeling of the hydrological and the hydrochemical behavior of hydrosystems – Application to nitrate transport and denitrification, Water Resour. Res., 37(8), 2179-2190, 2001 a.

Pinault J.-L., V. Plagnes, L. Aquilina and M. Bakalowicz, Inverse modeling of the hydrological and the hydrochemical behavior of hydrosystems - Characterization of karst system functioning, Water Resour. Res., 37(8), 2191-2204, 2001 b.

Pinault J-L (2001) – Manuel utilisateur de TEMPO: logiciel de traitement et de modélisation des séries temporelles en hydrogéologie et en hydrogéochimie. Projet Modhydro. Rap. BRGM/RP-51459 – FR, 221 p., 206 Fig, 5 tabl., 2 ann.

Pinault J-L, N. Doerfliger, B. Ladouche and M. Bakalowicz, Characterizing a coastal karst aquifer using an inverse modeling approach. The saline springs of Thau, Southern France, Water Resour. Res., 40, W08501, doi:10.1029/2003WR002553.

Pinault, J.-L., N. Amraoui, and C. Golaz (2005), Groundwater-induced flooding in macropore-dominated hydrological system in the context of climate changes, Water Resour. Res., 41, W05001, doi:10.1029/2004WR003169

Postma, D., Boesen, C., Kristiansen, H., Larsen, F., 1991. Nitrate reduction in an unconfined sandy aquifer: water chemistry, reduction processes, and geochemical modeling. Water Resource Research 27(8), 2027–2045.

Price M., R.G. Low and C. McCann, Mechanisms of water storage and flow in the unsaturated zone of the chalk aquifer, Journal of Hydrology, 223, 54-71, 2000.

Racke, K.D., M.W. Skidmore, D.J. Hamilton, J.B. Unsworth, J. Miyamoto, and S.Z. Cohen. 1997. Pesticide fate in tropical soils. Pure Appl. Chem. 69:1349–1371.

Ritter, W.F., R.W. Scarborough, and A.E.M. Chimside. 1994. Contamination of groundwater by triazines, metolachlor and alachlor. J. Contam. Hydrol. 15:73–92.

Robinson, K. W. *et al.,* (2003). Water-Quality Trends in New England Rivers During the 20th Century. Pembroke, New Hampshire, U.S. Geological Survey.03-4012. pp. 20

Schnabel, J. (2002). Lacamas Lake restoration program: WY 2000 and WY 2001 water quality monitoring. Clark county, Washington, USA, State of Washington Department of Ecology & Lacamas Lake restoration program advisory committee. pp. 88

Smith, D. G. and P. B. McCann (2000). Water quality trend detection in the presence of changes in analytical laboratory protocols. New York, USA, New York Department of Environmental Protection**:** 13.

Sposito, G., L. Martin-Neto, and A. Yang. 1996. Atrazine complexation by soil humic acids. J. Environ. Qual. 25:1203–1209.

Sültenfuß, J., Roether, W., and Rhein, M. (2004) The Bremen Mass Spectrometric Facility for the Measurement of Helium Isotopes, Neon, and Tritium in Water. IAEA publication IAEA-CN-119/7

Tanaka, H. (1987) - Fuzzy data analysis by possibilistic linear models. Fuzzy Sets Syst., 24(3):363–376.

Tanaka, H. and Guo, P. J. (1999) - Possibilistic Data Analysis for Operations Research. Studies in Fuzziness and Soft Computing, Vol. 29. Heidelberg.

Thurman, E.M., D.A. Goolsby, M.T. Meyer, and D.W. Kolpin. 1991. Herbicides in surface waters of the Midwestern United States: The effect of spring flush. Environ. Sci. Technol. 25:1794–1796.

Thurman, E.M., D.A. Goolsby, M.T. Meyer, M.S. Mills, M.L. Pomes, and D.W. Kolpin. 1992. A reconnaissance study of herbicides and their metabolites in surface water of the Midwestern United States using immunoassay and gas chromatography/mass spectrometry. Environ. Sci. Technol. 26:2440–2447.

Tindall, J.A., and W.K. Vencill. 1995. Transport of atrazine, 2,4-D, and dicamba through preferential flowpaths in an unsaturated clay-ean soil near Centralia, Missouri. J. Hydrol. 166:37–59.

Yue, S. *et al.,* (2002). "Power of the Mann-Kendall and Spearman's rho tests for detecting monotonic trends in hydrological series." Journal of Hydrology **259**: 254-271.

Wellings S.R., Recharge of the upper chalk aquifer at a site in Hampshire, England., 1. Water balance and unsaturated flow, Journal of Hydrology, 69, 259-273, 1984.

Zadeh, L.. (1978). “Fuzzy sets as a basis for a theory of possibility”. Fuzzy Sets and Systems, 1, 3-28.

Zetterqvist, L. (1991). "Statistical estimation and interpretation of trends in water quality time series." Water Resources Research **27**(7): 1637-1648.

Zhang, X. and F. W. Zwiers (2004). "Comment on "Applicability of prewhitening to eliminate the influence of serial correlation on the Mann-Kendall test" by Sheng Yue and Chun Yuan Wang." Water Resources Research **40**(In Press): In Press.

Appendices
(separate document)